Investigation of recycled materials in hot-mix asphalt mixtures

by

Ya Gao

B.S. Dalian Ocean University, China, 2012
M.S. Kansas State University, 2019

AN ABSTRACT OF A DISSERTATION

submitted in partial fulfillment of the requirements for the degree

DOCTOR OF PHILOSOPHY

Department of Civil Engineering
College of Engineering

KANSAS STATE UNIVERSITY
Manhattan, Kansas

2024

Abstract

In the United States, asphalt, concrete, aggregates, and other materials are used in large quantities to build highway pavements. Hot-mix asphalt (HMA) mixtures typically contain approximately 93-96% aggregates and 4-7% asphalt binder. Recycled materials can replace these two main components, which provide economic and environmental benefits. However, the recycled materials affect the properties of asphalt cement and HMA mixture and, in turn, the durability of asphalt pavements. Thus, evaluating HMA containing recycled materials is a significant research pursuit. This study investigated the performance of HMA mixtures containing carbon char and fly ash. The rheological properties of Recycled Engine Oil Bottom (REOB) blended binders were also investigated. Finally, research was done to determine recycled asphalt pavement (RAP) content in HMA during production in the drum mix plants.

Results showed that small quantities of carbon char can improve moisture resistance but reduce rutting resistance. Adding about 15% fly ash to the asphalt binder would perform similarly in rutting, fracture cracking, and moisture susceptibility to the HMA mixture without fly ash. No interaction between the recycled material and the asphalt binder was apparent in both cases. A hand-held XRF spectrometer can detect some of the "signature" elements present in REOB. The addition of REOB reduced the binder stiffness at high temperatures and improved the low-temperature properties. The theoretical RAP quantities in the produced HMA mix in drum mix plants varied due to differences in the RAP burn-off test results between the labs in the QC/QA process. More frequent RAP binder determination was suggested for better process control of input RAP quantity in the mix production process.

Using recycled materials in HMA mixtures looks enticing due to increasing environmental awareness and the need for sustainable construction practices. However, carefully

selecting and managing recycled materials are needed to achieve sustainable and cost-effective road construction practices while meeting performance requirements. The fundamental interaction between recycled material and asphalt binders should be studied first to ensure the role of recycled materials. The QC/QA process during HMA production using RAP should be enhanced since the input RAP properties determine the RAP quantity being used and should be within a specified limit.

Investigation of recycled materials in hot-mix asphalt mixtures

by

Ya Gao

B.S. Dalian Ocean University, China, 2012
M.S. Kansas State University, 2019

A DISSERTATION

submitted in partial fulfillment of the requirements for the degree

DOCTOR OF PHILOSOPHY

Department of Civil Engineering
College of Engineering

KANSAS STATE UNIVERSITY
Manhattan, Kansas

2024

Approved by:

Major Professor
Dr. Mustaque Hossain

Copyright

Abstract

In the United States, asphalt, concrete, aggregates, and other materials are used in large quantities to build highway pavements. Hot-mix asphalt (HMA) mixtures typically contain approximately 93-96% aggregates and 4-7% asphalt binder. Recycled materials can replace these two main components, which provide economic and environmental benefits. However, the recycled materials affect the properties of asphalt cement and HMA mixture and, in turn, the durability and strength of the asphalt pavements. Thus, the evaluation of HMA containing recycled materials is significant. This research investigated the performance of HMA mixtures containing carbon char and fly ash. The rheological properties of Recycled Engine Oil Bottom (REOB) blended binders were also investigated. Finally, research was done to determine recycled asphalt pavement (RAP) content in HMA during production in the drum mix plants.

Results showed that small quantities of carbon char can improve moisture resistance but reduce rutting resistance. Adding about 15% fly ash to the asphalt binder would perform similarly in rutting, fracture cracking, and moisture susceptibility to the HMA mixture without fly ash. Statistical analyses confirmed these observations. No interaction between the recycled material and the asphalt binder was apparent in both cases from the SEM study. A hand-held XRF spectrometer can detect some of the "signature" elements present in REOB. The addition of REOB reduced the binder stiffness at high temperatures and improved the low-temperature properties. Statistical analysis confirmed this finding. Statistical and Monte Carlo simulation analyses also confirmed that the theoretical RAP quantities in the produced mix varied due to differences in the RAP burn-off test results from the Quality Control/Quality Assurance (QC/QA) process labs. More frequent RAP binder determination was suggested for better process control of input RAP quantity in the mix production/QC process.

Using recycled materials in HMA mixtures looks enticing due to increasing environmental awareness and the need for sustainable construction practices. However, carefully selecting and managing recycled materials are needed to achieve sustainable and cost-effective road construction practices while meeting performance requirements. The fundamental interaction between recycled material and asphalt binders should be studied first to ensure the role of recycled materials. The QC/QA process during HMA production using RAP should be enhanced since the input RAP properties determine the RAP quantity being used and should be within a specified limit.

Table of Contents

List of Figures

List of Tables

Acknowledgments

I want to express my deepest gratitude to all those who have supported and guided me throughout this research project.

First and foremost, I am profoundly grateful to Dr. Mustaque Hossain, my supervisor, for his invaluable guidance, insightful feedback, and unwavering support. His expertise and dedication were instrumental in the completion of this thesis. I sincerely thank the members of my committee, Dr. Christopher A. Jones, Dr. Husain Aziz, and Dr. Christopher I. Vahl, for their valuable suggestions and constructive criticism, which significantly improved the quality of this work. I also want to acknowledge the Kansas Department of Transportation, whose financial support made this research possible.

I am also thankful to Kansas State University, Department of Civil Engineering, for providing the necessary resources and a conducive environment for my research. Special thanks to all my colleagues in the department for their collaborative spirit and technical assistance.

My heartfelt appreciation goes to my friends for their camaraderie, encouragement, and helpful discussions that enriched my research experience.

Finally, I am deeply indebted to my family for their unwavering support and encouragement throughout my academic journey. Thank you for believing in me and providing me with the foundation to pursue my dreams.

This thesis is dedicated to all those who have contributed to my academic and personal growth. Your support and encouragement have been my driving force.

Chapter 1 - Introduction

1.1 Background

It has been recognized that the volume of waste products is increasing rapidly as the world's population grows. The primary ways of disposing of waste materials are landfills, incineration, and recycling (Kandhal, 1992). However, the insufficient capacity of landfills could not fulfill the increment of discarded materials, resulting in a rise in the price of landfilling. The emission of harmful chemicals and pollutants from waste incineration creates air pollution. Environmental and economic concerns have encouraged us to put extensive effort into developing the usage of recycled waste materials.

Waste materials are usually called "resources in the wrong places," but many still have worthy physical or chemical properties and can be used or recycled as construction materials (Golestani, 2015; Chiu et al., 2008). Annually, over a half billion tons of residuals are produced in the United States that can be reused, such as construction and demolition (C&D) debris, combustion products, waste tires, slags, and so on (Golestani, 2015). In Europe and the United States, according to the type of material, recycled materials used in construction are classified as industrial byproducts, road byproducts, and demolition byproducts (Pihl and Milvang-Jensen, 2001; Chiu et al., 2008). Industrial byproducts are the excess or residual materials during a primary production process from industrial, commercial, mining, and agricultural operations (MPCA, 2014; EPA, 2007), such as steel and iron slags or dust; bottom ash and fly ash from combustion processes; and cut-offs by sawmills. Road byproducts, including reclaimed asphalt pavement (RAP) and reclaimed concrete pavement (RCP), are the materials collected from pavement rehabilitation or reconstruction. Demolition byproducts include debris from demolished buildings, roads, or bridges, including crushed concrete, reclaimed asphalt shingles (RAS), glasses, bricks, etc.

1.2 Problem Statement

Over 160,000 miles of highway pavements in the United States are built or rebuilt annually using large quantities of asphalt, concrete, aggregate, and other materials (FHWA, 2015). Asphalt pavement is the primary type of road surface covering over 94% of U.S. roads (FHWA, 2021). Typically, asphalt mixtures contain 93-96% aggregates and 4-7% asphalt binder. These two main components could be replaced by recycled material that can provide economic and environmental benefits.

Using recycled materials in pavement construction can benefit economically by diverting materials from landfills and reducing the need for virgin materials (Horvath, 2003; Lee et al., 2010). For instance, the average tipping fee for landfills in the U.S. is approximately $37/ton. The marginal benefit of recycling road construction materials is more than $41/ton, including processing and transportation costs, counting the avoided cost of virgin materials (Horvath, 2003). Approximately $3.3 billion annually is saved by using RAP in road construction. On average, producers can save $7.8 per ton by using 21.1% RAP in HMA production (NAPA, 2024). A Minnesota study indicated that an 18% saving occurred when using 40% RAP (Horvath, 2003).

Utilizing recycled materials instead of virgin materials in pavement construction offers a possible solution for waste management and supports achieving sustainability goals in the infrastructure sector (Salehi et al., 2021). In 2019, more than 97 million tons of RAP were recycled, which saved approximately 58.9 million cubic yards of landfill space (NAPA, 2024). In 2021, the estimated net reduction of greenhouse gas (GHG) emissions from a new mixture using RAP is 2.6 million metric tons (MMT) of CO2-equivalent (CO2e) emissions, which is the same as the annual emissions from approximately 574,000 passenger vehicles (Williams et al., 2022). Figure 1.1 shows the yearly and cumulative GHG emissions reductions in new asphalt mixtures using RAP in previous years. The cumulative GHG emissions reduction from 2009 to 2021 is 26.1 MMT CO2e.

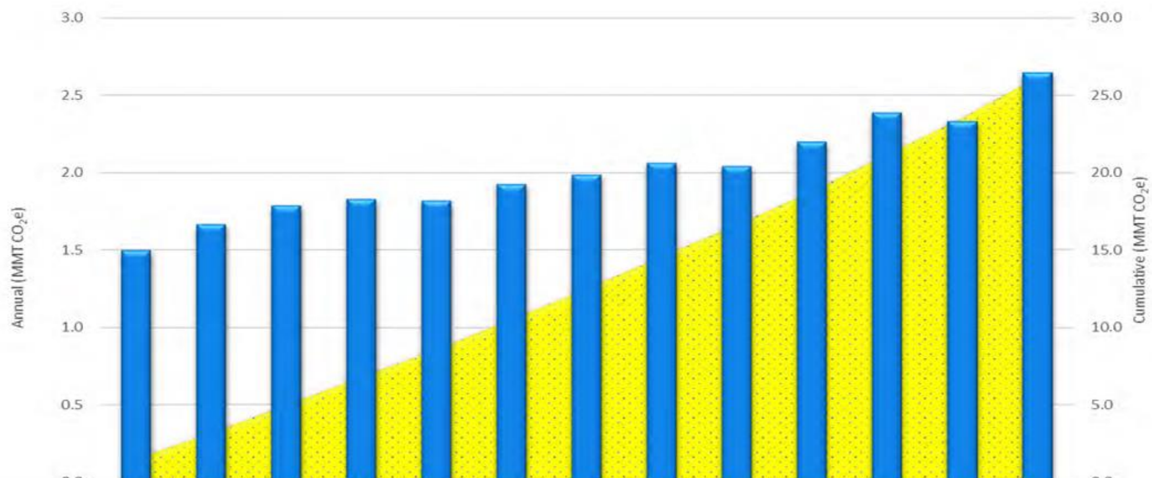

GHG Emissions	2009	2010	2011	2012	2013	2014	2015	2016	2017	2018	2019	2020	2021
Cumulative	1.5	3.2	4.9	6.8	8.6	10.5	12.5	14.5	16.6	18.8	21.2	23.5	26.1
Annual	1.5	1.7	1.8	1.8	1.8	1.9	2.0	2.1	2.0	2.2	2.4	2.3	2.6

Figure 1.1. GHG Emissions Reduction from Use of RAP in New Asphalt Mixtures, 2009–2021 (Williams et al., 2022)

Although beneficial, the recycled materials could affect the properties of the asphalt cement and hot-mix asphalt (HMA) mixture and the durability of the asphalt pavements. Thus, HMA containing recycled materials must be evaluated thoroughly and carefully.

1.3 Objectives

This research investigated multiple recycled materials, including carbon char, fly ash, re-refined engine oil bottom (REOB), and RAP usage in drum mix plants. The main objectives of this research were:

- Investigate the performance of HMA mixtures with various carbon char contents and compare that with a control mixture without carbon char.
- Evaluate the performance of HMA mixtures with various fly ash contents and compare that with a control mixture without fly ash.
- Investigate the effects of REOB on the rheological properties of asphalt binder blended with REOB.
- Investigate the RAP quantity used in HMA from drum mix plant production data and compare it with the calculated results.

1.4 Dissertation Outline

This dissertation is divided into six chapters, including this introductory chapter (Chapter 1). Chapter 2 introduces the investigation of carbon char in HMA mixtures. Chapter 3 discusses the performance of the HMA mixture with coal combustion products. Effects of REOB on asphalt binder's rheological properties are provided in Chapter 4. Chapter 5 discusses the investigation of the quantity of recycled asphalt pavement in asphalt mixture. Finally, Chapter 6 presents the conclusions and recommendations from this study.

Chapter 2 - Evaluation of Carbon Char in Hot-Mix Asphalt Mixture

2.1 Introduction

Carbon black results from incomplete combustion or thermal decomposition of heavy petroleum products. Approximately 14 million tons of carbon black are produced worldwide, and about 70% is used as a reinforcing filler in automobile tires (RCB Nanotechnologies, 2023). According to the U.S. Environmental Protection Agency (EPA), in 2003, approximately 290 million scrap tires were generated in the United States. Due to the non-biodegradable nature of tires, inappropriately disposing of the waste tires would impact the environment and human health. In 2003, over 80% of waste tires were reentered to the market, such as used as fuel, used in civil engineering projects, exported, etc. Among these, about 4.3% of scrap tires were processed, manufactured to ground rubber, and used to modify asphalt cement (EPA, 2016).

Carbon char, also known as raw recovered carbon black (rCB), is a by-product of the thermal decomposition of scrap tires containing carbon black. Usually, the pyrolysis process of tires produces 55% oil, 25% carbon char, 9% steel, 5% fiber, and 6% gas (Park et al., 1996). The residual of the pyrolysis process needs to be refined to gain a high-value product. The refined material is so-called rCB only if the wire and fabric are removed and milled.

2.2 Literature Review

Since the 1960s, recycled tire rubber has been used in the asphalt paving industry (Bukowski and Harman, 2014). Alfayez et al. (2020) discussed two methods of crumb rubber addition to asphalt mixture. In the early 1970s, the wet process, in which crumb rubber was added to the asphalt cement to modify the chemical and physical properties, was used to prevent early reflection of fatigue cracking in resurfaced pavements (Alfayez et al., 2020). The rubber-modified binder could increase the viscosity, improving the resistance of rutting and permanent deformation, lowering creep compliance, improving the elasticity, and increasing the stiffness (Kim et al., 2010). In the dry process, recycled tire rubber was used to replace part of the aggregates in the mix. However, volume instability and strength reduction occurred from the replacement (Gong et al., 2019).

Carbon black has also previously shown benefits in asphalt mixtures. Since the 1960s, many researchers have investigated carbon black use (Martin, 1962; Rostler et al., 1977; Vallerga & Gridley, 1980).

Yao and Monismith (1986) and Park et al. (1996) found that using carbon black increased the rutting resistance at high temperatures and decreased the temperature susceptibility and low-temperature cracking of HMA.

Ahmedzade and Geckil (2007) investigated the mechanical properties of HMA incorporating carbon black. In their research, carbon black was used as a filler. Marshall stability and flow tests showed that HMA with carbon black had higher stability and lower flow values, indicating high stiffness and resistance to permanent deformation. The higher creep stiffness obtained from the carbon black HMA showed a better rutting resistance. Such a mixture's high tensile strength values could enhance moisture damage resistance.

Notani et al. (2020) investigated the rheological performance of carbon black-modified asphalt binder. They found that increasing carbon black content could make the binder stiffer, and the lowest penetration value was observed at 15% of carbon black content. The viscosity increased as the carbon black content increased. Furthermore, the $G^*/\sin\delta$ values increased with a higher carbon black content, which improved rutting resistance.

Use of carbon black in the asphalt mixture is somewhat limited due to the high cost (Park et al., 1996). Because of the relatively high carbon black content in pyrolyzed carbon char, it has the potential to become an additive in the asphalt mixture. Using carbon char would also promote using waste products for sustainability and the economy.

2.3 Study Objectives

This study focused on investigating the performance of HMA mixtures with various carbon char contents and then comparing it with the performance of a control mixture (with no carbon char). Modified Lottman and Hamburg wheel tracking device (HWTD) tests were conducted on the Superpave mixtures for evaluation.

2.4 Materials

2.4.1 Carbon Char

In this research, Blizzard Energy, Inc. in Kansas provided carbon char powder, as shown in Figure 2.1, produced from combusting waste tires to recover oil.

Figure 2.1. Carbon Char

2.4.1.1 Scanning Electron Microscopy

The scanning electron microscopy (SEM) test was conducted to explore the microstructure. Blizzard Energy, Inc. provided the test results. Figure 2.2 shows the SEM image of carbon char with 1000 times magnification. The main elements and components detected by SEM are shown in Table 2.1. The detected elements are Carbon (C), O (Oxygen), Sulfur (S), and Iron (Fe), and the components of carbon char are elemental C, elemental S, iron carbonate (FeCO3), and iron-sulfur (FeS).

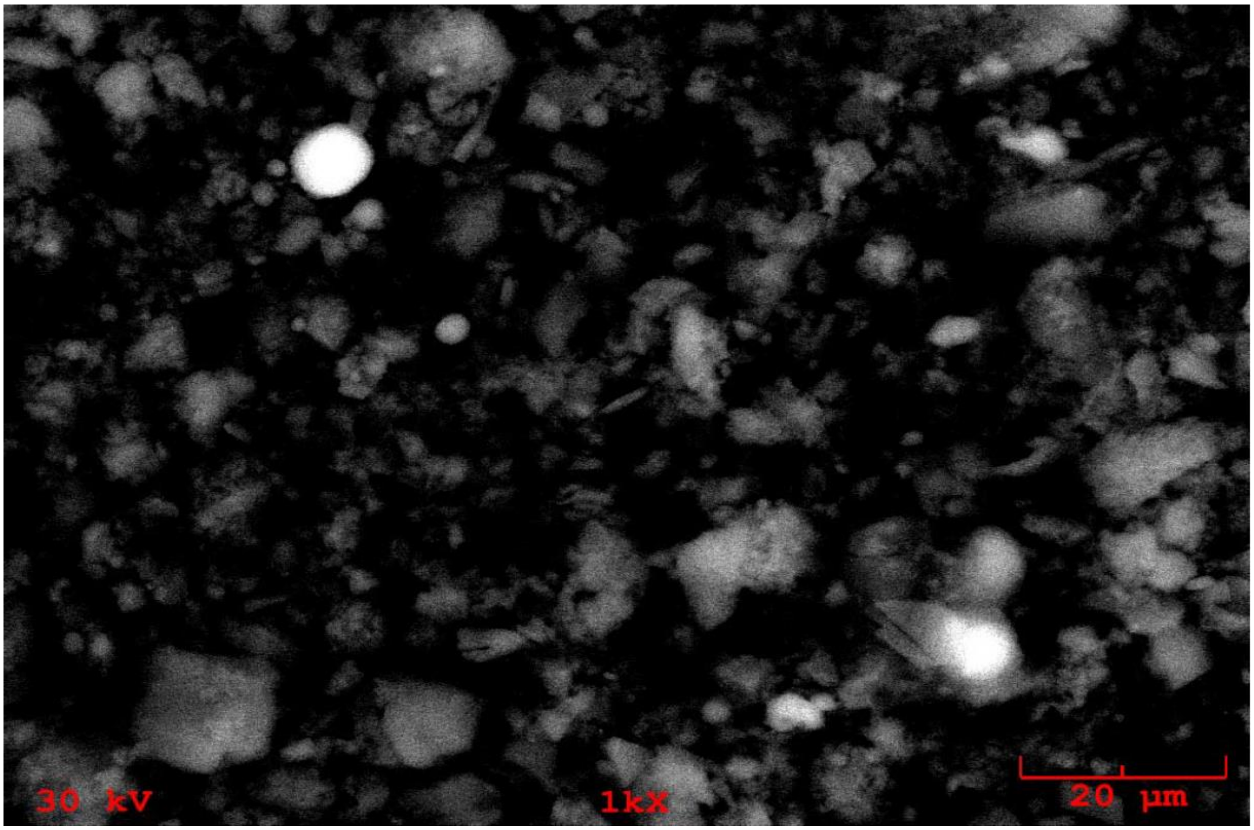

Figure 2.2. SEM Result of Carbon Char (source: Blizzard Energy, Inc.)

Table 2.1. Main Elements and Components of Carbon Char (source: Blizzard Energy, Inc.)

Element	%	Component	%	Comment
C	58.50	C	55.14	Elemental Carbon
O	13.40	S	10.40	Elemental Sulfur
S	11.17	$FeCO_3$	32.35	Iron Carbonate
Fe	16.93	FeS	2.11	Iron Sulfide
Total	100	Total	100	

2.4.2 Aggregates

In this study, HMA mixtures containing RAP used five virgin aggregates (CS-1, CS-2A, CS-2, SSG, and SSG-1). Virgin aggregates and RAP were collected from Shilling Construction Co. Inc. in Riley County, Kansas. The gradation of each aggregate product is shown in Table 2.2.

Table 2.2. Aggregate Gradation

Aggregate Type	% Retained								
	½	3/8	#4	#8	#16	#30	#50	#100	#200
CS-1	36	73	95	99	99	99	99	99	99.0
CS-2A			5	48	78	88	92	94	95.8
CS-2			24	50	62	69	75	78	80.2
SSG				25	60	80	91	98	99.0
SSG-1		7	73	99	99	99	99	99	99.0
RAP	4	10	26	44	60	71	83	88	90.6

2.4.3 Binder Preparation

A PG 58-28 asphalt binder was used for the HMA mixtures. Carbon char at mass percentages of 5%, 10%, 15%, and 20% were blended with heated asphalt cement. First, the asphalt binder was heated to the mixing temperature corresponding to the binder PG grade. Then, carbon char was added to the binder. A spiral mixer was installed on a drill to mix the carbon char and binder. After mixing, a rotational viscometer (RV) test was performed on the blends to see what percentages of carbon char would be workable. The test for the Superpave PG asphalt binder is always conducted at 135°C, and typical viscosity values for the asphalt binder at this temperature are 200 cP to 2000 cP (Pavement Interactive). The viscosity of the virgin binder used in this research is 310 cP. Based on the test results tabulated in Table 2.3, viscosity values of the blends with 5% and 10% carbon char fall in this viscosity range, indicating good workability. However, we could not get any reading on the viscometer for blends with 15% and 20% carbon char. As shown in Figure 2.3, some carbon char seemed to "bunch" up around the test spindle, resulting in viscosity readings of these two blends that were out of range of the RV used. Therefore, 5% and 10% carbon char blends were adopted for this study. Furthermore, as time passed, carbon char settled in the binder. Thus, carbon char was blended with the binder before using it in the asphalt mixtures.

Table 2.3. Viscosity Test Results

Carbon Char Content (%)	Viscosity (cP)
0	310
5	340
10	352

Figure 2.3. Bunch up of Carbon Char around Test Spindle

2.4.4 Mix Design

HMA mixtures were developed in the laboratory following the Kansas Department of Transportation (KDOT) requirements. KDOT defines mixtures by their nominal maximum aggregate size (NMAS). In this study, a 12.5 mm NMAS mix design was developed. The mixture gradation is shown in Figure 2.4. Table 2.4 shows the percentages of aggregates used, the gradation of the combined blend, and KDOT requirements. In this study, PG 58-28 was needed in the mixture because of the use of 15% recycled asphalt pavement (RAP) materials. As was the binder, all aggregates were heated within the mixing temperature range. RAP was heated at 60℃. Aggregates were then mixed with a binder with various carbon char percentages using a mechanical mixer. After mixing, the loose mixtures were aged for two hours at the compaction temperature. Then, a Superpave gyratory compactor was used to compact the asphalt mixtures with the maximum number of gyrations selected based on the design equivalent single-axel loads

(ESALs). The compacted cylindrical samples with 150 mm diameter were expected to achieve the 4% air voids target. Two compacted samples and 1,500 g of loose mixture for each asphalt mixture were prepared, respectively, for the bulk specific gravity (G_{mb}) and theoretical maximum specific gravity (G_{mm}) tests to compute air voids. Based on the required air voids, the control mix (0% carbon char) was found to have 6.1% asphalt binder. Asphalt content was 6.7% in mixtures with 5% and 10% carbon char.

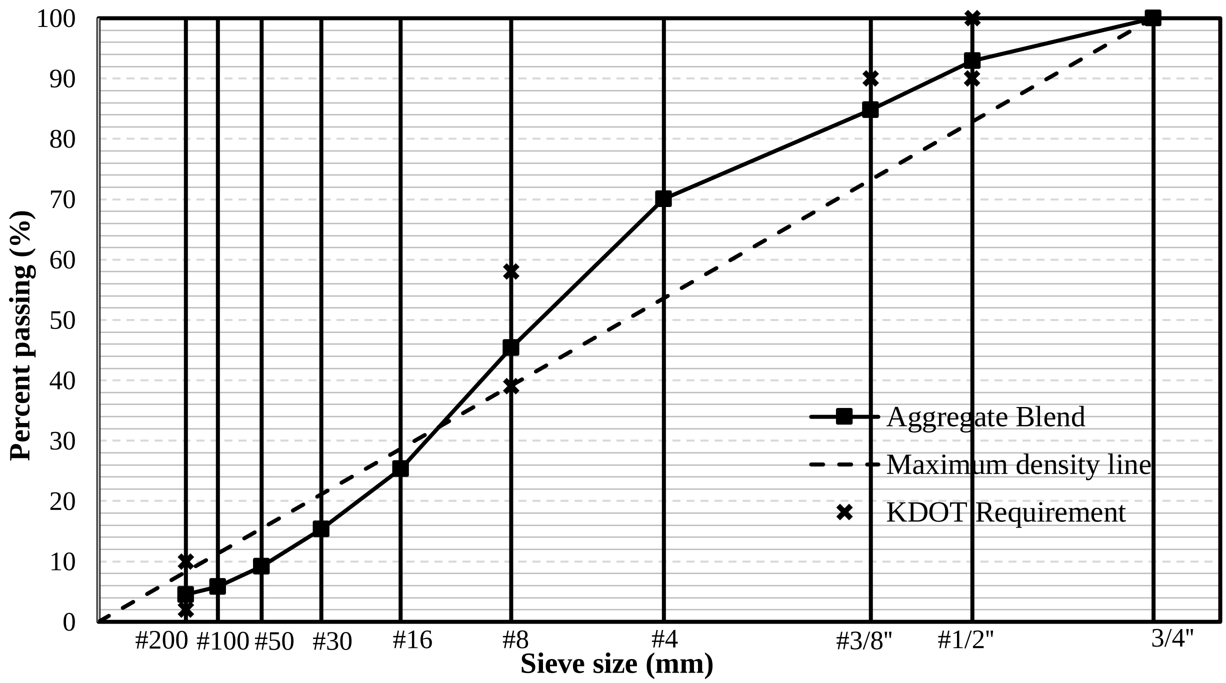

Figure 2.4. 0.45 Power Chart for Blended Aggregates

Table 2.4. Percentages of Aggregates, Gradation of Blend, and KDOT Requirements

Aggregate Type	% in Mix	% Retained								
		1/2	3/8	#4	#8	#16	#30	#50	#100	#200
CS-1	18	6	13	17	18	18	18	18	18	17.8
CS-2A	24			1	12	19	21	22	23	23.0
CS-2	8			2	4	5	6	6	6	6.4
SSG	27			0	7	16	22	25	26	26.7
SSG-1	8		1	6	8	8	8	8	8	7.9
RAP	15	1	2	4	7	9	11	12	13	13.6
Design Single Point		7	15	30	55	75	85	91	94	95.5
SR-12.5A Master Limits		0-10	10 Min.		42-61					90-98

2.4.4.1 Scanning Electron Microscopy for Compact Mixture

After determining the mix design, an SEM test was done on the compact mixtures. This test was conducted on the cutoff surfaces of the compact mix without carbon char and the one with the highest carbon char content, 10%, for easy observation due to the significant difference in carbon char content. Figure 2.5 shows the SEM images of compacted mixtures with 300. 2,000, and 4,000 magnifications. The red square areas in lower magnification images were enlarged in the following pictures for a more specific observation. From the photos, it is hard to distinguish the existence of carbon char since the color of carbon char is black and the same as an asphalt binder. The cutoff surface of the mixture with a higher percentage of carbon char is rougher and has more round particles. However, a convincing conclusion that using carbon char would affect the volumetric property of the HMA mixture is not able to sum up.

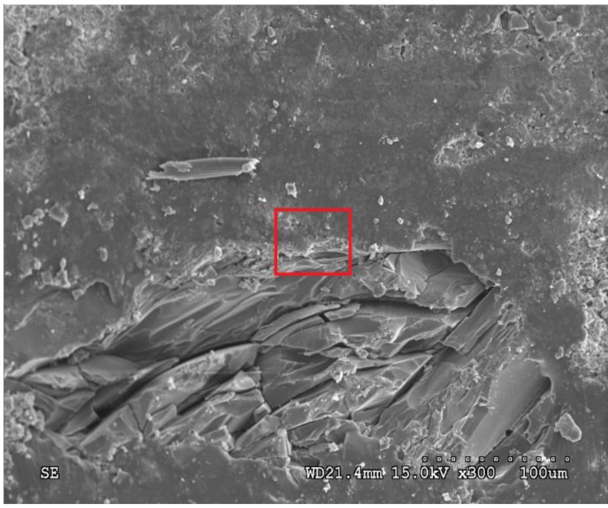

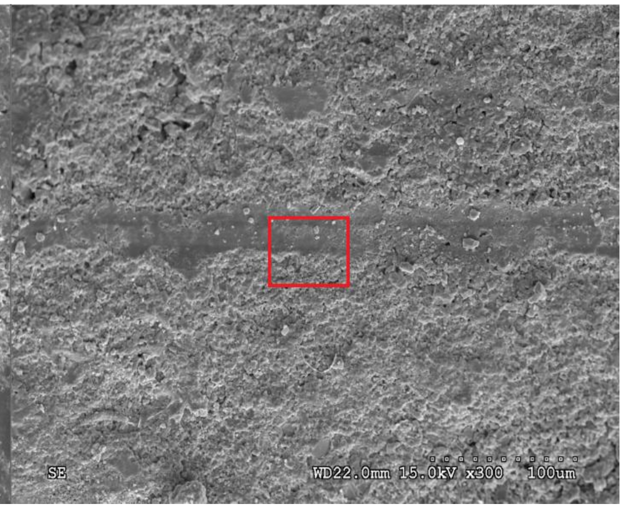

(a) 0% Carbon Char in 300 Magnification (b) 10% Carbon Char in 300 Magnification

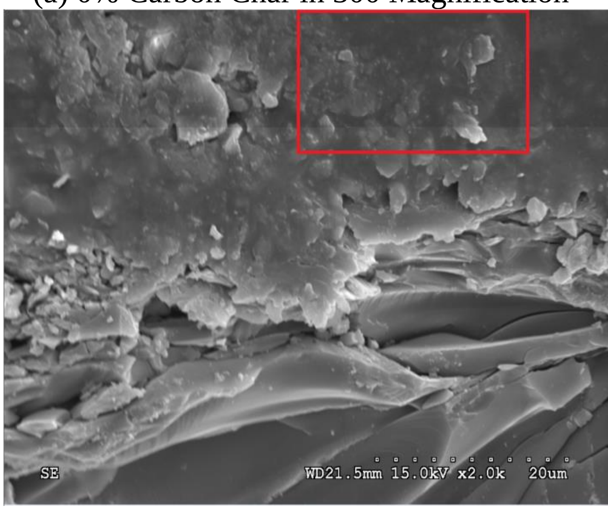

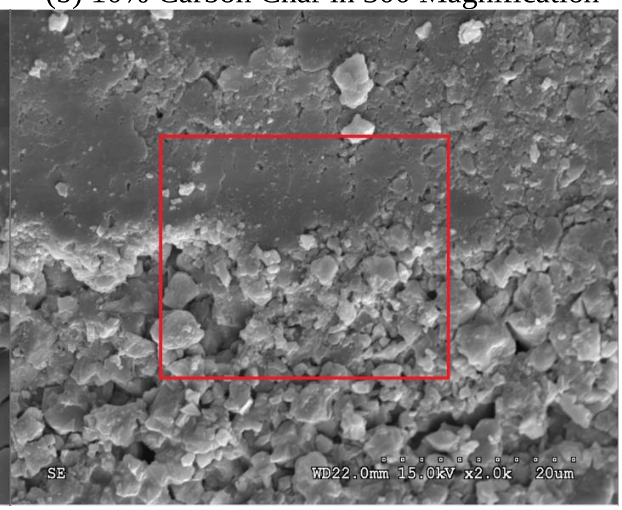

(c) 0% Carbon Char in 2000 Magnification (d) 10% Carbon Char in 2000 Magnification

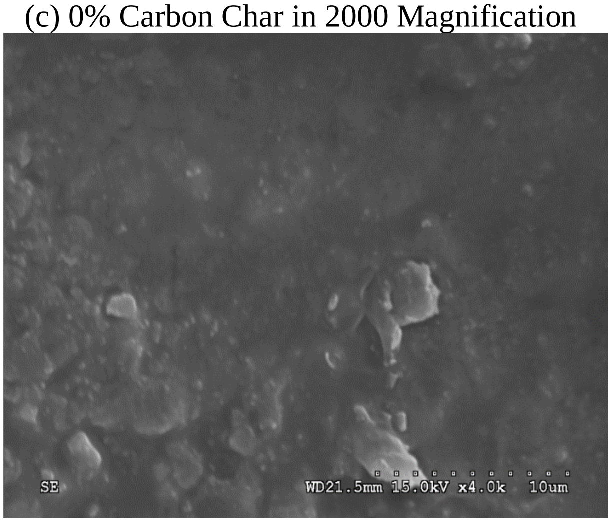

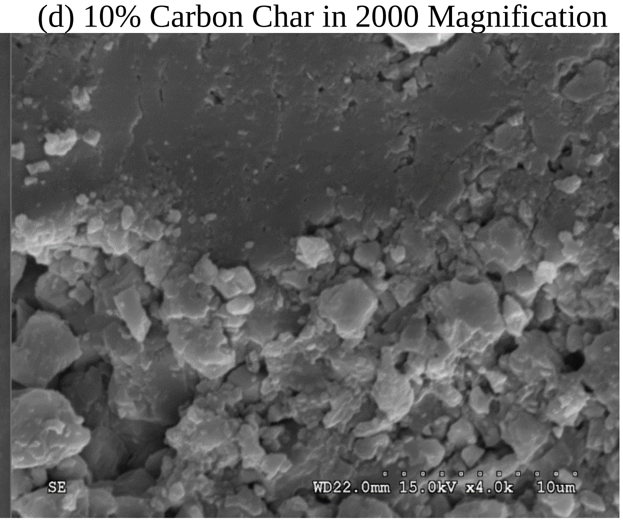

(e) 0% Carbon Char in 4000 Magnification (f) 10% Carbon Char in 4000 Magnification

Figure 2.5. SEM Images for Compact Mixture with 0% and 10% Carbon Char in 300, 2000, and 4000 Magnifications

2.5 Experimental Work

2.5.1 Modified Lottman (KT-56) Test

The modified Lottman test evaluates the moisture susceptibility or stripping potential of HMA mixtures. This study followed the KDOT test method KT-56, Resistance of Compacted Asphalt Mixture to Moisture-induced Damage (KDOT 2022). This moisture susceptibility test required six samples with 150 mm diameter, 95±5 mm height, and 7±0.5% air voids. The samples were sorted into two subsets of three specimens each by getting approximately equal average air voids. One subset was taken as a control or unconditioned group tested when dry. The other subset was conditioned through a freeze-thaw cycle. The conditioned samples were first vacuum-saturated until the volume of water was between 70% and 80% of the air volume. After saturation, the specimens were frozen at -18±3 °C for at least 16 hours. Then, the specimens were placed in a hot water bath with a temperature of 60±1 °C for 24±1 hours, followed by immersion in a 25±0.5 °C water tank for 2 hours ± 10 minutes. Finally, the indirect tensile strength (ITS) test (Figure 2.6) was conducted on conditioned and unconditioned samples with a loading speed of 50 mm per minute until failure. The peak loads were recorded to calculate ITS by using Equation 2.1.

$$ITS = \frac{2000 \times P}{\pi \times t \times D} \qquad \text{Equation 2.1}$$

Where,

ITS = indirect tensile strength (kPa);

P = maximum load (N);

t = specimen thickness (mm); and

D = specimen diameter.

Then, the tensile strength ratio (TSR) was calculated using Equation 2.2.

$$TSR = \frac{ITS_C}{ITS_{UC}} \qquad \text{Equation 2.2}$$

Where,

TSR = tensile strength ratio;

ITS_c = average indirect tensile strength of conditioned subset; and

ITS_{uc} = average indirect tensile strength of unconditioned subset.

Figure 2.6. Indirect Tensile Strength Test Setup

2.5.2 Hamburg Wheel Tracking Device (HWTD) Test

The HWDT is one of the most common tests for evaluating the effects of rutting and moisture damage. The HWDT simulates the wheel load by rolling a pair of steel wheels back and forth over the surface of HMA specimens submerged in hot water at 50˚C. The test procedure followed is the Tex-242-F test method of the Texas Department of Transportation (TxDOT)

(TxDOT 2014). Test specimens were compacted to 7±1% air voids with 150 mm diameter and 62±2 mm height. A set of tests required four specimens with three replicates; therefore, 12 specimens were prepared for each mixture. The edges of test specimens were trimmed according to the fabricated molds to form the test specimen configuration (Figure 2.7). Before the test, the number of maximum wheel passes, and the maximum rut depth must be input into the operational software. The test criteria of the Tex-242-F test method are summarized in Table 2.5.

Table 2.5. Hamburg Wheel Tracking Test Criteria

Binder Grade	Number of Wheel Passes	Maximum Rut Depth (mm)
PG 64-22	10,000	12.5
PG 70-22	15,000	12.5
PG 76-22	20,000	12.5

Figure 2.7. HWTD Setup

For this study, 40,000-wheel passes and a 20-mm maximum rut depth were set as the failure criteria. The test started once the water temperature reached 50℃. An LVDT measured the rut depth of every 100-wheel pass at 11 points along the wheel path. The test automatically stopped when either the desired number of wheel passes was reached or the maximum rut depth was reached, and the number of passes to failure and rut depth was recorded at the end of the test.

2.6 Results and Discussion

2.6.1 Modified Lottman (KT-56) Test Results

The KT-56 test results for all mixtures are listed in Table 2.6. As shown in Table 2.6, all mixtures met the KDOT criterion of a minimum 80% TSR. Thus, all mixtures exhibited good moisture susceptibility. Mixtures containing 10% carbon char had the highest TSR, which indicated that adding 10% carbon char can improve moisture resistance to a limited extent. Even though the conditioned and unconditioned tensile strength of the 10% carbon char mixture is not the highest, the better performance after the condition process results in a higher TSR. Based on the average tensile strength of conditioned and unconditioned samples as a function of carbon char content, the highest tensile strength was observed for the control mix (0% carbon char). The average tensile strength of unconditioned samples decreased when the carbon char content increased. The average tensile strength of conditioned samples decreased when adding 5% carbon char, but tensile strength recovered when adding the carbon char to 10%.

Table 2.6. Modified Lottman Test Results

Carbon Char Content		Air Voids (%)	Tensile Strength (kPa)	Avg. (kPa)	TSR (%)
0%	Conditioned	7.1	320	275	86.6
		7.0	243		
		6.8	262		
	Unconditioned	6.9	274	318	
		6.7	300		
		7.2	379		
5%	Conditioned	7.2	220	237	82.0
		7.0	287		
		7.0	205		
	Unconditioned	7.1	215	290	
		7.0	276		
		6.9	378		
10%	Conditioned	7.0	228	262	92.7
		7.0	193		
		7.0	364		
	Unconditioned	7.0	242	282	
		7.0	251		
		7.0	353		

2.6.2 HWTD Test Results

The HWTD test results are shown in Table 2.7. All the mixtures with carbon char failed to pass the HWTD test. The control mix (0% carbon char) failed with a 20-mm rut depth at 9,849 passes. The 5% and 10% carbon char mixtures failed at 6,717 and 6,979 passes, respectively. Therefore, adding carbon char in an HMA mixture would reduce the rutting resistance.

Table 2.7. HWTD Test Results

Carbon Char Content	Left Wheel		Right Wheel		Average		Average No. of Passes
	No. of Passes	Rut Depth (mm)	No. of Passes	Rut Depth (mm)	No. of Passes.	Rut Depth (mm)	
	12,147	20.02	10,163	20.00	11,155	20.01	
0%	10,153	20.29	6,931	20.01	8,542	20.15	9,849
	-*	-	-	-	-	-	
	6,820	20.07	5,794	20.00	6,307	20.04	
5%	5,212	20.02	6,920	20.02	6,066	20.02	6,717
	8,733	20.40	6,001	20.02	7,367	20.21	
	7,896	20.10	8,104	20.01	8,000	20.06	
10%	5,886	20.08	6,030	20.01	5,958	20.05	6,979
	-*	-	-	-	-	-	

* Data missing due to unexpected equipment problems during the test

To further evaluate mixture performance, the post-compaction consolidation, the creep slope, the stripping slope, and the stripping inflection point can be obtained by plotting a curve between rut depth and the number of wheel passes, as shown in Figure 2.8. The deformation at 1,000-wheel passes is called post-compaction consolidation. The wheel is assumed to densify the mixture within the first 1,000-wheel passes (Yildirim et al., 2007). The creep slope is the inverse of the deformation rate with the curve's linear region from post-compaction to stripping (if it occurs). It is the number of wheel passes required to create 1 mm of rut depth. A steep slope is related to rutting susceptibility (Yildirim et al., 2007). The stripping slope is the inverse of the deformation rate with the linear region of the deformation curve after stripping starts, and it is the number of wheel passes creating 1 mm of rut depth after the stripping reflection point. Stripping slope is related to moisture damage (Yildirim et al., 2007). The stripping reflection point is the number of wheel passes at the creep and stripping slope interaction points. Generally, a high creep slope, stripping reflection point, and stripping slope indicate lower moisture susceptibility (Yildirim et al., 2007).

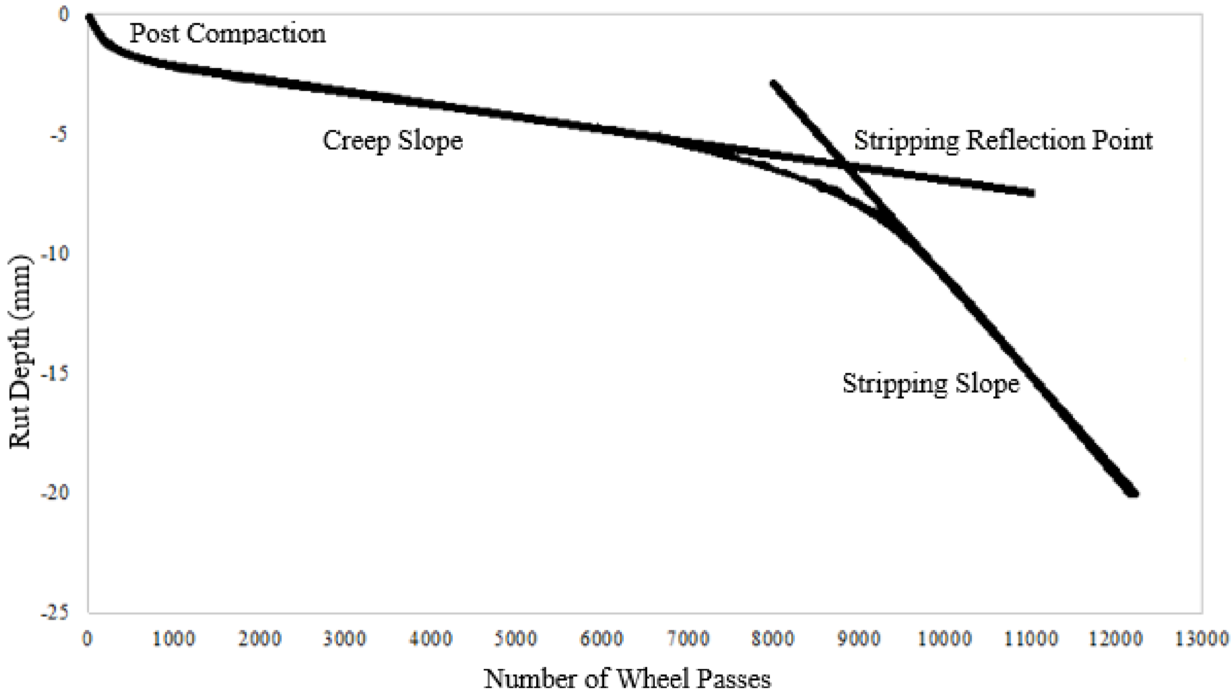

Figure 2.8. Typical HWTD Outputs

Table 2.8 shows the test results of the creep slope, stripping reflection point, and stripping slope of mixtures with various carbon char content. The highest creep slope, stripping slope, and stripping inflection point were observed for the mixture without carbon char. The number of wheel passes at failure was also the highest for this mix. Therefore, the mix without carbon char is more resistant to rutting and moisture damage. However, the creep slope, stripping slope, and stripping inflection point of the mix with 10% carbon char is higher than the mixture with 5% carbon char.

Table 2.8. HWTD Test Output Parameters

Carbon Char Content	Creep Slope	Stripping Reflection Point	Stripping Slope
0%	5,671	6,151	832
5%	1,867	2,948	301
10%	2,415	3,988	774

2.6.3 Design and Evaluation of HMA Mixtures with 3% Air Voids

To further evaluate the effects of carbon char on HMA mixtures, mixtures with 3% air voids were designed and tested. The same 12.5-mm NMAS mix design for mixtures with 4% air voids was used to achieve 3% air voids by adding more asphalt binder. The carbon char was mixed with a PG 58-28 binder at different percentages (0%, 5%, and 10%).

A Hamburg wheel tracking device (HWTD) test was conducted on these new mixtures with 3% air voids. The test results are shown in Table 2.8. All the mixtures failed to pass the HWTD test criteria. The control mix (0% carbon char) failed with a 20-mm rut depth at 3,584 passes. The 5% and 10% carbon char mixtures failed at 3,733 and 4,263 passes, respectively. The average number of passes increased as the carbon char content increased. Adding carbon char to the HMA mixture slightly increases the rutting resistance. However, the overall number of passed dropped significantly compared with the HWTD test results of 4% air voids mixtures. Thus, the mixtures with 3% air voids are less rutting resistant than the mixtures with 4% air voids.

Table 2.9. HWTD Test Results for 3% Air Voids Mixtures

Carbon Char Content (%)	Left Wheel		Right Wheel		Average		Average No. of Passes
	No. of Passes	Rut Depth (mm)	No. of Passes	Rut Depth (mm)	No. of Passes.	Rut Depth (mm)	
0	3,639	-20.05	3,519	-20.22	3,579	-20.14	3,584
	2,762	-20.01	4,256	-20.07	3,509	-20.04	
	3,350	-20.03	3,976	-20.04	3,663	-20.04	
5	3,261	-20.02	3,669	-20.02	3,465	-20.02	3,733
	3,222	-20.05	3,344	-20.05	3,283	-20.05	
	5,104	-20.04	3,800	-19.24	4,452	-19.64	
10	3,900	-20.05	4,406	-20.02	4,153	-20.04	4,263
	3,466	-20.05	3,600	-20.09	3,533	-20.07	
	6,134	-20.42	4,072	-20.02	5,103	-20.22	

Table 2.10 shows the creep slope, stripping reflection point, and stripping slope of mixtures with various carbon char contents. The lowest creep slope, stripping slope, and stripping inflection point were observed for the mixture without carbon char. The creep slope, stripping slope, and stripping inflection point of the mixtures increased as the carbon char content increased. The mix with 3% air voids became more moisture resistant when more carbon char was added. However, the values of creep slope, stripping slope, and stripping inflection point with 3% air voids were much lower than those for mixtures with 4% air voids. Therefore, mixtures with 3% air voids were more moisture-susceptible than mixtures with 4% air voids.

Table 2.10. HWTD Test Output Parameters

Carbon Char Content (%)	Creep Slope	Stripping Reflection Point	Stripping Slope
0	369	1,890	159
5	422	1,962	174
10	514	2,456	247

2.6.4 Statistical Analysis

Statistical Analysis System (SAS)® software was used to perform statistical analysis. The GLMMIX procedure in SAS was used to fit the models of the tests. This approach combines the characteristics of several models with the ability to account for both fixed and random effects, any distributions of the response variable (SAS Institute Inc., 2018). The least squares means (LS-means) were also calculated to compare levels of categorical variables. Least squares are predictions or averages from a linear model commonly used to summarize factor effects (Lenth, 2016).

2.6.4.1 Modified Lottman (KT-56) Test

The experimental design for the Modified Lottman test was a two-way factorial treatment structure, where two treatment factors were (i) carbon char content at three levels - 0%, 5%, and 10%; (ii) conditioning with two levels - conditioned and unconditioned. The strength differences among mixtures with various carbon char contents were analyzed in a linear model:

$$\mathbf{y}_{ijk} = \boldsymbol{\mu} + \boldsymbol{\alpha}_i + \boldsymbol{\beta}_j + (\boldsymbol{\alpha\beta})_{ij} + \boldsymbol{\varepsilon}_{ijk} \qquad \text{Equation 2.3}$$

Where,

y is the response variable (ITS);

μ is the intercept;

α_i is the effect of i^{th} level of carbon char content; i = 1, 2, 3;

β_j is the effect of j^{th} level of conditioning state, j = 1, 2;

$(\alpha\beta)_{ij}$ is the interaction between i^{th} carbon char content and j^{th} conditioning state, and

ε_{ijk} is the response error for the k^{th} sample from the i^{th} carbon char content and j^{th} conditioning state, assumed to be normally distributed with mean 0 and variance σ^2.

The Type III test results are shown in Table 2.11. Type III tests provide insight into the significance of each factor and interaction in the model, considering the effects of all other factors and interactions. When interpreting the Type III results, the highest-order interactions are considered first, then moved to the lower-order interactions before considering the main factors. Because interactions can reveal complex relationships and ensure the potential interactions that could influence the main factors are accounted for. All the p-values in Table 2.11 are larger than 0.05, indicating that there is no significant interaction between carbon char content and conditioning, and none of the effects, carbon char content, and conditioning are statistically significant. This implies that, in the presence of the other variables in the model, these effects do not significantly influence the tensile strength.

Table 2.11. Type III Tests of Tensile Strength

Effect	Num DF	Den DF	F value	Pr > F
Carbon Char Content	2	12	0.42	0.6644
Conditioning	1	12	1.58	0.2327
Carbon Char Content * Conditioning	2	12	0.09	0.9109

The LS-means results are shown in Table 2.12 and Table 2.13.

Table 2.12. Differences of LS-Means for Multiple Comparisons of Tensile Strength

Carbon Char Content (%)	Carbon Char Content (%)	Estimate	Standard Error	DF	t value	Pr > |t|
0	5	33.12	37.43	12	0.88	0.3937
0	10	24.73	37.43	12	0.66	0.5212
5	10	-8.38	37.43	12	-0.22	0.8265

Table 2.13. T Grouping for Carbon Char Content LS-Means of Tensile Strength (α = 0.05)

Carbon Char Content (%)	Estimate	
0	296.50	A
		A
10	271.77	A
		A
5	263.38	A

*LS-means with the same letter are not significantly different.

Table 2.12 shows the pairwise comparisons of the LS-means of tensile strength for various carbon char levels. The p-values in Table 2.12 are all larger than 0.05, showing no significant difference between the LS-means of tensile strengths derived from two different carbon char contents. Adding carbon char will not significantly affect the mixture's tensile strength.

Table 2.13 illustrates the same conclusion. Table 2.13 listed the estimated LS-means of tensile strength at various levels of carbon char content in decreasing order, and all the LS-means share the same letter. This confirms that there is no significant evidence suggesting that the LS-means of tensile strength for different percentages of carbon char differ. Therefore, the tensile strength does not vary significantly across carbon char content.

2.6.4.2 HWTD Test

For the HWTD test, the two mix designs with different design air voids were tested. Therefore, the analysis is performed in two cases. The first case was to study the influence of carbon char content separately with different design air voids, 3%, and 4%. In this case, a one-way treatment experiment was designed to evaluate the effectiveness of carbon char content on rutting resistance (in terms of number of passes to failure in HWTD). The single factor/treatment, carbon char content, had three levels - 0%, 5%, and 10%. A linear model was used to analyze the data:

$$\mathbf{y}_{ij} = \mu + \alpha_i + \varepsilon_{ij} \qquad \text{Equation 2.4}$$

Where,

y is the response variable (no. of passes to failure in HWTD);

μ is the intercept;

α_i is the effect of i^{th} level of carbon char content; i = 1, 2, 3; and

ε_{ij} is the response error for the j^{th} sample from the i^{th} carbon char content, assumed to be normally distributed with mean 0 and variance σ^2.

SAS software was used again to perform the statistical analysis. Table 2.14 to Table 2.16 show the analysis results for mixtures with 4% air voids.

The Type III test results are shown in Table 2.14. The p-value is larger than 0.05, indicating that carbon char content does not significantly influence the number of passes to failure in the HWDT test for mixtures with 4% air voids.

Table 2.14. Type III Tests of Passes Number

Effect	Num DF	Den DF	F value	Pr > F
Carbon Char Content	2	4	4.34	0.0996

The LS-means results are shown in Table 2.15 and Table 2.16.

Table 2.15. Differences of LS-Means for Multiple Comparisons of Passes Number

Carbon Char Content (%)	Carbon Char Content (%)	Estimate	Standard Error	DF	t value	Pr > │t│
0	5	3268.50	1159.82	4	2.82	0.0479
0	10	2869.50	1270.52	4	2.26	0.0868
5	10	-399.00	1159.82	4	-0.34	0.7482

Table 2.16. T Grouping for Carbon Char Content LS-Means of Passes Number (α = 0.05)

Carbon Char Content (%)	Estimate		
0	9848.50		A
			A
10	6979.00	B	A
		B	
5	6580.00	B	

*LS-means with the same letter are not significantly different.

As shown in Table 2.15, the p-value of comparing 0% carbon char to 5% carbon char is smaller than 0.05; the p-value of comparing 0% carbon char to 10% carbon char and comparing

5% carbon char to 10% carbon char is larger than 0.05. These results demonstrate that the LS-means difference of the pass number at failure between the mixture without carbon char and the mixed with 5% carbon char is significant. However, the other comparisons are not significant. Table 2.16 illustrates the same conclusion. Therefore, for the mixtures with 4% air voids, adding 5% of carbon char significantly affects the rutting potential, but increasing the carbon char content to 10% would slightly improve the rutting resistance.

Tables 2.17 to 2.19 show the analysis results for samples with 3% air voids. The Type III test results are shown in Table 2.17. The p-value is larger than 0.05, implying that there is no significant evidence to suggest that carbon char content would affect the number of passes to failure in the HWDT test for the mixture with 3% air voids. The LS-means results are shown in Table 2.18 and Table 2.19.

Table 2.17. Type III Tests of Passes Number

Effect	Num DF	Den DF	F value	Pr > F
Carbon Char Content	2	6	1.12	0.3870

Table 2.18. Differences of LS-Means for Multiple Comparisons of Passes Number

Carbon Char Content (%)	Carbon Char Content (%)	Estimate	Standard Error	DF	t value	Pr > |t|
0	5	-149.67	477.70	6	-0.31	0.7647
0	10	-679.33	477.70	6	-1.42	0.2048
5	10	-529.67	477.70	6	-1.11	0.3100

Table 2.19. T Grouping for Carbon Char Content LS-Means of Passes Number (α = 0.05)

Carbon Char Content (%)	Estimate	
10	4263.00	A
		A
5	3733.33	A
		A

0	3583.67	A

*LS-means with the same letter are not significantly different.

Table 2.18 shows that all the p-values are larger than 0.05, suggesting no significant difference between the LS means of wheel pass number to failure derived from two different carbon char contents. Table 2.19 reveals the same conclusion. Adding carbon char would slightly increase the pass number to failure, but the differences are insignificant. Therefore, adding carbon char will not significantly affect the mixture's rutting potential for the mix with 3% air voids.

The second case of statistical analysis for this HWTD test is to consider carbon char content (with three levels: 0%, 5%, and 10%) and air voids (with two levels: 4% and 3%) as two-way factorial design. The following linear model was used to evaluate the differences in rutting resistance among mixtures with various carbon char content and design air voids:

$$\boldsymbol{y_{ijk} = \mu + \alpha_i + \beta_j + (\alpha\beta)_{ij} + \varepsilon_{ijk}} \qquad \text{Equation 2.5}$$

Where,

y is the response variable (no. of passes to failure in HWTD);

μ is the intercept;

α_i is the effect of i^{th} level of carbon char content; i = 1, 2, 3;

β_j is the effect of j^{th} level of air voids, j = 1, 2;

$(\alpha\beta)_{ij}$ is the interaction between i^{th} carbon char content and j^{th} condition state, and

ε_{ijk} is the response error for the k^{th} sample from the i^{th} carbon char content and j^{th} air voids, assumed to be normally distributed with mean 0 and variance σ^2.

The Type III test results are shown in Table 2.20. The p-value for carbon char content is 0.0556, which is very close to 0.05; the p-values for air voids and the interaction of carbon char content and air voids are smaller than 0.05. These results imply that the effect of carbon char content depends on air voids, and all the factors are statistically significant on pass number to failure.

Table 2.20. Type III Tests of Passes Number

Effect	Num DF	Den DF	F value	Pr > F
Carbon Char Content	2	10	3.91	0.0556
Air Voids	1	10	70.44	<.0001
Carbon Char Content * Air Voids	2	10	5.90	0.0203

The LS-means results of carbon char contents are shown in Tables 2.21 and 2.22.

Table 2.21. Differences of LS-for Multiple Carbon Char Content Comparisons of Passes Number

Carbon Char Content (%)	Carbon Char Content (%)	Estimate	Standard Error	DF	t value	Pr > |t|
0	5	1559.42	564.93	10	2.76	0.0201
0	10	1095.08	595.49	10	1.84	0.0958
5	10	-464.33	564.93	10	-0.82	0.4303

Table 2.22. T Grouping for Carbon Char Content LS-Means of Passes Number (Alpha = 0.05)

Carbon Char Content (%)	Estimate		
0	6716.08		A
			A
10	5621.00	B	A
		B	
5	5156.67	B	

*LS-means with the same letter are not significantly different.

Table 2.21 shows the pairwise comparisons of the LS-means of the wheel pass numbers for various levels of carbon char content. The p-value of comparing 0% and 5% carbon char content is smaller than 0.05, which means a significant difference is shown between the mixtures with 0% and 5% carbon char. The others do not differ significantly from each other. Table 2.22

confirms the same conclusion. The rutting potential will significantly increase by adding 5% carbon char; however, increasing the carbon char content to 10% would slightly improve the rutting resistance.

The LS-means results of air voids are shown in Tables 2.23 and 2.24.

Table 2.23. Differences of LS-Means for Multiple Air Voids Comparisons of Passes Number

Air Voids (%)	Air Voids (%)	Estimate	Standard Error	DF	t value	Pr > │t│
3	4	-3942.50	469.73	10	-8.39	<.0001

Table 2.24. T Grouping for Air Voids Least Squares Means of Passes Number (α = 0.05)

Air Voids (%)	Estimate	
4	7802.50	A
3	3860.00	B

*LS-means with the same letter are not significantly different.

As shown in Table 2.23, the p-value comparing 3% and 4% air voids is smaller than 0.05, which means a significant difference in the LS-means of the number of wheel passes showed up between the mixtures with 3% and 4% air voids. Table 2.24 implies the same conclusion. The rutting potential will significantly decrease when reduced design air voids are used.

2.7 Conclusions

This research aimed to investigate asphalt mixture performance with various carbon char content. Mixtures with 0%, 5%, and 10% carbon char were tested in modified Lottman and HWDT tests. The following conclusions were drawn based on the analysis of the test results:

- Modified Lottman test results illustrated that all mixtures achieved higher TSR than the minimum 80% KDOT requirement. Moisture resistance slightly decreased with 5% carbon char, but TSR increased with 10% carbon char in the HMA.

- The HWDT test results showed that all mixtures failed at 20 mm rut depth. However, based on the number of wheel passes to failure, we can also conclude that the mix without carbon char has a higher rutting resistance than the mixtures with it. HWDT output parameters of creep slope, stripping slope, and denying reflection point also indicate a low moisture resistance of HMA mixtures with 5% carbon char.
- The HWDT test results of 3% air voids mixtures showed that all mixtures failed at 20 mm rut depth. As the carbon char content increased, rutting and moisture resistance slightly improved. However, the mixtures with 3% air voids are less rutting and moisture resistant than those with 4%.
- Statistical analyses confirmed these observations.

Chapter 3 - Evaluation of Coal Combustion Products in Hot-Mix Asphalt Mixture

3.1 Introduction

Coal combustion products (CCPs), or fly ash, are a by-product of coal ignition during electricity generation. Fly ash has been effectively used in Portland cement concrete, embankments, and soil stabilization. However, the applications of fly ash in hot-mix asphalt (HMA) pavements are minimal (Asi et al., 2005; Tapkin, 2008; Bautista 2015; Mistry et al. 2016). According to the American Coal Ash Association (ACAA), only 48% of 129 million tons of CCPs are used in different applications, and the rest (52%) are placed in landfills. Moreover, only 0.13% of CCPs are used as mineral fillers in HMA (Faheem et al. 2017). Recently, the Environmental Protection Agency (EPA) changed the emission requirements of electric power generation, resulting in a large volume of fly ash in many coal-fired power stations that cannot be used as replacements for Portland cement in concrete because of sulfur. Therefore, agencies are investigating different methods of using these by-products beneficially, such as using in asphalt binders.

3.2 Literature Review

In the past decades, many researchers conducted limited investigations of the performance of HMA mixtures with CCPs. In the early stage of the inquiry of fly ash in asphalt, higher stability was noted in HMA with fly ash after immersing in water (Zimmer, 1970; Henning, 1974). In 1982, Rosner et al. studied Class C and Class F fly ash as a mineral filler and anti-stripping agent for asphalt mixture. The moisture susceptibility test was conducted, and the retained strength of the samples with fly ash was higher than any other samples with other filler materials. Tons et al. (1983) used Class F fly ash to replace asphalt cement in various percentages and conducted performance tests on asphalt mixture specimens. They found that moisture damage resistance, rutting resistance, fatigue life, and tensile strength were improved. Bautista (2015) found that using fly ash improved the properties of asphalt mastic more than those with limestone fines as mineral filler. Mistry and Roy (2016) studied the potential use of fly ash through the Marshall mix design. It was discovered that adding up to 4% of fly ash would provide considerable economic savings, better stability, and lesser deformation. Faheem et al. (2017) investigated eight types of CCPs: Class C fly ash, Class F fly ash, and spray dryer absorber (SDA) CCP mixed with three types of asphalt binders. They concluded that CCPs can act as enhancers and extenders to the binder and potentially retarding aging, improving rutting resistance and fatigue life.

Mirković et al. (2019) studied the mixture properties with three types of fly ash different chemical compositions. In their research, the mineral filler was replaced by fly ash with 20%, 50%, 75%, and 100%. All fly ash ash-asphalt mixtures achieved higher stability and lower flow at high temperatures. Compared to the control mix, the indirect tensile strength (IDT) results of asphalt mixtures with different types of fly ash varied significantly due to their different chemical compositions. One of the fly ash mixtures' TSR decreased while the fly ash content increased. The other two mixtures showed an increasing trend as fly ash content increased, indicating moisture resistance improvement. Among these two fly ashes, the one with high lime (CaO) content delivered superior TSR. The rut depth est results for all fly ash mixtures presented acceptable rutting resistance.

3.3 Study Objective

This study evaluated the performance of HMA mixtures with various fly ash content and compared them with a control mixture without fly ash. For evaluation, the Hamburg wheel tracking device (HWTD), modified Lottman, dynamic modulus, and simplified viscoelastic continuum damage (S-VECD) tests were conducted on Superpave HMA mixtures with fly ash.

3.4 Materials

3.4.1 Coal Combustion Products

In this study, local CCPs, as shown in Figure 3.1, were supplied by Kansas City Fly Ash (KCFA) LLC/Eagle Materials from the Kansas City Power & Light (KCP&L) sources. The ash was ASTM Class C fly ash. It was blended with an asphalt binder at various percentages, 5%, 10%, and 15%, by mass of the asphalt binder, as proposed by the Kansas Department of Transportation (KDOT).

Figure 3.1. Fly Ash

3.4.1.1 Scanning Electron Microscopy

The scanning electron microscopy (SEM) test was conducted to explore the microstructure characteristics. Figure 3.2 shows the SEM image of fly ash with 2,000 times magnification. The main elements detected by SEM are shown in Table 3.1. The detected elements include O, Ca, S, and Si.

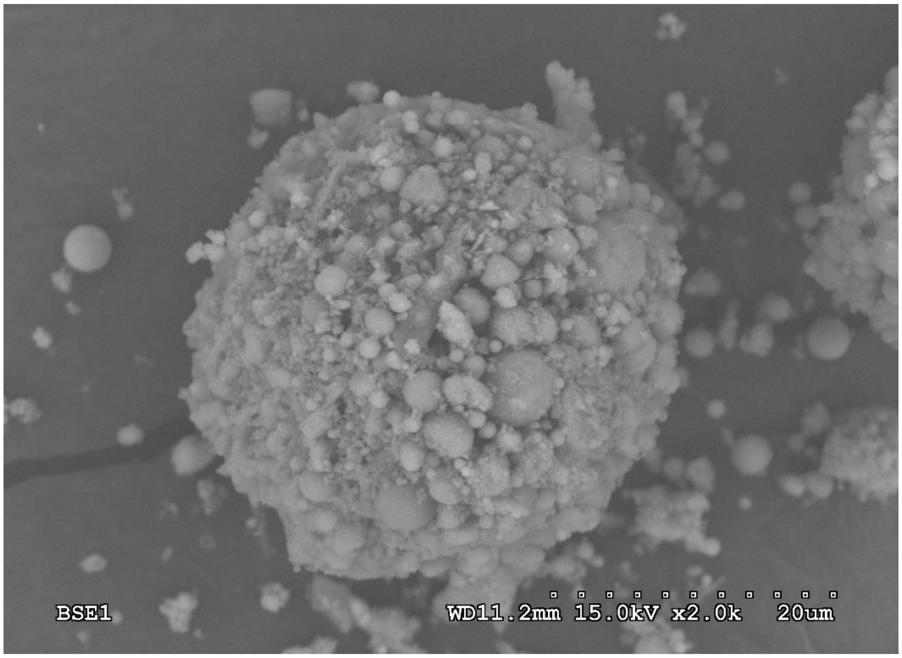

Figure 3.2. SEM Results of Fly Ash

Table 3.1. Main Elements of Fly Ash

Element	Atomic %
O	59.09
Ca	15.04
S	9.24
Si	6.90
Al	4.82
Te	3.19
Mg	1.72
Total	100

3.4.2 Aggregates

In this study, HMA mixtures used five virgin aggregates (CS-1, CS-2A, CS-2, SSG, and SSG-1) and RAP. Virgin aggregates and RAP were collected from Shilling Construction Co. Inc. in Riley County, Kansas. The gradation of each aggregate is shown in Table 3.2.

Table 3.2. Aggregate Gradation

Aggregate Type	% Retained									
	3/4	1/2	3/8	#4	#8	#16	#30	#50	#100	#200
CS-1		36	73	95	99	99	99	99	99	99.0
CS-2A				5	48	78	88	92	94	95.8
CS-2				24	50	62	69	75	78	80.2
SSG					25	60	80	91	98	99.0
SSG-1			7	73	99	99	99	99	99	99.0
RAP		4	10	26	44	60	71	83	88	90.6

3.4.3 Binder Preparation

Fly ash was blended with heated asphalt cement at 5%, 10%, and 15% mass percentages. A PG 58-28 asphalt binder was used in this research for the HMA mixtures. The viscosity of the asphalt binder was 312 cP. A spiral mixer installed on a drill was used to mix the fly ash and binder to obtain a “somewhat” homogeneous binder. After mixing, a rotational viscometer (RV) test was conducted to check the workability of the blended binders. Usually, the RV test for the Superpave PG asphalt binder is conducted at 135°C, and typical viscosity values for the asphalt binder at this temperature are 200 cP to 2000 cP (Pavement Interactive). Based on the test results tabulated in Table 3.3, all blends' viscosity values fall in this range, indicating good workability. However, separation occurred in the binders with 10% and 15% fly ash as time passed. Therefore, fly ash was blended with the binder just before putting into the asphalt mixtures.

Table 3.3. Viscosity Test Results

Fly Ash Content (%)	Viscosity (cP)
0	312
5	330
10	352
15	375

3.4.4 Mix Design

HMA mixtures were developed in the laboratory following KDOT requirements. A 12.5-mm nominal maximum aggregate size (NMAS) mix design was developed in this project. The mixture gradation is shown in Figure 3.3. Table 3.4 shows the gradation of the combined blend and KDOT requirements. Since the percentage of RAP materials used in this study was 20%, a PG 58-28 was needed. All aggregates were heated within the mixing temperature range as the binder was blended. RAP was heated to 60℃. The mixtures were prepared using a mechanical mixer. After mixing, loose mixtures were aged for two hours at the compaction temperature. Then, a Superpave gyratory compactor was used to compact the asphalt mixture with the maximum number of gyrations selected based on design cumulative equivalent single axle loads (ESALs). A target air void of 4% was expected for the compacted cylindrical samples. Two compacted specimens were made for the bulk specific gravity (G_{mb}) test, and 1,500 g of loose mixture was used for the theoretical maximum specific gravity (G_{mm}) test to compute the air voids of compacted specimens. Based on the required air voids, the asphalt binder content of mixtures with 0%, 5%, 10%, and 15% fly ash was 6%, 6.2%, 6.5%, and 6.8%.

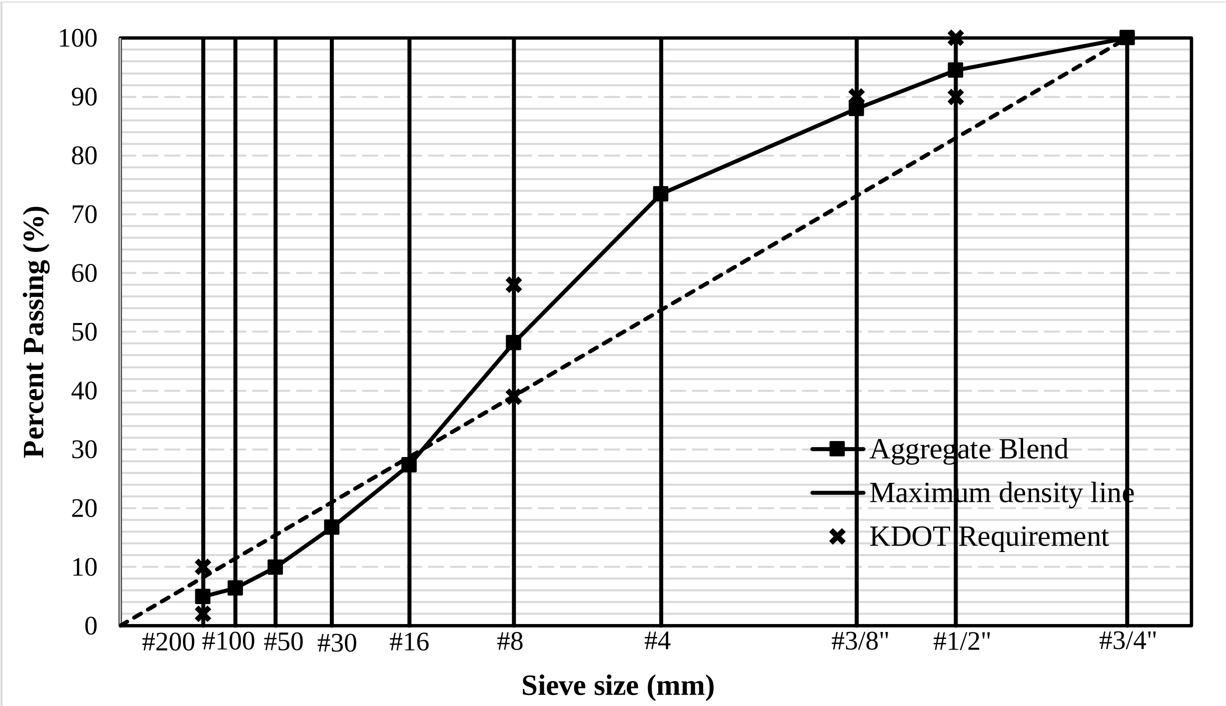

Figure 3.3. 0.45 Power Chart for Blended Aggregates

Table 3.4. Percentages of Aggregates, Gradation of Blend, and KDOT Requirements

Aggregate Type	% in Mix	% Retained									
		3/4	1/2	3/8	#4	#8	#16	#30	#50	#100	#200
CS-1	13		5	10	12	13	13	13	13	13	12.9
CS-2A	24				1	12	19	21	22	23	23.0
CS-2	8				2	4	5	6	6	6	6.4
SSG	27				0	7	16	22	25	27	26.7
SSG-1	8			1	6	8	8	8	8	8	7.9
RAP	20		1	2	5	9	12	14	17	18	18.1
Design Single Point			5	12	27	52	73	83	90	94	95.0
SR-12.5A Master Limits		0-2	0-10	10 Min.		42-61					90-98

3.4.4.1 Scanning Electron Microscopy for Compact Mixture

SEM test was done on compact mixtures. This test was conducted on the sliced surface of the compact mix without fly ash and the one with 15% fly ash. Figure 3.4 shows the SEM images of compacted mixtures with 300, 2000, and 4000 times magnifications. The red square areas in lower magnification images were enlarged in the following pictures for a more specific observation, except the x2,000 figure without fly ash. The photos show a rougher surface on the compacted mixture's sliced surface with 15% fly ash.

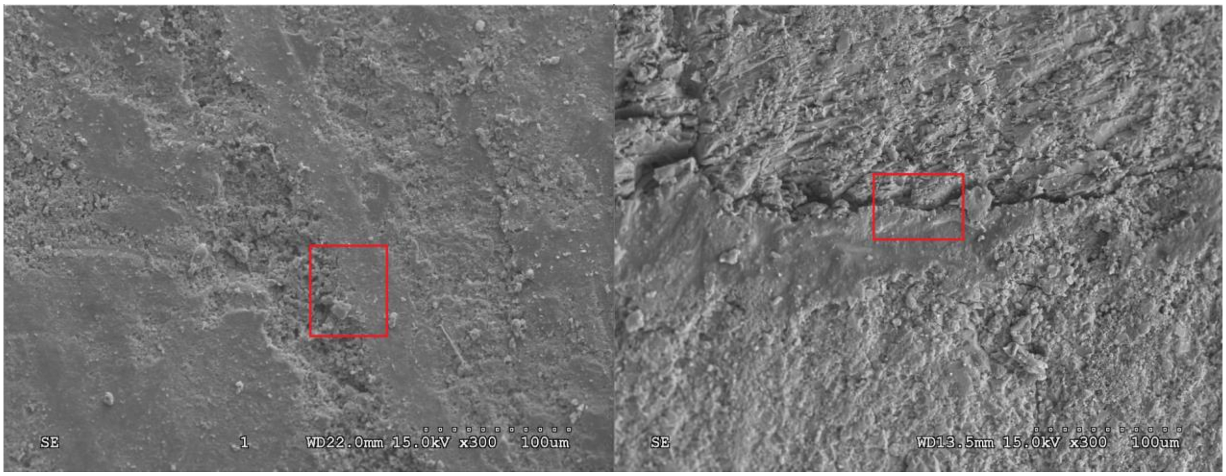

(a) 0% Fly Ash in 300 Magnification (b) 10% Fly Ash in 300 Magnification

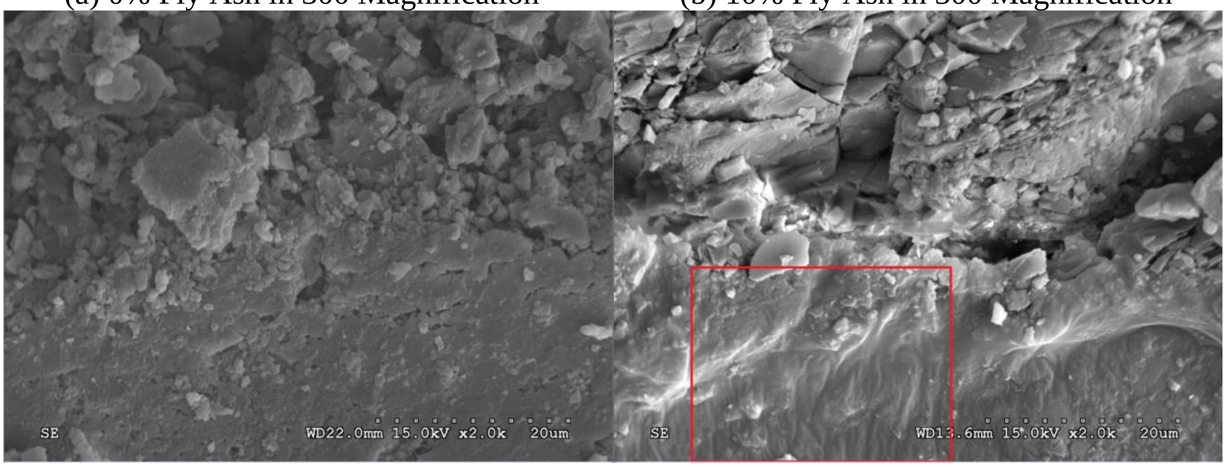

(c) 0% Fly Ash in 2000 Magnification (d) 10% Fly Ash in 2000 Magnification

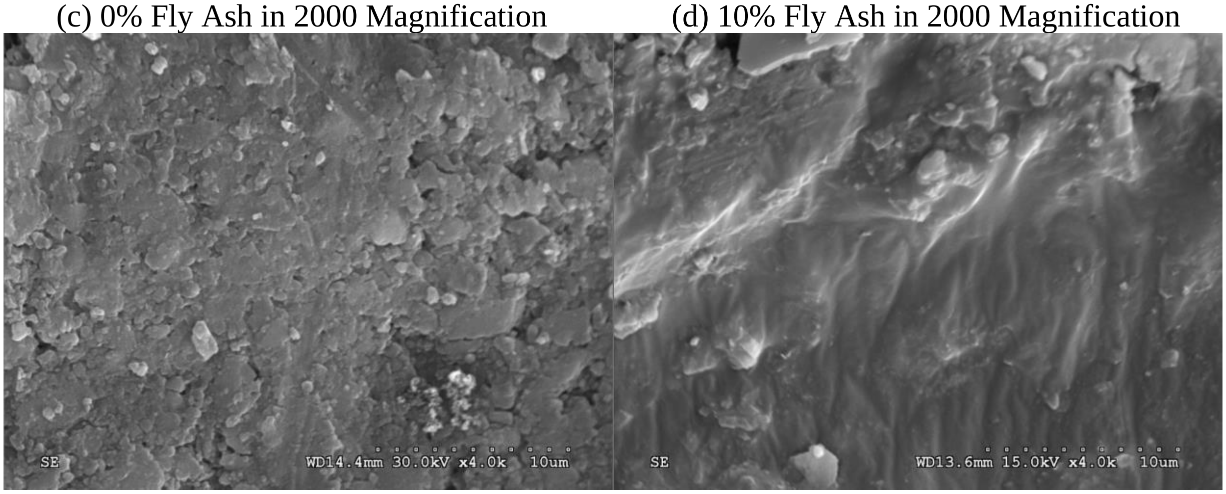

(e) 0% Fly Ash in 4000 Magnification (f) 10% Fly Ash in 4000 Magnification

Figure 3.4. SEM Images for Compact Mixture with 0% and 10% Carbon Char in 300, 2000, and 4000 Magnifications

3.5 Experimental Work

3.5.1 HWTD Test

The HWTD is now an accepted test for evaluating the effects of rutting and moisture damage. The details of the sample preparation and test setup were stated in the previous chapter (Section 2.5.2).

2.5.2 Modified Lottman Test

The modified Lottman test evaluates the moisture susceptibility or stripping potential of HMA mixtures. The details are described in Section 2.5.1.

2.5.3 Dynamic Modulus Test

Dynamic modulus is a fundamental property of HMA mixtures. It defines the viscoelastic nature of HMA mixtures and describes the stiffness over a wide range of temperatures and loading frequencies (Witczak and Bari 2004). This study performed the dynamic modulus test according to the AASHTO TP 62-07 Standard Method of Test for Determining Dynamic Modulus of Hot Mix Asphalt (2009). Compacted samples with 150 mm diameter and 170 mm height were prepared before coring. For each mixture, three samples were fabricated with 7±0.5% target air voids after coring and trimming to 100 mm diameter and 150 mm height. Six metal studs were glued to the sides of the samples to attach the LVDTs. The tests were conducted at temperatures of 4˚C, 21˚C, and 37˚C, and frequencies of 24, 10, 5, 1, 0.5 and 0.1 Hz in this study. The samples were preconditioned in an environmental chamber before being set up in the Asphalt Mixture Performance Tester (AMPT) machine. After setup, the test started once the test temperature reached, and the AMPT software automatically collected test results.

2.5.4 Simplified Viscoelastic Continuum Damage (S-VECD) Test

The S-VECD test is usually conducted to evaluate the fatigue behavior of HMA mixtures. This study performed the S-VECD tests according to the AASHTO TP 107 standard test method for Determining the Damage Characteristic Curve of Asphalt Mixtures from Direct Tension Cyclic Fatigue Tests (2018). Compacted samples with 150 mm diameter and 180 mm height were fabricated. After coring and trimming the compacted samples to 100 mm diameter and 130±2.5 mm height, samples with air voids of 7±0.5% were adopted for the S-VECD tests. The top and bottom platen and the metal studs for the Linear Variable Differential Transformers (LVDTs) were glued to the samples and cured at least 10 hours before the test. The test specimens were put into an environmental chamber for at least two hours to reach the test temperature of 18 ˚C. After preconditioning, the test specimen was set up in the test machine and quickly tightened to the bottom and top support platen. Once the test temperature was reached, a fingerprint dynamic modulus test at 10 Hz was first performed with a target strain range of 50 to 75 micro-strain. After the fingerprint test, the specimen was left to rest for a minimum of 15 minutes before starting the fatigue test. A peak-to-peak strain of 300 µs (s1) was required on the first sample. The number of cycles to failure (Nf_1) would determine the theme for the second and third test samples, as shown in Table 3.5 (AASHTO TP 107-14 2014). The test stopped when the samples failed, and a sudden drop would appear in the dynamic modulus-phase angle graph. All test outputs are automatically collected and can be exported from the software for analysis.

Table 3.5. On-specimen strain Levels for the Second and Third Specimens

Case	Sample 2	Sample 3
500< Nf_1<1,000	s_1 - 100	s_1 - 150
1,000< Nf_1<5,000	s_1 - 50	s_1 - 100
5,000< Nf_1<20,000	s_1 + 50	s_1 - 50
20,000< Nf_1<100,000	s_1 + 100	s_1 + 50
100,000< Nf_1	s_1 + 150	s_1 + 100

3.6 Results and Discussions

3.6.1 HWTD Test Results

The HWTD test results are shown in Table 3.6. Figure 3.5 shows the test output of a mixture sample with 15% fly ash. All mixtures failed since the maximum rut depth was reached. The control mix (0% fly ash) failed with 12,263 passes at 20-mm rut depth. The 5% and 10% fly ash mixtures failed at 7,520 and 6,941 passes, respectively. The rutting resistance was reduced when the fly ash content increased to 10%. However, the number of passes to failure bounced back to 11,283, close to that for the control mix. Therefore, adding 15% fly ash to an HMA mixture would increase the rutting resistance.

Table 3.6. HWTD Test Results

Fly Ash Content	Asphalt Content	Left Wheel		Right Wheel		Average		Average No. of Passes
		Pass No.	Rut Depth (mm)	Pass No.	Rut Depth (mm)	Pass No.	Rut Depth (mm)	
0%	6.0%	9,682	20.3	7,284	20.01	8,483	20.16	12,263
		10,576	20.05	27,854	20.02	19,215	20.04	
		10,550	20.1	7,634	20.26	9,092	20.18	
5%	6.2%	-	-	-	-	-	-	7,520
		6,562	20.05	6,406	20.11	6,484	20.08	
		10,624	20.10	6,488	20.01	8,556	20.06	
10%	6.5%	4,900	20.05	9,288	20.08	7,094	20.07	6,941
		7,146	20.05	6,428	20.01	6,787	20.03	
		6,922	20.05	6,500	20.1	6,711	20.08	
15%	6.8%	8,930	20.12	10,402	20.04	9,666	20.08	11,283
		13,906	20.23	11,894	20.01	12,900	20.12	
		11,088	20.02	13,192	20.35	12,140	20.19	

*Data missing due to the unexpected machine problems during the test

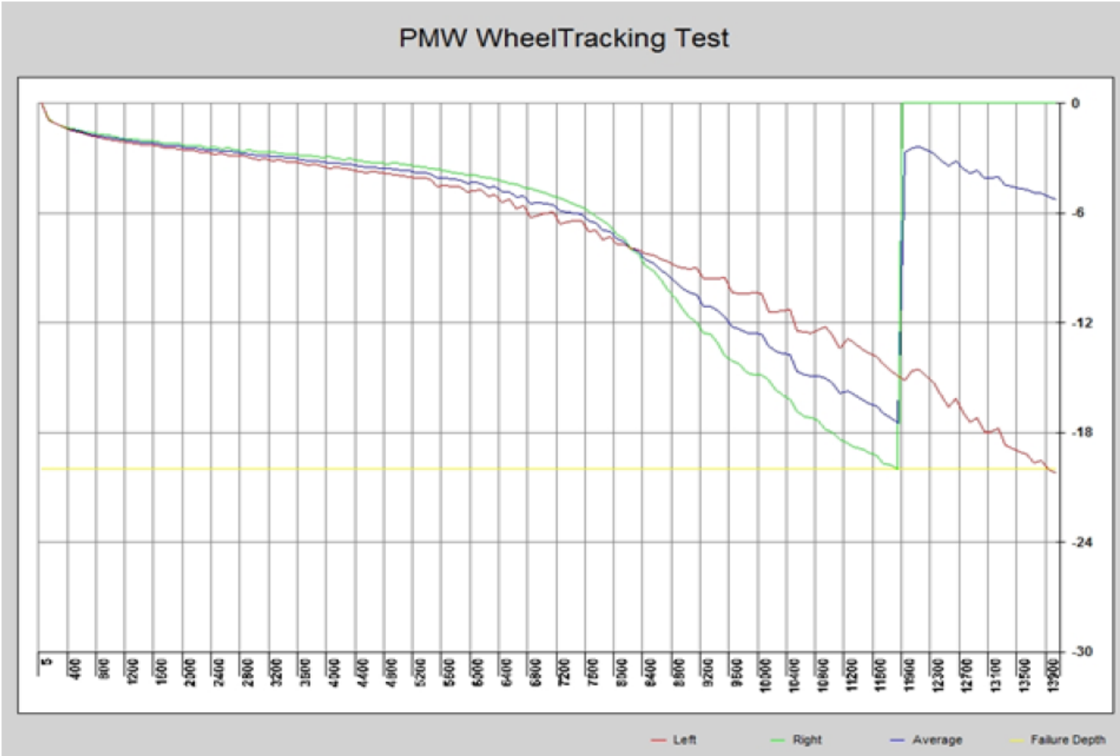

Figure 3.5. HWTD Output of Mixture with 15% Fly Ash

Table 3.7 shows the test results of the creep slope, stripping inflection point, and stripping slope of mixtures with various fly ash contents. The highest wheel pass number at failure, creep slope, stripping slope, and stripping inflection point were observed for the control mix. Therefore, the control mixture without fly ash was more resistant to rutting and moisture damage. The mixture's creep, stripping, and stripping inflection point decreased when adding 5% and 10% fly ash. However, those values increased when the fly ash content reached 15%. The creep slope and stripping slope were almost the same as the control group.

Table 3.7. HWTD Test Output Parameters

Fly Ash Content	Creep Slope	Stripping Reflection Point	Stripping Slope
0%	2,108	7,422	361
5%	1,161	4,193	277
10%	1,125	3,648	221
15%	2,104	6,645	360

Since all mixtures failed in the HWTD test, the best-performing mix (with 15% fly ash) was selected to conduct more performance tests and compare with the control group (without fly ash).

3.6.2 Modified Lottman (KT-56) Test Results

The KT-56 test results for all mixtures are listed in Table 3.8. As shown in Table 3.8, all mixtures met the KDOT criterion of a minimum 80% TSR. Mixtures containing 15% fly ash had the minimum required TSR, which indicated that adding 15% fly ash could maintain moisture resistance. Based on the average tensile strength of conditioned and unconditioned samples as a function of fly ash content, the highest tensile strength was observed for the mixture with 15% fly ash.

Table 3.8. Modified Lottman Test Results

Fly Ash Content		Air Voids (%)	Tensile Strength (kPa)	Avg. (kPa)	TSR (%)
0%	Conditioned	7.1	239	246	80
		6.6	274		
		7.0	226		
	Unconditioned	6.9	305	307	
		6.8	290		
		7.0	328		
15%	Conditioned	6.9	331	261	80
		6.9	233		
		6.9	219		
	Unconditioned	7.0	356	327	
		6.9	317		
		6.9	309		

3.6.3 Dynamic Modulus Test Results

To compare the test results for different mixtures, a master curve, as shown in Figure 3.6, was prepared by shifting different test temperatures to a reference temperature, 18 ˚C, and the test temperature of S-VECD. Based on the master curve, the dynamic modulus of the mixture with 15% of fly ash was slightly higher. A mixture with 15% fly ash is somewhat stiffer and susceptible to fracture cracking than the control mix.

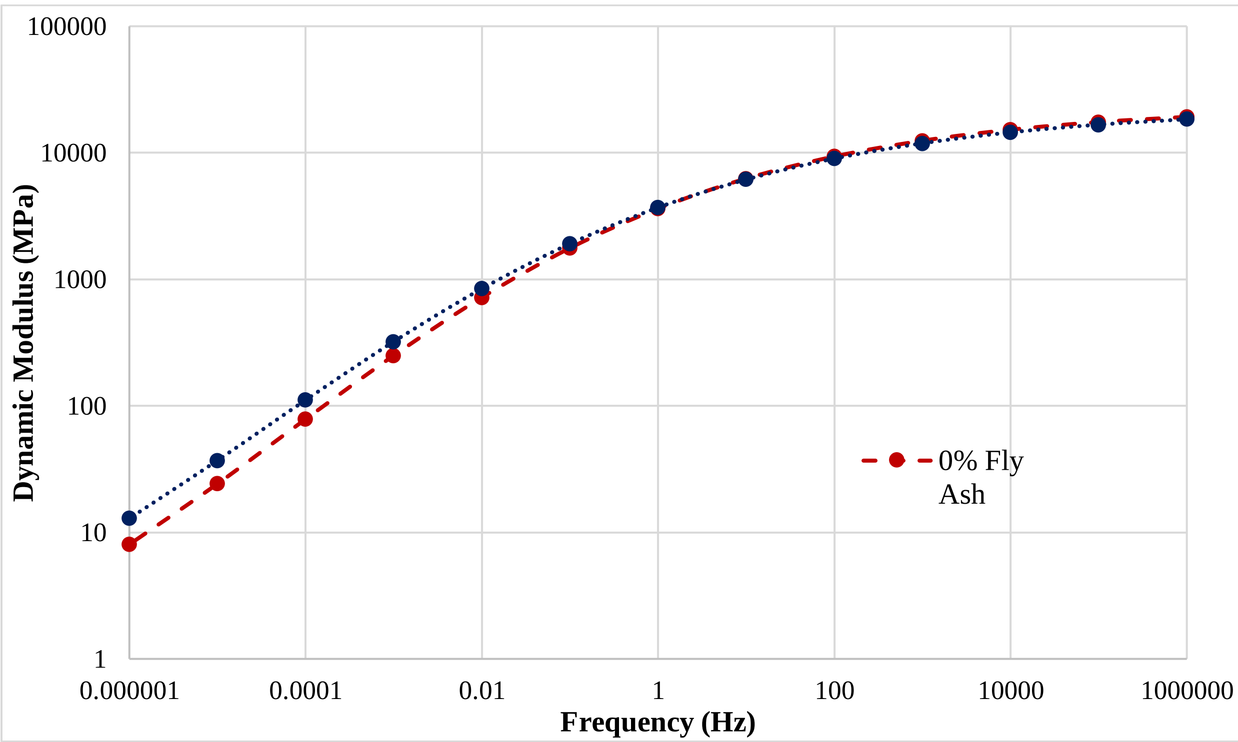

Figure 3.6. Dynamic Modulus Master Curve at 18 ˚C

3.6.4 S-VECD Test Results

A damage characteristic curve (C-S) was developed using the test results to study the mixture resistance of fatigue cracking. The following power model, Equation 3.1, was used to investigate damage parameters for various mixtures:

$$C = 1 - yS^{z} \qquad \text{Equation 3.1}$$

Where:

C = pseudo stiffness at failure;

S = damage internal state variable at failure; and

y, z = fitting coefficients for the power model.

Alpha-Fatigue software was used to obtain the fatigue damage characteristics using results from the S-VECD tests and previously described dynamic modulus tests. The software automatically calculated fitting coefficients y, z, and pseudo strains at failure. The damage Characteristic Curve was developed using the power model above by changing pseudo stiffness (C) from 1 to the value at failure (Tavakol and Hossain 2016). Figure 3.7 illustrates the damage characteristic curves of the control mix and mixture with 15% of fly ash. For a given normalized pseudo stiffness (C), higher damage (S) indicated a better resistance to wear (Xie et al. 2015). In the figure, the C-S curves of the control mix and 15% fly ash mixture were very close, indicating that these two mixtures had similar resistance to damage.

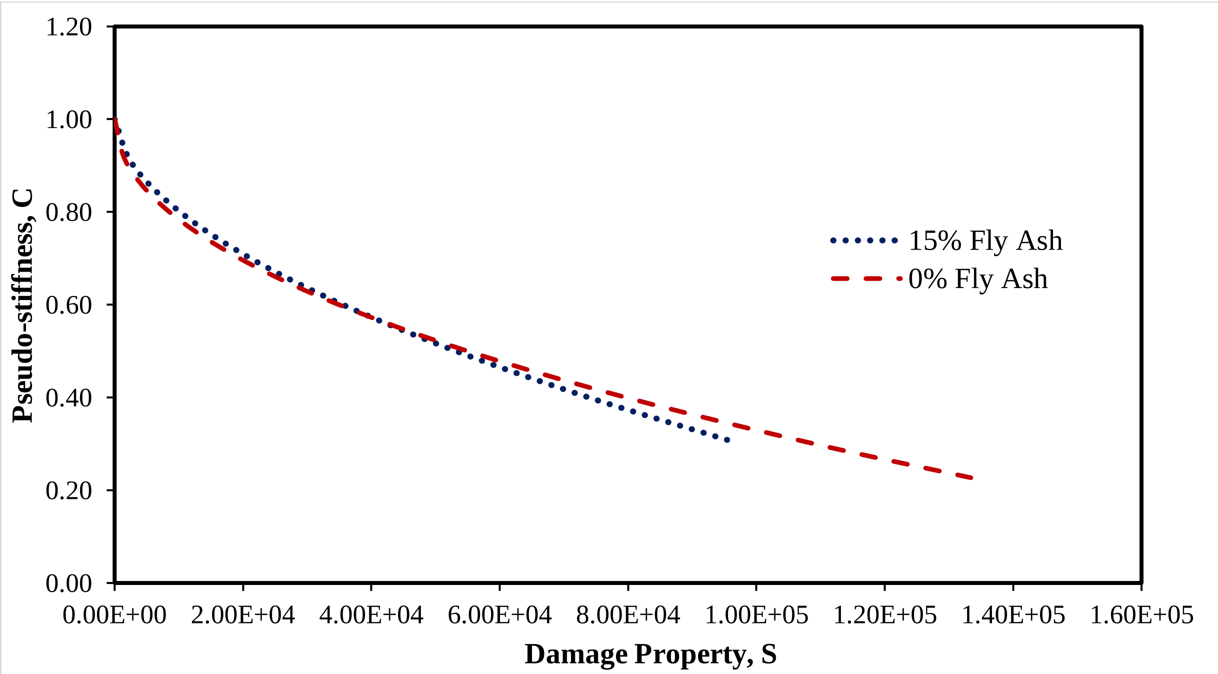

Figure 3.7. Damage Characteristic Curve at 18 ˚C

3.6.5 Statistical Analysis

3.6.5.1 HWTD Test

In this test, a one-way experiment was designed with one treatment: fly ash content including four levels: 0%, 5%, 10%, and 15%. The following linear model was used to investigate the differences in rutting resistance (in terms of number of wheel passes to failure in HWTD) among various mixtures with varying fly ash contents:

$$\mathbf{y}_{ij} = \boldsymbol{\mu} + \boldsymbol{\alpha}_i + \boldsymbol{\varepsilon}_{ij} \qquad \text{Equation 3.2}$$

Where,

y is the response variable (no. of passes to failure in HWTD);

μ is the intercept;

α_i is the effect of i^{th} level of fly ash content; i = 1, 2, 3, 4; and

ε_{ij} is the response error for the j^{th} sample from the i^{th} fly ash content, assumed to be normally distributed with mean 0 and variance σ^2.

The Type III test results are shown in Table 3.9. The p-value is larger than 0.05, demonstrating that fly ash content does not significantly influence the number of wheel passes to failure.

Table 3.9. Type III Tests of Passes Number

Effect	Num DF	Den DF	F value	Pr > F
Fly Ash Content (%)	3	7	1.85	0.2268

Table 3.10. Differences of LS-Means for Multiple Comparisons of Number of Passes

Fly Ash Content (%)	Fly Ash Content (%)	Estimate	Standard Error	DF	t Value	Pr > │t│
0	5	4743.33	3098.04	7	1.53	0.1696
0	10	5399.33	2770.97	7	1.95	0.0924
0	15	694.67	2770.97	7	0.25	0.8092
5	10	656.00	3098.04	7	0.21	0.8383
5	15	-4048.67	3098.04	7	-1.31	0.2326
10	15	-4704.67	2770.97	7	-1.70	0.1333

Table 3.11. T Grouping for Fly Ash Content LS-Means of Passes Number (α = 0.05)

Fly Ash Content (%)	Estimate	
0	12263	A
		A
15	11569	A
		A
5	7520	A
		A
10	6864	A

*LS-means with the same letter are not significantly different.

LS-means results of fly ash contents are shown in Table 3.10 and Table 3.11. All the p-values in Table 3.10 are more significant than 0.05, implying that the difference in pass number between fly ash contents is insignificant. The analysis results in Table 3.11 demonstrate the same conclusion. Therefore, adding fly ash insignificantly affects the rutting potential irrespective of the fly ash quantity. Based on the estimated LS-means values, the mixture with 15% fly ash shows higher pass numbers than other mixtures containing fly ash.

3.6.5.2 Modified Lottman (KT-56) Test

For this text, the experimental design is a two-way, full factorial. There are two treatment factors: (i) fly ash content at two levels**,** 0% and 15%; (ii) condition state with two levels**:** conditioned and unconditioned. A linear model was used to explore the strength differences of mixtures with various fly ash contents, as shown below:

$$\mathbf{y}_{ijk} = \boldsymbol{\mu} + \boldsymbol{\alpha}_i + \boldsymbol{\beta}_j + (\boldsymbol{\alpha\beta})_{ij} + \boldsymbol{\varepsilon}_{ijk} \qquad \text{Equation 3.3}$$

Where,

y is the response variable (ITS);

μ is the intercept;

α_i is the effect of i^{th} level of fly ash content; i = 1, 2;

β_j is the effect of j^{th} level of condition state, j = 1, 2;

$(\alpha\beta)_{ij}$ is the interaction between i^{th} fly ash content and j^{th} condition state, and

ε_{ijk} is the response error for the k^{th} sample from the i^{th} fly ash content and j^{th} condition state, assumed to be normally distributed with mean 0 and variance σ^2.

The Type III test results are shown in Table 3.12. The p-value of the condition is smaller than 0.05, and the p-values of fly ash content and the interaction between fly ash content and condition are more significant than 0.05. This means that the effect of fly ash content does not depend on the conditioning. Only the conditioning is statistically significant, which implies that the conditioning has a considerable influence on the tensile strength. Fly ash content will not significantly influence tensile strength.

Table 3.12. Type III Tests of Tensile Strength

Effect	Num DF	Den DF	F value	Pr > F
Fly Ash Content	1	8	0.66	0.4393
Conditioning	1	8	9.16	0.0164
Fly Ash Content * Conditioning	1	8	0.01	0.9086

Table 3.13. Differences of LS-Means for Multiple Comparisons of Tensile Strength

Fly Ash Content (%)	Fly Ash Content (%)	Estimate	Standard Error	DF	t value	Pr > |t|
0	15	-17.17	21.09	8	-0.81	0.4393

Table 3.14. T Grouping for Carbon Char Content LS-Means of Tensile Strength (Alpha = 0.05)

Fly Ash Content (%)	Estimate	
15	294.17	A
		A
0	277.00	A

*LS-means with the same letter are not significantly different.

The LS-means results are shown in Table 3.13 and Table 3.14. Table 3.13 compares the LS means of tensile strength of the mixtures with 0% and 15% fly ash. The p-value is larger than 0.05, indicating no significant difference between the mixtures containing 0% and 15% fly ash. Adding fly ash will not significantly affect the mixture's tensile strength. Table 3.14 demonstrates the same conclusion.

3.6.5.3 Dynamic Modulus Test

For the Dynamic Modulus test, a three-way experiment was designed to evaluate the differences in viscoelastic properties of the mixtures with varying fly ash content. The three treatment factors were (i) fly ash content at two levels, 0% and 15%; (ii) temperature with three levels: 4 °C, 21 °C and 37 °C; (iii) frequency with three levels: 0.1 Hz, 1 Hz, and 10 Hz. A linear model was used to conduct the statistical analysis:

$$y_{ijkl} = \mu + \alpha_i + \beta_j + (\alpha\beta)_{ij} + \gamma_k + (\alpha\gamma)_{ik} + (\beta\gamma)_{jk} + (\alpha\beta\gamma)_{ijk} + \varepsilon_{ijkl} \quad \text{Equation 3.4}$$

Where,

y is the response variable (ITS);

μ is the intercept;

α_i is the effect of i^{th} level of fly ash content; i = 1, 2;

β_j is the effect of j^{th} level of temperature, j = 1, 2, 3;

γ_k is the effect of k^{th} level of frequency, k = 1, 2, 3;

$(\alpha\beta)_{ij}$, $(\alpha\gamma)_{ik}$, $(\beta\gamma)_{jk}$, $(\alpha\beta\gamma)_{ijk}$ are the interactions between all effects, and

ε_{ijkl} is the response error for the l^{th} sample from the i^{th} fly ash content, j^{th} temperature, and k^{th} frequency, assumed to be normally distributed with mean 0 and variance σ^2.

The Type III test results are shown in Table 3.15. Except for the interaction between fly ash content and frequency and the three-way interaction between all the effects, all the other factors and interactions have p-values smaller than 0.05. These results demonstrate that the interaction of fly ash content, temperature, and frequency is insignificant, suggesting that the third factor will not influence the effect of two other factors. The influence of fly ash content is dependent on temperature but not dependent on frequency. The effect of temperature highly depends on frequency. Fly ash content, temperature, and frequency significantly influence dynamic modulus.

Table 3.15. Type III Tests of Dynamic Modulus

Effect	Num DF	Den DF	F value	Pr > F
Fly Ash Content	1	36	5.83	0.0209
Temperature	2	36	1661.76	<.0001
Fly Ash Content*Temperature	2	36	6.94	0.0028
Frequency	2	36	389.94	<.0001
Fly Ash Content * Frequency	2	36	0.72	0.4915
Temperature * Frequency	4	36	62.26	<.0001
Fly Ash Content * Temperature * Frequency	4	36	1.24	0.3105

Table 3.16. Differences of LS-Means for Multiple Comparisons of Dynamic Modulus

Fly Ash Content (%)	Fly Ash Content (%)	Estimate	Standard Error	DF	t value	Pr > │t│
0	15	-40.86	16.92	36	-2.42	0.0209

Table 3.17. T Grouping for Carbon Char Content LS-Means of Dynamic Modulus (α = 0.05)

Fly Ash Content (%)	Estimate	
15	636.50	A
0	595.64	B

*LS-means with the same letter are not significantly different.

LS-means results are illustrated in Table 3.16 and Table 3.17. Table 3.16 compares the LS means of dynamic modulus of the mixtures with 0% and 15% fly ash. The p-value is less than 0.05, showing that the dynamic modulus for the mixture containing 0% and 15% fly ash differ significantly. Table 3.17 demonstrates the same conclusion. Using fly ash will significantly affect the mixture's dynamic modulus. Therefore, a higher fly ash content will stiffen the mix and make it more susceptible to fracture cracking.

3.6.6 Economic Analysis

All test results in this study showed that asphalt mixture with 15% fly ash performs similarly in rutting, fatigue cracking, and stripping resistance compared to a mix without any fly ash. However, added fly ash results in an increase in virgin binder content when doing the mix design. Therefore, an economic analysis was conducted to check whether using 15% fly ash would be economic.

Since the mix design and the materials used are all identical except for the binder and fly ash content, therefore, the price comparison was done only considering the binder and fly ash parts. Table 3.18 shows the binder content of mixtures with 0% and 15% of fly ash. The price of PG 58-28 binders is about $470 per ton, and the average cost of fly ash is about $60 per ton. The added virgin binder and fly ash cost can be calculated based on these prices.

Let us assume building a one-mile-long 2-lane HMA overlay project which was placed with a thickness of 50 mm. The standard lane width for most roads in Kansas is typically 3.66 meters (12 feet) per lane. The volume of a one-mile-long 2-lane overlay can be calculated which equals 589 m^3. Assuming the air voids of a newly constructed overlay is 8%, the quantity of HMA mixture building a one-mile-long overlay can be calculated with the known G_{mm} of each mixture, and the results are shown in Table 3.18. For the control mix (no fly ash), the cost only includes added virgin binder (as shown in Table 3.12), which is 66 * $470 = $30,856. The price for a mixture with 15% of fly ash is 76 *(1-15%) * $470 + 76 * 15% * $60 = $31,083. Therefore, the cost of building a one-mile-long overlay with mixtures containing 15% fly ash would be $228 more expensive than only using virgin binders.

Table 3.18. Added Binder Price for a One-Mile-Long Overlay

Fly Ash Content (%)	G_{mm}	HMA Quantity (ton)	Total Binder Content (%)	Added Binder Content (%)	Added Binder Mass (ton)	Added Binder Price
0	2.423	1313	6.0	5.0	66	30,856
15	2.421	1312	6.8	5.8	76	31,083

3.7 Conclusions

This research aimed to investigate asphalt mixture performance with various fly ash contents. Mixtures with 0%, 5%, 10%, and 15% fly ash were tested in HWTD, modified Lottman, dynamic modulus, and S-VECD tests to evaluate mixture performance. The following conclusions can be made based on the analysis of the test results:

- The HWTD test results showed that all mixtures failed at 20 mm rut depth. Based on the number of wheel passes to failure, we could conclude that the control mixture without fly ash had the highest rutting resistance. Meanwhile, a mix with 15% fly ash also had a relatively high rutting resistance compared to the 5% and 10% fly ash varieties. HWTD output parameters of creep slope, stripping slope, and stripping inflection point also indicated the same conclusion- the control mix and mixture containing 15% fly ash have relatively high moisture resistance.
- Modified Lottman test results illustrated that the control and 15% fly ash mixtures met the minimum 80% TSR requirement of KDOT
- Dynamic modulus test results indicate that the stiffness of the mixture with 15% fly ash was slightly higher than the control mix at lower frequencies, but the difference was insignificant. Also, these two mixtures showed approximately the same fatigue performance according to the respective S-VECD test results.

All tests indicated that asphalt mastic with fly ash would unlikely enhance pavement performance in terms of rutting, fatigue cracking, and moisture susceptibility resistance. Statistical analyses confirmed these observations.

Chapter 4 - Effects of REOB on Asphalt Binder's Rheological Properties

4.1 Introduction

Re-refined engine oil bottom (REOB) is a non-distillable waste engine oil residue. REOB has been used in the paving industry since the 1980s as a blending agent to soften base binder to improve low-temperature properties (AI, 2016; Arnold and Shastry, 2015; FHWA, 2015; Kaskow et al., 2018; Karki and Zhou, 2018). The current trend of using recycled asphalt pavement (RAP) and recycled asphalt shingles (RAS) in hot-mix asphalt (HMA) mixtures has resuscitated the use of softener in virgin binder (AI, 2016). The use of REOB has recently gained more attention for the sake of sustainability. The Federal Highway Administration (FHWA) has found that approximately 20 percent of 1,000 samples coming from different states in the U.S. contained some amount of REOB (Arnold and Shastry, 2015; FHWA, 2015; Ozer et al., 2016; You et al., 2018). However, some state highway agencies, such as KDOT, are concerned about the potential adverse effect of REOB on binder and pavement performance. Specifically, using REOB as a softening agent to lower the low-performance grade (PG) concerns KDOT, as many low-temperature cracking problems have recently been reported. However, the suppliers do not typically furnish the chemical composition of commercial asphalt cement.

4.2 Literature Review

In recent years, X-ray fluorescence (XRF) devices have been used to identify metallic elements in asphalt cement. Thus, the methods to determine the presence of REOB are essential. XRF technique is commonly used to detect REOB in asphalt binders. In 2015, Arnold and

Shastry (2015) found that XRF to be a qualitative tool to identify the presence of REOB in asphalt binders. REOB contains some metals from engine wear, which were present in the additives in the original oil, such as iron, copper, zinc, calcium, and molybdenum (Arnold and Shastry 2015). XRF can readily determine the presence of these metals. The researchers suggested that calcium, zinc, copper, and molybdenum can be used as markers to show that a binder contains REOB (Arnold and Shastry 2015). Inductively coupled plasma (ICP) is also a powerful tool for detecting and determining the approximate amounts of elements in REOB present in asphalt. In addition, cross-checking by IPC would be a good practice for any large-scale XRF program (Oelofse, 2018).

Some researchers indicated a positive influence of REOB on pavement performance, such as rut resistance, moisture damage resistance, extended fatigue life, and cracking resistance (D'Angelo et al., 2013; Wielinski, 2014; Barborak et al., 2016; You et al., 2018). On the other hand, some others believe that adding REOB to an asphalt binder causes expedited aging, resulting in brittle asphalt binders and premature failure in pavements (Hesp and Shurvell, 2013; Ozer et al., 2016; Barborak et al., 2016; Bennert et al., 2016; Kaskow et al., 2018). A trace amount of residual waste materials in REOB, such as iron, copper, zinc, calcium, and molybdenum, has been blamed for the poor performance. Thus, a better understanding of the effects of REOB on the rheological properties of asphalt binder and pavement performance across all climatic conditions (i.e., low, medium, and high temperature) is essential for making a better-informed decision. In this paper, the effects of REOB on the rheological properties of asphalt binders have been discussed.

4.3 Objective

The primary objective of this study is to investigate the effects of REOB on the rheological properties of asphalt binder. A PG 64-22 asphalt binder and a REOB were blended at different percentages (i.e., 0%, 3%, 6%, 9%, and 12% by mass of the asphalt binder) to produce five different binder samples. Using the dynamic shear rheometer and bending beam rheometer, these blended asphalt binders were evaluated in terms of stiffness and resilience at high, medium, and low-temperature ranges. In addition, the effect of REOB on the aging characteristics of the asphalt binders was investigated at different long-term aging times (i.e., 20 hours vs. 40 hours of pressure aging vessel).

4.4 Materials

This research utilized a PG 64-22 binder (unmodified) and one type of REOB obtained from a binder supplier in Kansas. The PG 64-22 binder, without any REOB, was the control sample. The REOB used in this study was analyzed by an XRF device, and eight elements of metallic wastes, which were molybdenum, zirconium, strontium, lead, zinc, copper, iron, and calcium, were detected, as shown in the second column of Table 4.1. Among these elements, zinc had the highest amount, 5,057 ppm or mg/kg. The zinc, calcium, and iron content were also relatively high at 586.2 ppm and 544.9 ppm. Besides that, 246.7 ppm of molybdenum were also detected. These eight elements totaled 0.67% of the REOB. The rest of the REOB is the remaining engine oil fraction (AI, 2016). Also presented in the table is a typical composition of REOB, according to Shastry (2018). The specific elements include a considerable amount of phosphorus and sulfur (up to 1.9% each). Calcium and zinc have relatively higher contents, followed by phosphorus and sulfur. Iron, copper, and molybdenum are also present at relatively lower ranges. These elements, calcium, zinc, copper, and molybdenum are fingerprints that show the presence of REOB in asphalt binders (Arnold and Shastry, 2015). The total percentage ranges from 4.3 to 6.0% for these elements in the REOB, which is much higher than that of the REOB used in this study. When these REOB constituents are compared to the typical ranges, only iron and zinc fall into the field; molybdenum is slightly lower than the range, and calcium and copper contents are far below the lower range. The most significant difference between the two is that there is no phosphorus and sulfur in the REOB used in this study.

Table 4.1. Element Contents in REOB

Elements	Content in REOB under Study (ppm)	Typical Content in REOB (ppm) (Shastry, 2018)
Phosphorus	-	1.5 – 1.9%
Sulfur	-	1.5 – 1.9%
Calcium	586	7,200 – 10,900
Iron	545	370 – 1,800
Copper	190	700 – 1,500
Zinc	5,057	4,500 – 7,200
Molybdenum	247	300 - 700
Zirconium	9.7	-
Strontium	7.4	-
Lead	67.0	-
Total (%)	0.67	4.3 – 6.0

- means under the detection limit.

The five blended binder samples were short-term and long-term aged using the Rolling Thin-Film Oven (RTFO) and the Pressure Aging Vessel (PAV). Additionally, binder samples were PAV-aged at two different aging times (i.e., 20 hours and 40 hours) at 100° C to evaluate the effect of REOB on aging characteristics. At all aging stages from original to 40-hour PAV aging, the DSR tests were conducted. The BBR test was born on the 20-hour PAV-aged and 40-hour PAV-aged binders. Based on the binder test results, continuous PG grades of the five blended binder samples were determined and shown in Table 4.2. The high-temperature grade of the binder samples decreases as the REOB content increases, which implies a potential reduction in high-temperature performance. The low-temperature phase of the binder samples decreases as well, suggesting an improvement in the low-temperature performance of the binder. The improvement in low-temperature performance is highly desirable. However, the decrease in high-temperature performance grade may not be desirable. If maintaining the high-temperature performance grade at a certain level is demanded, one must consider having a base binder with a higher high-temperature PG grade when working with REOB.

Table 4.2. Continuous Blended Binder Grade

% REOB	0	3	6	9	12
Binder Grade	64-22	65-24	63-24	61-26	58-26

4.5 Experimental Work

4.5.1 XRF

An XRF spectrometer is an X-ray instrument used to detect the inorganic elements in materials and determine quantities of the ingredients detected. The fundamental principle of XRF is the interactions between X-rays with atoms in samples (Wirth, 2018). The sample is illuminated by an X-ray beam with enough energy to interact with the atoms in the sample. Outer electrons displace the electrons in the inner orbital shells of the atoms. During the displacement, energy is released. This energy release is fluorescent radiation, which can be detected and measured by the XRF device. The fluorescent energy detected is unique to each element in the sample (Wirth, 2018; Bruker, 2018).

Arnold and Shastry (2015) found that XRF can be used as a qualitative tool to identify the presence of REOB in asphalt binders. REOB contains some metallic elements from engine wear and the additives in the original oil. Iron, copper, zinc, calcium, and molybdenum (Arnold and Shastry, 2015; Shastry, 2018). XRF can readily determine the presence of these metallic elements.

(a) (b)

Figure 4.1. (a) Test Samples with Different REOB Content and (b) XRF Device

In this research, five blended binder samples were heated to 150 °C, stirred thoroughly, poured into Petri dishes, and cooled to room temperature before the test, as shown in Figure 4.1 (a). Three samples were prepared for each blended binder. The REOB oil was also stirred and poured into three Petri dishes. A handheld X-ray fluorescence analyzer, as shown in Figure 4.1 (b), was used in this study. Before the actual test, a reference sample was tested first to calibrate the XRF device. The analyzer window, located in the front of the device and emits the X-ray onto the sample, was placed right on top of the petri dish containing the sample. Once triggered, the XRF device analyzed the sample for 120 seconds, displaying the results on the screen. Testing was done on three replicate samples. For each sample, three measurements were obtained at three different positions on the sample's surface.

4.5.1 ICP

Figure 4.2 shows the ICP device used in this study. ICP is an analytical technique used for the detection of chemical elements. Two types of ICP are commonly used: inductively coupled plasma mass spectrometry (ICP-MS) and inductively coupled plasma optical emission spectrometry (ICP-OES). ICP-MS comprises two parts: inductively coupled plasma and the mass spectrometer. The plasma is formed in inductively heated argon gas, then the sample is introduced into the plasma, and the elements' atoms in the sample are converted to ions. Then, the irons are transformed into the mass spectrometer and are separated according to their mass-to-charge ratio. A detector receives the ion signals, and the intensity of the signals is directly proportional to the concentration of the elements in the sample (Montaser 1998). ICP-OES combines an ICP with an optical emission spectrometer. The mechanism of ICP-OES is like that of ICP-MS, except the elements' wavelengths are measured. In ICP-OES, the ionization is accompanied by light emission, and the sunlight is introduced into the optical chamber and separated into different wavelengths. Light intensity is measured to analyze every element (Lichte et al. 1987). Compared with ICP-OES, ICP-MS is more precise, sensitive, and faster.

Figure 4.2. Inductively Coupled Plasma Optical Emission Spectrometer

The binder samples must be dissolved into a solution to test the elements in asphalt binder on ICP and AAS instruments. In this study, nitric acid was used in the digestion process. 10mL nitric acid was added into 0.5g asphalt binder and heated to 175℃ for 10 minutes. Then, the dissolved solutions were transformed into falcon tubes, as shown in Figure 4.3, after cooling down.

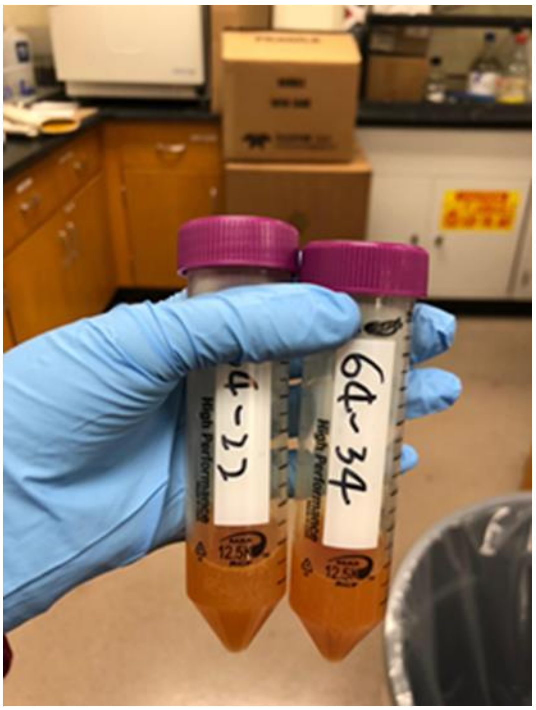

Figure 4.3. Dissolved Solution for ICP and AAS

4.5.3 Dynamic Shear Rheometer (DSR)

Figure 4.4 shows the DSR device used in this study. The DSR determines the viscoelastic behavior of asphalt binders at intermediate and high temperatures. The testing followed AASHTO T 315: Determining the Rheological Properties of Asphalt Binder Using a Dynamic Shear Rheometer (DSR). In this research, frequency sweep and temperature sweep tests were performed for the blended binder samples. The angular frequency applied was from 0.1 rad/s to 100 rad/s. For the temperature sweep, samples were tested at 40°C, 55°C, and 70°C. The DSR tests were performed on unaged, RTFO-aged, 20-hour PAV-aged, and 40-hour PAV-aged blended binder samples. Test samples were prepared using 25 mm diameter and 8 mm diameter silicon molds depending on the test temperatures, i.e., 25 mm diameter samples were tested at 55°C and 70°C. In comparison, 8 mm diameter samples were tested at 40 °C.

Figure 4.4. DSR Device

Table 4.3. Target Strain Values

Target Strain Values (%)		Aging Condition		
		Unaged	RTFO	PAV
Temperature	40 °C	9	8	0.8
	55 °C	12	10	1
	70 °C	12	10	1

Table 4.3 summarizes target shear strain values for different temperatures and aging conditions. Two replicates were tested for each blended binder with varying aging conditions.

Based on the measured shear stress and the applied shear strain, the complex shear modulus (G*) values were calculated as the ratio of max shear stress to max shear strain at different temperatures and angular frequencies. Phase angles were also measured as the phase differences between the shear stress and shear strain waveforms.

4.5.4 Bending Beam Rheometer (BBR)

Figure 4.5 shows the BBR device and test setup used in this study. The BBR test determines the low-temperature stiffness and relaxation properties of asphalt binders. The testing was conducted by AASHTO T 313: Determining the Flexural Creep Stiffness of Asphalt Binder Using the Bending Beam Rheometer (BBR). This research tested the blended binder samples with 20-hour- and 40-hour PAV aging. The test was conducted at two low temperatures, i.e., -6 °C and -18 °C. This temperature range was selected to ensure that critical temperatures would occur within the field. For each blended binder, three replicate samples were tested. Aluminum molds were used to fabricate asphalt beam samples.

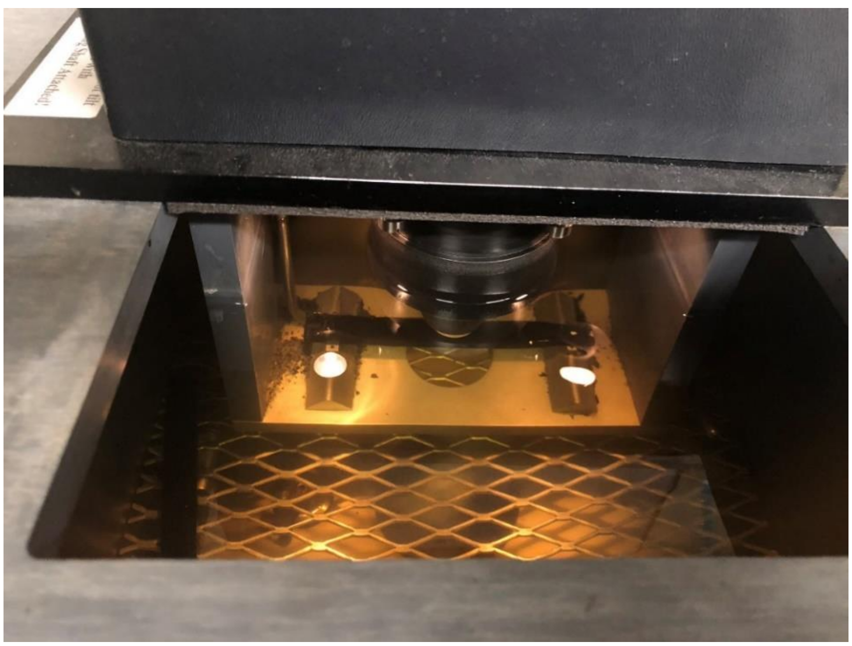

Figure 4.5. BBR Device and Test Set-up

After demolding, the test samples were immediately placed into the bath and conditioned for 60 minutes at the test temperature. After conditioning, the beam was set on the test support, as shown in Figure 4.5. Then, the constant creep loading of 980 mN was applied for 240 seconds, and the stiffness and m-value were recorded. Stiffness and m-values measured at 60 seconds were compared to the specification criteria, i.e., stiffness less than 300 MPa and m-value greater than 0.3.

4.6 Results and Discussions

4.6.1 XRF Test Results

The XRF test results of all detected metallic elements are shown in Table 4.4. For REOB, calcium, copper, zinc, molybdenum, and iron were the five primary elements that were found. As discussed earlier, calcium, copper, zinc, and molybdenum are known to be REOB fingerprint elements among these five elements. Some copper, zinc, and molybdenum were detected in the base binder (i.e., 0%), while calcium was not found. Besides these elements, the base binder contained nickel, uranium, tungsten, vanadium, and potassium, which were not found in REOB. Zirconium and strontium were found both in REOB and base binder. Based on the composition of the elements in REOB and base binder, it was expected that the total content of four fingerprint elements (i.e., calcium, copper, zinc, and molybdenum) would increase as the blend percentage of REOB increased in the blended binder samples. Clearly, copper, zinc, and molybdenum showed the expected increase, but the calcium contents were not detected up to the addition of 12% REOB. Thus, a hand-held XRF spectrometer can detect some of the "signature" elements of REOB.

Table 4.4. XRF Test Results

Elements	Element Content (ppm)					
	REOB	0%	3%	6%	9%	12%
Calcium	586.2	< LOD	< LOD	< LOD	< LOD	< LOD
Copper	189.6	15.4	21.2	29.2	31.6	35.0
Zinc	5,057.0	122.8	295.1	451.4	587.2	681.1
Molybdenum	246.7	20.7	29.3	37.1	44.4	49.8
Iron	544.9	< LOD	23.1	56.3	66.4	69.1
Nickel	< LOD	75.6	69.1	70.5	69.7	69.4
Zirconium	9.7	8.7	8.7	9.3	9.3	9.1
Strontium	7.4	2.6	2.8	3.3	3.7	3.6
Uranium	< LOD	2.8	< LOD	< LOD	< LOD	< LOD
Lead	67.0	< LOD	< LOD	0.9	4.0	5.1
Tungsten	< LOD	13.6	4.1	4.4	< LOD	5.7
Vanadium	< LOD	29.1	55.0	52.5	52.7	53.5
Potassium	< LOD	83.8	< LOD	< LOD	< LOD	< LOD

*<LOD means limit of detection.

4.6.2 ICP Test Results

The ICP test results of detected elements of calcium, copper, zinc, molybdenum, iron, nickel, phosphorus, and sulfur are shown in Table 4.5. The fingerprint elements in REOB are all detected by ICP and in the base binder (0% REOB). However, limited calcium and copper are seen in the binders blended with different percentages of REOB. There are also two other elements, phosphorus and sulfur, that ICP can detect. However, these two elements are not fingerprint elements of REOB. Compared with the element contents from XRF, the element contents detected by ICP are lower, possibly because of the incomplete digestion process of the binder into acid.

Table 4.5. ICP Test Results

Elements	Element Content (ppm)					
	REOB	0%	3%	6%	9%	12%
Calcium	205.7	22.6	< LOD	< LOD	< LOD	< LOD
Copper	4.9	0.8	< LOD	< LOD	< LOD	< LOD
Zinc	95.1	8.4	12.7	14.0	13.7	15.8
Molybdenum	25.3	8.5	0.9	1.3	1.4	1.8
Iron	9.4	< LOD	120.0	281.2	114.6	116.5
Nickel	4.3	5.5	1.0	0.9	0.8	0.8
Phosphorus	141.7	24.0	< LOD	< LOD	< LOD	< LOD
Sulfur	349.8	853.7	859.4	843.7	769.4	778.0

*<LOD means limit of detection.

4.6.3 DSR Test Results

The DSR test results of all blended binders are shown in Figure 4.6 and Figure 4.7 below. Figure 4.6 (a) shows the complex modulus, G* master curves of five unaged binder samples, and Figure 4.6 (b) presents the G* master curve of five 40-hour PAV-aged binder samples. All master curves were constructed at a reference temperature of 55 °C. The master curves show that the G* increases with frequency for unaged and 40-hrs PAV-aged binders. Also, as REOB content increases, the G* values decrease, which indicates that the blended binder becomes softer at high temperatures when REOB is added. Although not depicted in Figure 4, the stiffness of blended binders continuously increased as the aging process continued.

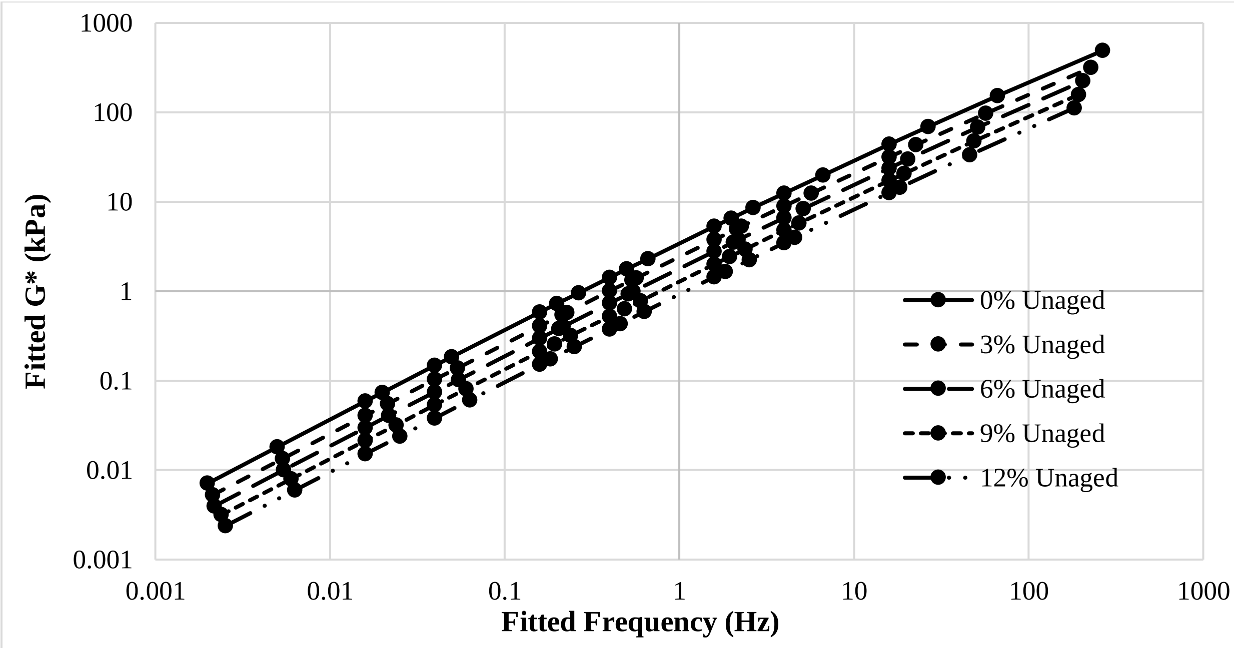

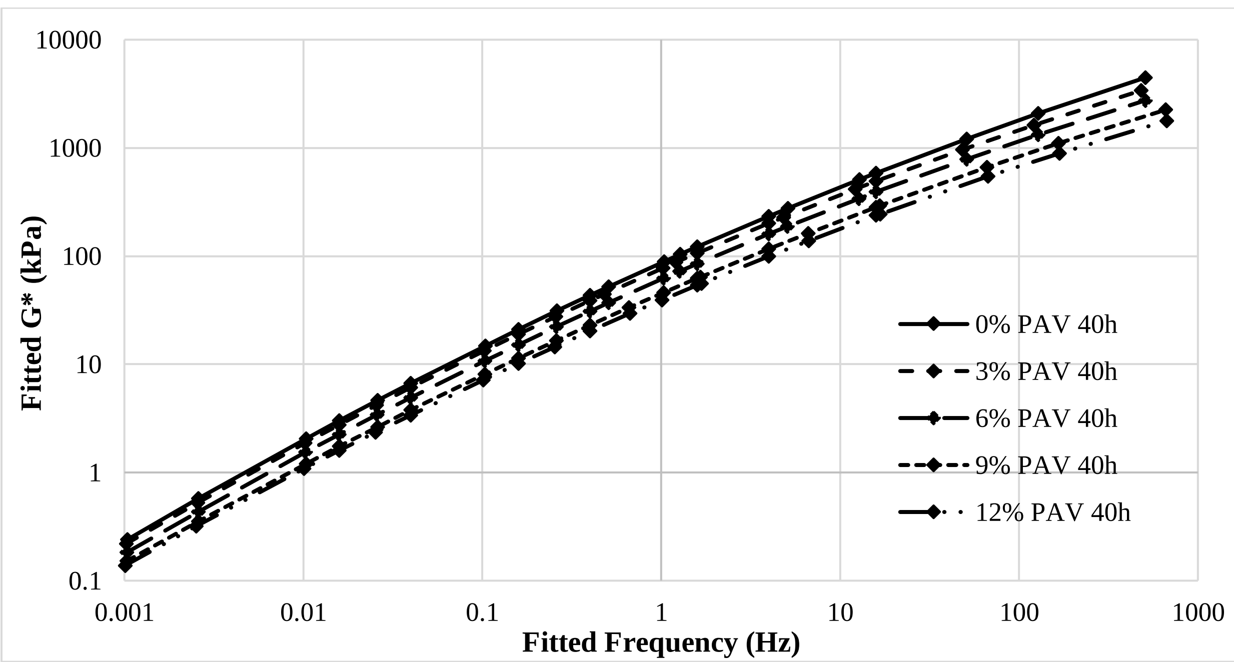

Figure 4.6. Master Curve of Fitted Complex Shear Modulus at 55 °C (a) Unaged Binder (b) 40 Hours PAV Aged Binder

Figure 4.7 shows the changes in phase angle for the binders at various REOB contents at 40 °C and 10 radians/second (1.59 Hz) and at four aging stages. Since the REOB is expected to soften the asphalt binder, the phase angle is supposed to increase when the REOB content rises.

The unaged binder shows an increasing trend as expected, and the RTFO aged binder shows a slight increase in phase angle as the REOB content increases. On the other hand, both 20-hour PAV- and 40-hour PAV-aged binders show a decreasing trend, which implies that the blended binder becomes more elastic as the REOB content increases. This opposite trend of phase angle with increasing REOB may indicate that some of the elements in REOB are sensitive to aging. Thus, expedited aging occurs with the binder that contains a higher percentage of REOB. The possibility of accelerated aging of high REOB binders was also observed by Bennert et al. (2016).

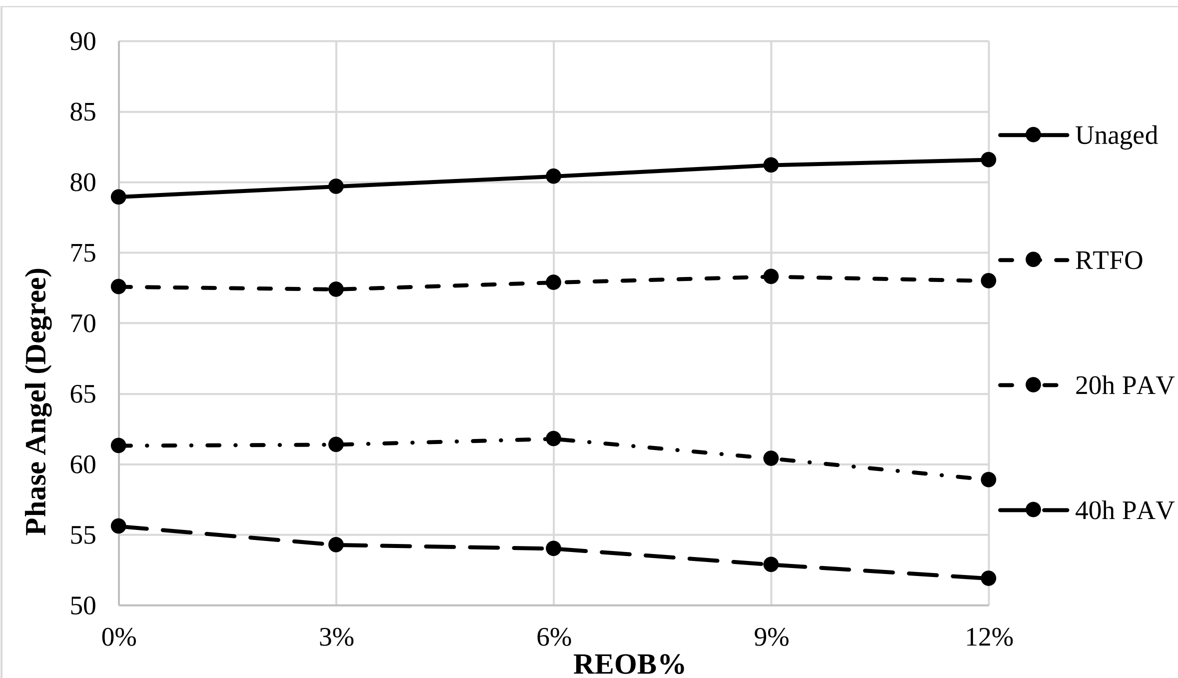

Figure 4.7. Phase Angle vs REOB Content at 40 °C and 10 Radians/Second

4.6.4 BBR Test Results

The BBR test results of all blended binders are shown in Figures 4.8 and 4.9. Figure 4.8 shows the stiffness versus loading time at -18 °C for 40-hour PAV-aged blended binders with various percentages of REOB. As indicated in Figure 6, the stiffness decreases as the REOB content increases. The trend is consistent at different test temperatures at -6 °C and with other aging conditions of 20-hour PAV.

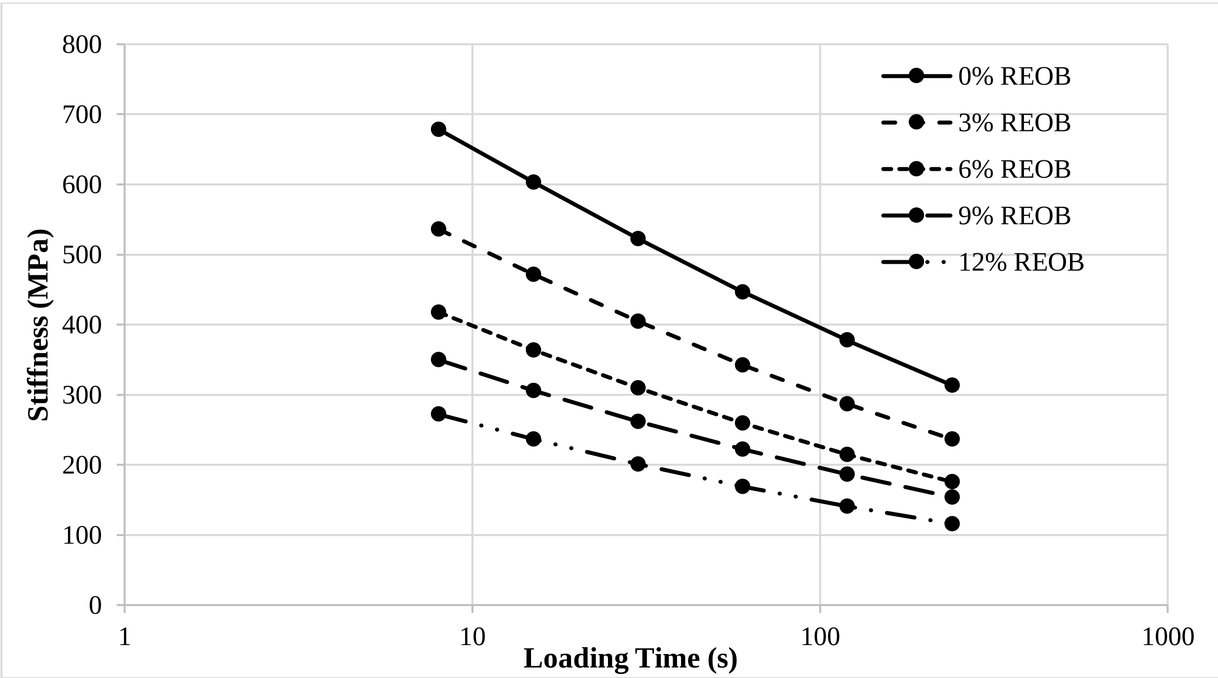

Figure 4.8. Stiffness vs Loading Time at -18 °C for 40 Hours PAV Aged Binder

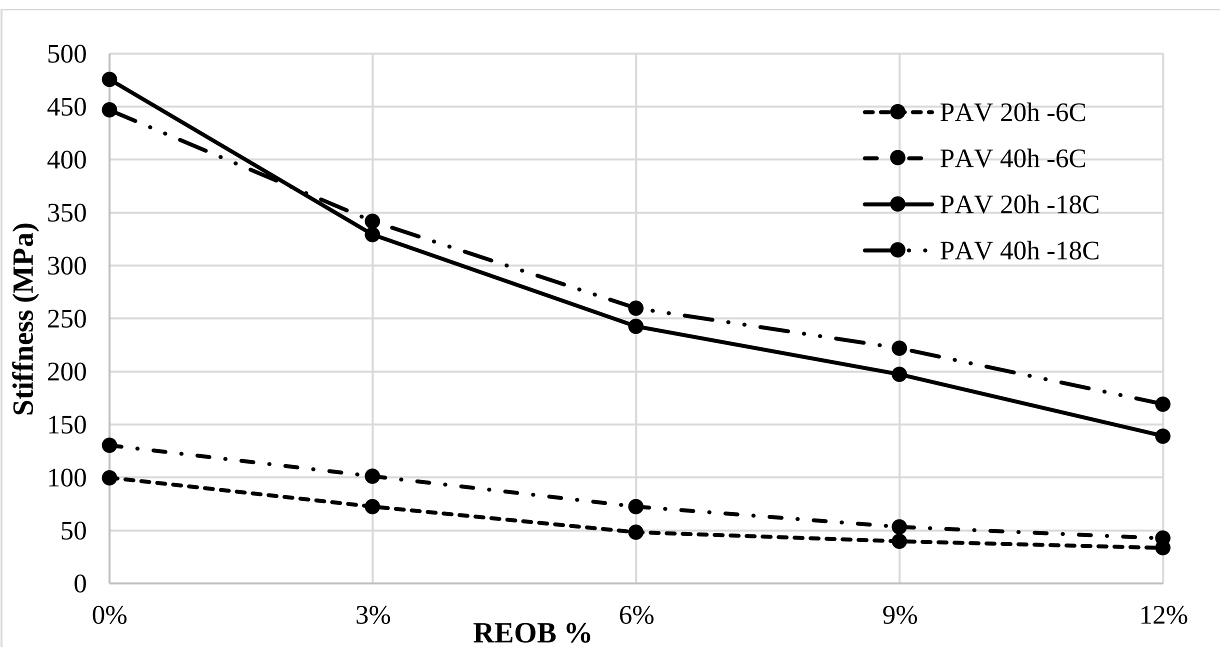

(a) Stiffness

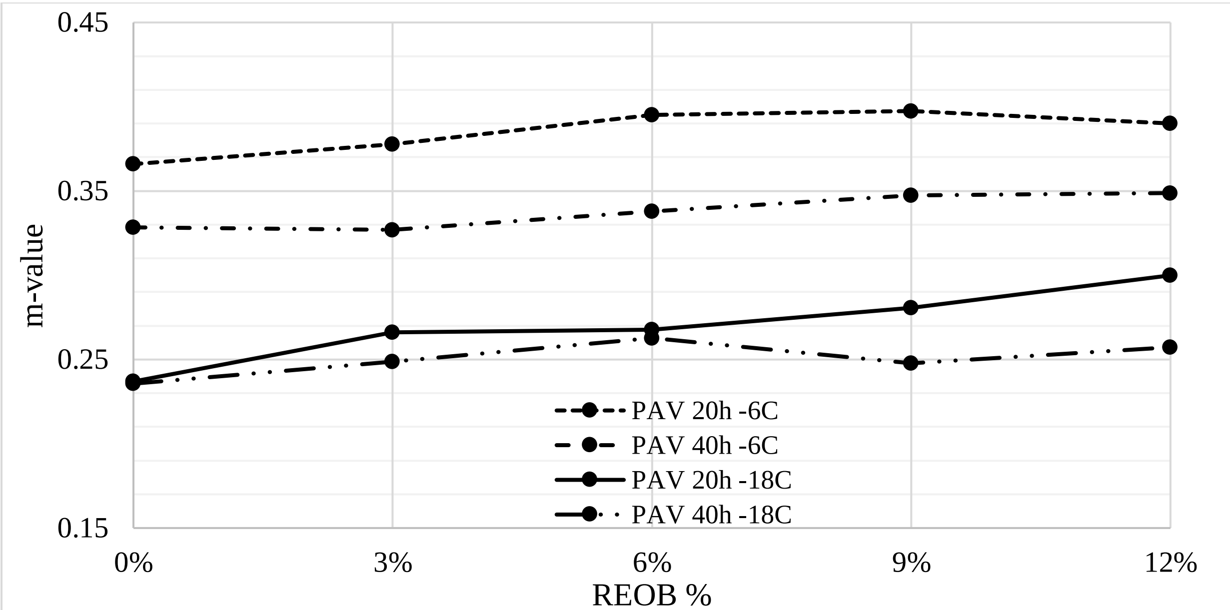

(b) m-value

Figure 4.9. BBR Test Results

Figure 4.9 shows the stiffness and m-value results. As the REOB content increases, the stiffness of the asphalt binder decreases (also observed in Figure 4.8), and the m-value slightly improves, though the changes in the m-value are not as apparent as the stiffness. As expected, binders with extended aging time (e.g., 40 hours of PAV) show slight increases in stiffness and decreases in m-values. Considering tiny fractions of metallic wastes (i.e., 0.67%) and much higher oil fraction in the REOB used in this study, this softening effect of REOB on asphalt binder is reasonable.

Table 4.6. ΔT Results

	20-hour PAV			40-hour PAV		
	T_s	T_m	ΔT	T_s	T_m	ΔT
0%	-12.3	-12	-0.3	-12.2	-9.4	-2.8
3%	-16.6	-14.3	-2.3	-15.8	-9.9	-5.9
6%	-21.5	-14.3	-7.2	-20.5	-11.8	-8.7
9%	-25.8	-15.9	-9.9	-23.6	-11.5	-12.1
12%	-25.7	-18	-7.7	-30.5	-12.3	-18.2

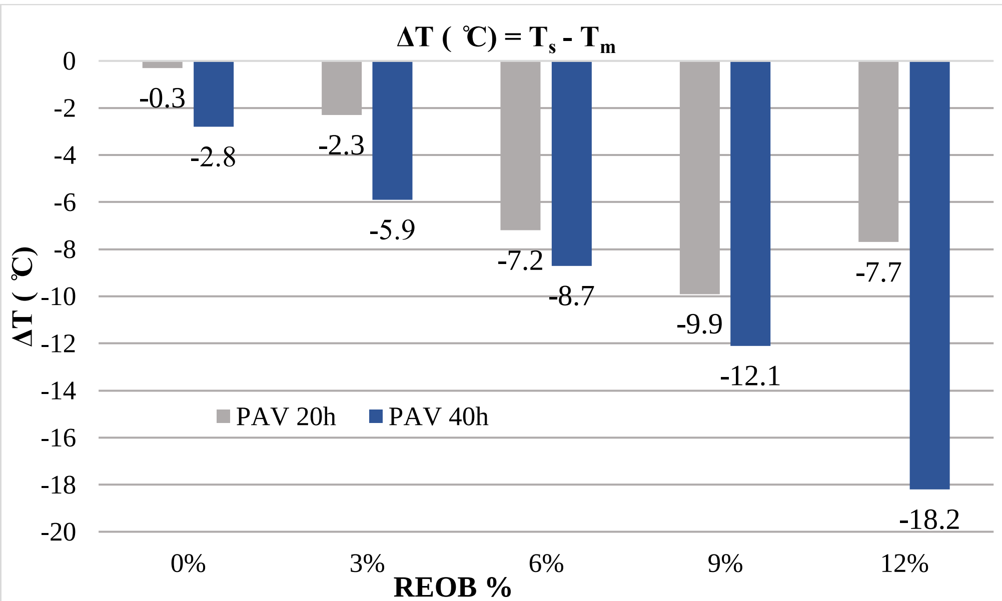

Figure 4.10. ΔT Results

Table 4.6 and Figure 4.10 show the difference in critical temperatures, ΔT. ΔT is calculated as the difference between the required low temperature determined by the stiffness (T_s) and the necessary low temperature determined by the m-value (T_m) (Reinke et al., 2016). Anderson et al. (2011) reported that ΔT is a parameter that captures the relaxation properties of bitumen and correlates to non-loading associated cracking. The negative value of ΔT indicates that the asphalt binder's low-temperature grade is determined by the m-value (i.e., m-controlled). As the REOB content increases, the negative ΔT value drops rapidly for both 20-hour and 40-hour PAV-aged binder samples, except for the 12% REOB and 20-hour PAV-aged binder. As provided in Table 4.6, this rapid drop of ΔT is due to the sharp decline in T_s, while the change in T_m is not as profound as T_s. Notably, the difference in ΔT after 40 hours of PAV aging is much higher than that of 20 hours of PAV aging, which indicates the asphalt binder becomes more m-controlled as aging continues. In other words, the REOB used in this study significantly improved the stiffness of the blended binders at low temperatures. At the same time, the relative improvement in relaxation property was not as significant.

4.6.5 Statistical Analysis

4.6.5.1 DSR Test

In the DSR test, statistical analysis was conducted for two response variables, complex shear modulus, and phase angle, separately with the same three independent variables. A three-way factorial was designed to examine the differences in rheological properties on binders with varying content of REOB. The independent variables are: (i) REOB content at five levels: 0%, 3%, 6%, 9%, and 12%; (ii) aging condition with four levels: unaged, RTFO, PAV-20h, and PAV-40h; (iii) temperature with three levels: 40 °C, 55 °C, and 70 °C. The linear model as shown below is used:

$$\mathbf{y}_{ijkl} = \boldsymbol{\mu} + \boldsymbol{\alpha}_i + \boldsymbol{\beta}_j + (\boldsymbol{\alpha\beta})_{ij} + \boldsymbol{\gamma}_k + (\boldsymbol{\alpha\gamma})_{ik} + (\boldsymbol{\beta\gamma})_{jk} + (\boldsymbol{\alpha\beta\gamma})_{ijk} + \boldsymbol{\varepsilon}_{ijkl} \quad \text{Equation 4.1}$$

Where,

y is the response variable (complex shear modulus or phase angle);

μ is the intercept;

α_i is the effect of i^{th} level of REOB content; i = 1, 2, 3, 4, 5;

β_j is the effect of j^{th} level of aging condition, j = 1, 2, 3, 4;

γ_k is the effect of k^{th} level of temperature, k = 1, 2, 3;

$(\alpha\beta)_{ij}$, $(\alpha\gamma)_{ik}$, $(\beta\gamma)_{jk}$, $(\alpha\beta\gamma)_{ijk}$ are the interactions between all effects, and

ε_{ijkl} is the response error for the l^{th} sample from the i^{th} REOB content, j^{th} aging condition, and k^{th} temperature, assumed to be normally distributed with mean 0 and variance σ^2.

Table 4.7 illustrates the Type III test results for complex shear modulus. For all effects and interactions, the results show very low p-values (<.0001). The combined effect of REOB content, aging condition, and temperature significantly influences the complex shear modulus. The significance of two-way interactions indicates that the effect of one factor depends on the level of the other, and all the factors significantly affect the complex shear modulus.

Table 4.7. Type III Tests of Complex Shear Modulus

Effect	Num DF	Den DF	F value	Pr > F
REOB Content	4	60	497.58	<.0001
Aging Condition	3	60	5720.61	<.0001
REOB Content * Aging Condition	12	60	108.99	<.0001
Temperature	2	60	14650.4	<.0001
REOB Content * Temperature	8	60	372.26	<.0001
Aging Condition * Temperature	6	60	4119.82	<.0001
REOB Content * Aging Condition * Temperature	24	60	78.70	<.0001

Table 4.8. Differences of LS-Means for Multiple Comparisons of Complex Shear Modulus

REOB Content (%)	REOB Content (%)	Estimate	Standard Error	DF	t value	Pr > |t|
0	3	44.94	2.80	60	16.03	<.0001
0	6	77.21	2.80	60	27.54	<.0001
0	9	95.51	2.80	60	34.06	<.0001
0	12	111.04	2.80	60	39.60	<.0001
3	6	32.28	2.80	60	11.51	<.0001
3	9	50.57	2.80	60	18.04	<.0001
3	12	66.11	2.80	60	23.58	<.0001
6	9	18.29	2.80	60	6.52	<.0001
6	12	33.83	2.80	60	12.06	<.0001
9	12	15.53	2.80	60	5.54	<.0001

Table 4.9. T Grouping for REOB Content LS-Means of Complex Shear Modulus ($\alpha = 0.05$)

REOB Content (%)	Estimate	
0	191.45	A
3	146.51	B
6	114.23	C
9	95.94	D
12	80.41	E

*LS-means with the same letter are not significantly different.

LS-means results are illustrated in Table 4.8 and Table 4.9. Table 4.8 compares the complex shear modulus LS- means derived from various REOB contents. All the p-values are less than 0.0001, implying that the complex shear modulus differs significantly regardless of the REOB content. Table 4.9 demonstrates the same conclusion. Adding REOB will significantly affect the binder's complex shear modulus. The complex shear modulus decreases when REOB is added to the binder, indicating that the binder becomes softer.

Table 4.10 implies the Type III test results for phase angle. As shown in the table, all the p-values are smaller than 0.0001. This indicates that all the interactions and factors significantly affect the phase angle.

Table 4.10. Type III Tests of Phase Angle

Effect	Num DF	Den DF	F value	Pr > F
REOB Content	4	60	202.77	<.0001
Aging Condition	3	60	338033	<.0001
REOB Content * Aging Condition	12	60	2728.72	<.0001
Temperature	2	60	281629	<.0001
REOB Content * Temperature	8	60	56.00	<.0001
Aging Condition * Temperature	6	60	7159.39	<.0001
REOB Content * Aging Condition * Temperature	24	60	134.19	<.0001

Table 4.11. Differences of LS-Means for Multiple Comparisons of Phase Angle

REOB Content (%)	REOB Content (%)	Estimate	Standard Error	DF	t value	Pr > │t│
0	3	-0.05	0.03	60	-2.26	0.0275
0	6	0.02	0.03	60	0.81	0.4229
0	9	0.17	0.03	60	6.45	<.0001
0	12	0.58	0.03	60	22.59	<.0001
3	6	0.08	0.03	60	3.07	0.0032
3	9	0.23	0.03	60	8.71	<.0001
3	12	0.64	0.03	60	24.85	<.0001
6	9	0.15	0.03	60	5.65	<.0001
6	12	0.56	0.03	60	21.79	<.0001
9	12	0.42	0.03	60	16.14	<.0001

Table 4.12. T Grouping for REOB Content LS-Means of Phase Angle (α = 0.05)

REOB Content (%)	Estimate	
3	74.74	A
0	74.68	B
		B
6	74.66	B
9	74.51	C
12	74.10	D

*LS-means with the same letter are not significantly different.

Table 4.11 and Table 4.12 illustrate the LS-means result for the phase angle. Table 4.11 shows the comparison of the LS-means among different content of REOB. The comparison between 0% REOB and 6% REOB gives a larger p-value than 0.05. This indicates that the phase angle between 0% and 6% REOB binders differs insignificantly. All the other comparisons show statistically significant differences. Table 4.12 confirms the same conclusion. Adding 3% REOB increases the phase angle despite other independent variables, which means the biner becomes softer. However, as the phase angle decreases, the binder becomes stiffer when more REOB is added.

4.6.5.2 BBR Test

For the BBR test results, statistical analysis was also conducted for two response variables, stiffness, and m-value. The design was a three-way full factorial. The three independent variables are: (i) REOB content at five levels: 0%, 3%, 6%, 9%, and 12%; (ii) aging condition at two levels: PAV-20h, and PAV-40h; (iii) temperature at two levels: -6 °C, and -18 °C. The following linear model is used to evaluate the differences in low-temperature properties of the binders with varying REOB content:

$$y_{ijkl} = \mu + \alpha_i + \beta_j + (\alpha\beta)_{ij} + \gamma_k + (\alpha\gamma)_{ik} + (\beta\gamma)_{jk} + (\alpha\beta\gamma)_{ijk} + \varepsilon_{ijkl} \quad \text{Equation 4.2}$$

Where,

y is the response variable (stiffness or m-value);

μ is the intercept;

α_i is the effect of i^{th} level of REOB content; i = 1, 2, 3, 4, 5;

β_j is the effect of j^{th} level of aging condition, j = 1, 2;

γ_k is the effect of k^{th} level of temperature, k = 1, 2;

$(\alpha\beta)_{ij}$, $(\alpha\gamma)_{ik}$, $(\beta\gamma)_{jk}$, $(\alpha\beta\gamma)_{ijk}$ are the interactions between all effects, and

ε_{ijkl} is the response error for the l^{th} sample from the i^{th} REOB content, j^{th} aging condition, and k^{th} temperature, assumed to be normally distributed with mean 0 and variance σ^2.

Table 4.13 illustrates the Type III test results for complex shear modulus. Except for the interactions of REOB content, aging condition, and temperature, the rest of the effects and interactions have lower p-values than 0.05. This suggests that the three-way interaction of the REOB content, aging condition, and temperature significantly affects the stiffness. The effect of aging condition is not dependent on the REOB content or temperature. The treatments significantly affect the stiffness.

Table 4.13. Type III Tests of Stiffness

Effect	Num DF	Den DF	F value	Pr > F
REOB Content	4	36	558.01	<.0001
Aging Condition	1	36	31.07	<.0001
REOB Content * Aging Condition	4	36	1.92	0.1282
Temperature	1	36	5349.78	<.0001
REOB Content * Temperature	4	36	192.32	<.0001
Aging Condition * Temperature	1	36	3.27	0.0788
REOB Content * Aging Condition * Temperature	4	36	5.93	0.0009

Table 4.14. Differences of LS-Means for Multiple Comparisons of Stiffness

REOB Content (%)	REOB Content (%)	Estimate	Standard Error	DF	t value	Pr > |t|
0	3	77.28	4.53	36	17.07	<.0001
0	6	132.27	4.39	36	30.11	<.0001
0	9	159.99	4.66	36	34.34	<.0001
0	12	192.06	4.53	36	42.42	<.0001
3	6	54.99	4.53	36	12.15	<.0001
3	9	82.71	4.79	36	17.28	<.0001
3	12	114.79	4.66	36	24.64	<.0001
6	9	27.72	4.66	36	5.95	<.0001
6	12	59.80	4.53	36	13.21	<.0001
9	12	32.08	4.79	36	6.70	<.0001

Table 4.15. T Grouping for REOB Content LS-Means of Stiffness (Alpha = 0.05)

REOB Content (%)	Estimate	
0	288.16	A
3	210.88	B
6	155.89	C
9	128.17	D
12	96.10	E

*LS-means with the same letter are not significantly different.

Table 4.14 and Table 4.15 illustrate the LS-means results of Stiffness. Table 4.14 shows the comparison of the stiffness LS- means derived from different content of REOB. All the p-values are less than 0.0001, which implies the difference in stiffness between REOB contents is significant. Table 4.15 demonstrates the same conclusion. Adding REOB will significantly reduce the stiffness at low temperatures.

Table 4.16 implies the Type III test results for the m-value. All the p-values are smaller than 0.0001. These results indicate that all the interactions and factors significantly affect the m-value.

Table 4.16. Type III Tests of m-value

Effect	Num DF	Den DF	F value	Pr > F
REOB Content	4	36	197.28	<.0001
Aging Condition	1	36	1617.49	<.0001
REOB Content * Aging Condition	4	36	25.10	<.0001
Temperature	1	36	14634.4	<.0001
REOB Content * Temperature	4	36	20.62	<.0001
Aging Condition * Temperature	1	36	271.77	<.0001
REOB Content * Aging Condition * Temperature	4	36	29.66	<.0001

Table 4.17. Differences of LS-Means for Multiple Comparisons of m-value

REOB Content (%)	REOB Content (%)	Estimate	Standard Error	DF	t value	Pr > │t│
0	3	-0.01	0.001	36	-10.22	<.0001
0	6	-0.02	0.001	36	-19.28	<.0001
0	9	-0.03	0.001	36	-19.92	<.0001
0	12	-0.03	0.001	36	-25.02	<.0001
3	6	-0.01	0.001	36	-8.49	<.0001
3	9	-0.01	0.001	36	-9.73	<.0001
3	12	-0.02	0.001	36	-14.38	<.0001
6	9	-0.002	0.001	36	-1.74	0.0898
6	12	-0.01	0.001	36	-6.31	<.0001
9	12	-0.01	0.001	36	-4.27	0.0001

Table 4.18. T Grouping for REOB Content LS-Means of m-value (Alpha = 0.05)

REOB Content (%)	Estimate	
12	0.3242	A
9	0.3183	B
		B
6	0.3160	B
3	0.3050	C
0	0.2917	D

*LS-means with the same letter are not significantly different.

Table 4.17 and Table 4.18 show the m-value LS-means results. Table 4.17 compares the LS- means derived from different content of REOB. Only the p-value of the comparison of 6% REOB and 9% REOB is more significant than 0.05. This implies that the difference in m-value between 6% and 9% REOB binders is insignificant. All the other comparisons show statistically significant differences. Table 4.18 confirms the same conclusion. The m-value decreases when REOB content decreases. This indicates that the binder becomes softer while adding REOB.

4.7 Conclusions

This study blended a single source of REOB containing a small fraction of petroleum waste with a PG 64-22 unmodified asphalt binder at varying contents of 0%, 3%, 6%, 9%, and 12%. The DSR frequency-temperature sweep test and BBR test with 20 and 40 hours of PAV aging evaluated the rheological properties of the blended binders at high and low temperatures. Following is the summary of observations from this limited study:

- The addition of REOB effectively reduced the stiffness (e.g., G*) of the blended binders at high temperatures, indicating a good potential for using REOB as a softening or recycling agent. On the other hand, the effect of REOB on the phase angle showed mixed trends, which requires more investigation.

- The addition of REOB generally improved the low-temperature properties of asphalt binders (i.e., both stiffness and m-value). Unlike the observations by other researchers, the improvement in stiffness was much more profound than in the m-value by the addition of the REOB used in this study.
- These observations were confirmed by statistical analyses.
- With 0.67% of potentially detrimental metallic wastes in REOB, the softening effect of 99.33% of oil prevails. Therefore, based solely on the binder properties, well-prepared REOB can help mitigate the low-temperature cracking problems of asphalt pavements.
- The primary effective component in REOB is 99.33% oil. Considering the effects of REOB in HMA mixtures, the effective oil content in the HMA mixture with a binder content of 6% ranged approximately from 0.18% to 0.72% when the REOB content varied from 3% to 12%. The minimal REOB oil content in the total mixture is unlikely to influence the properties of the HMA mixtures. Therefore, further investigation of HMA mixtures containing varying REOB content was not done.

Chapter 5 - Quality Control and Quality Assurance of Recycled Materials Quantity in Hot-Mix Asphalt

5.1 Introduction

A hot-mix asphalt (HMA) plant aims to produce a homogeneous mixture by blending aggregates and asphalt binder at an elevated temperature. Using recycled materials such as Recycled Asphalt Pavement (RAP) and Recycled Asphalt Shingles (RAS) in HMA production can decrease the demand for new materials such as virgin binders and aggregates, which can consequently lower material costs and preserve natural resources. FHWA defines RAP as "removed or reprocessed pavement materials that contain asphalt binder and aggregates during resurfacing, rehabilitation, or reconstruction operations" (Copeland, 2011). RAP is a valuable alternative to virgin materials and is recycled more than other materials (Williams et al., 2022). Over 95% of RAP returned to produce new pavements, while the remaining 5% were used as unbound aggregate bases or subbases (Chesner et al. 2002; Williams et al. 2022). RAS is typically derived from tear-offs of roofs and manufactured shingle waste. Williams et al. (2022) stated that approximately 94.6 million tons of RAP and 630,000 tons of RAS were used in asphalt mixtures in 2021. RAP usage replaced 4.7 million tons of asphalt binder and more than 89 million tons of aggregate, resulting in $3.4 billion in savings. During the same year, using RAS reduced the need for 126,000 tons of asphalt binder and 315,000 tons of aggregate, saving over $69 million (Williams et al., 2022).

Drum mix plants, the primary HMA production plants used for most paving projects, including those for KDOT, use belts to feed virgin aggregates and RAP into a drum for HMA production. At the beginning of each project, the belts are calibrated to control the aggregate and RAP quantities during mixing. Based on the totalizer input, a specific amount of virgin binder is pumped from a storage tank (NAPA & APWA, 2000). Current KDOT specifications require a totalizer to determine the percentage of RAP fed into the drum. Data from many projects showed that the amount of RAP back-calculated from the total mass of the mixture from the bill of lading quantity and virgin binder content was higher than the maximum allowable RAP content. A similar issue is also being studied in the ongoing project NCHRP 09-69: Verifying Quantities of Materials Used in Asphalt Mixtures at Production Facilities. This study investigated the quality control and quality assurance (QC/QA) process regarding RAP quantity on multiple HMA projects. Drum mix plants, the primary hot-mix asphalt (HMA) production plants for most Kansas Department of Transportation (KDOT) projects, use belts to feed virgin aggregates and reclaimed asphalt pavement (RAP) into a drum for HMA production. At the beginning of each project, the belts are calibrated to control the aggregate and RAP quantities during mixing. Based on the totalizer input, a specific amount of virgin binder is pumped from a storage tank (NAPA & APWA, 2000).

5.2 KDOT HMA Mix Production Investigation

KDOT utilized a mass-balance approach to back-calculate the percentage of RAP in the HMA mixture that was being produced in the project. The added virgin asphalt binder and asphalt binder contributed by RAP constitute the total binder content of the mix. Therefore, the theoretical binder content of an HMA mixture at the maximum allowable RAP percentage can be calculated by Equation 5.1:

$$\boldsymbol{P_{bMixTheo}} = (\boldsymbol{AC} + \%\boldsymbol{RAP_{Max}} \times \boldsymbol{P_{bRAP}} \times (\boldsymbol{Q_{Mix}} - \boldsymbol{AC}))/\boldsymbol{Q_{Mix}} \qquad \text{Equation 5.1}$$

Where:

$P_{bMixTheo.}$ is theoretical binder content of the HMA mixture (%);

AC is amount of virgin binder and additives (ton);

$\%RAP_{Max}$ is maximum % RAP of JMF allowed in the mix, expressed as decimal (i.e., 25% = 0.25);

Pb RAP is % binder content of RAP based on the average QC/QA test results (determined from the Kansas test method KT-57: Determination of Asphalt Content and Gradation of Hot-Mix Asphalt Concrete by the Ignition Method (KDOT, 2022b)); and

Q_{Mix} is the total quantity of HMA mix produced (tons).

If QC/QA data is available for the HMA mixture and RAP and the quantities of produced HMA mixture and virgin binder used are known, then the theoretical %RAP can be calculated by Equation 5.2:

$$\%\boldsymbol{RAP_{Theo.}} = ((\boldsymbol{Q_{Mix}} \times \boldsymbol{P_{bMix}}) - \boldsymbol{AC})/(\boldsymbol{P_{bRAP}} \times (\boldsymbol{Q_{Mix}} - \boldsymbol{AC})) \qquad \text{Equation 5.2}$$

Where:

$\%RAP_{Theo}$. is theoretical %RAP; and

Pb_{Mix} is the average binder content of the HMA mixture based on the average QC/QA testing values.

Data was collected from eight projects in northwest Kansas. Back calculations were done for the theoretical binder content and corresponding RAP percentage following Equations 5.1 and 5.2 and assuming the following for all projects: D2S for P_{bMix} = 0. 2%; D2S for P_{bRAP} = 0. 2%; virgin binder scale tolerance = 0.5%; and mix scale tolerance = 0.5%. D2s is the measure of precision for the Kansas test method KT-57. The variations (2 x Std. Dev.) for P_b Mix and P_{bRAP} were computed from the data points for these variables for the project. P_{bMix} is determined for each sublot (750 tons of HMA), and P_{bRAP} for the first HMA lot (3,000 tons) and then one per 1,000 tons of RAP used. Table 5.1 shows an example of contrasts of the variables used in simulation calculations using Equations 5.1 and 5.2.

Table 5.1. Example Contrast used in Theoretical $P_{b\ Mix}$ and %RAP Calculations

P_{bMix}		P_{bRAP}		AC	Q_{Mix}
D2S	Proj. Var	D2S	Proj. Var	Scale Tol.	Scale Tol.
1	1	-1	-1	-1	1
1	1	-1	-1	0	1
1	1	-1	-1	-1	0
1	1	-1	-1	0	0
1	1	-1	-1	1	1
1	1	-1	-1	-1	-1
1	1	-1	-1	1	0

Figure 5.1 shows the distribution of back-calculated RAP percentages from one project for all possible combinations of P_{bMix}, P_{bRAP}, tons of asphalt binder used, and produced HMA mix. This project's maximum allowable RAP percentage was 40%, and 37% of RAP was in the JMF. The simulation results clearly show that, in many instances, the maximum RAP percentage was exceeded.

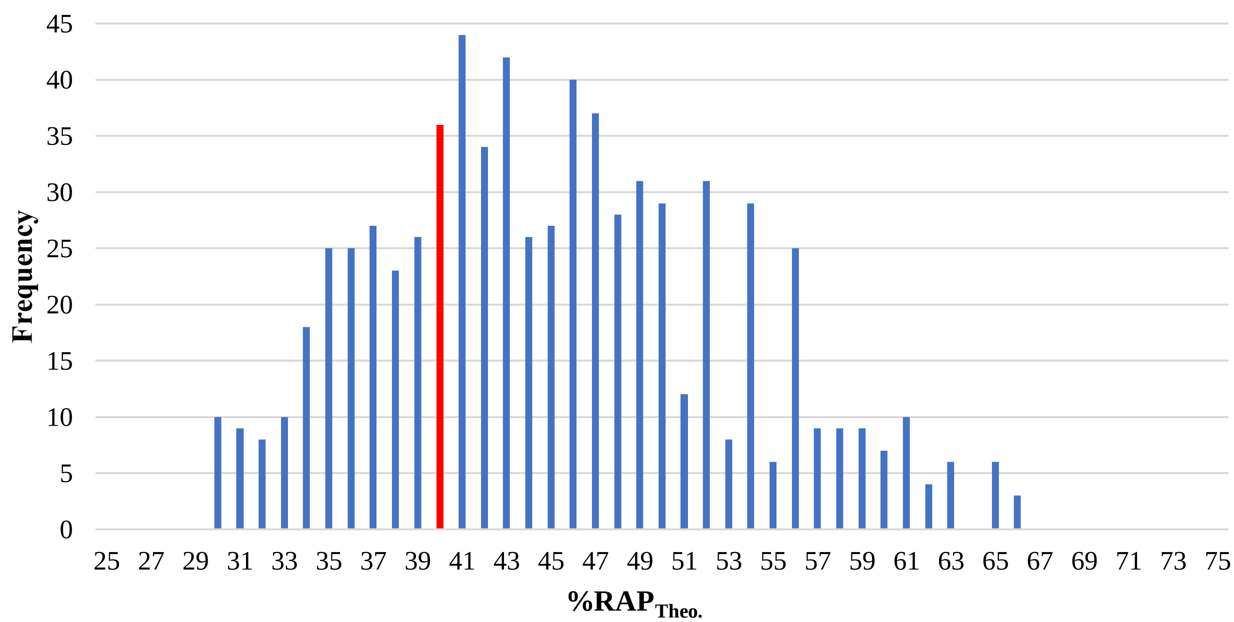

Figure 5.1. Distribution of Back-calculated RAP Quantities

The summary results of the analysis of all projects using Equations (1) and (2) are summarized in Table 5.2. The theoretical RAP percentages exceeded those in JMF and the maximum allowable quantity in all cases.

Table 5.2. Summaries of Theoretical P_b and Calculated RAP Contents

Project No.	P_b (%)		Quantity (tons)		Theo. P_b (%)	RAP (%)			Reclaimed Binder Ratio (RBR, %)		
	Mix	RAP	Binder	Mix		Theo.	JMF	Max.	JMF	Theo	Max.
1	5.72	5.18	1,081	24,947	5.57	28	24	25	21.7	26.0	22.6
2	4.96	5.63	605	23,770	4.74	44	37	40	42.0	52.3	45.4
3	5.24	5.67	361	13,214	4.94	45.4	37	40	40.0	52.1	43.3
4	5.20	4.80	3,220	85,678	4.91	31.2	24.6	25	22.7	30.5	23.1
5	5.20	5.08	491	15,921	5.05	43.0	39	40	38.1	43.3	39.1
6	4.94	5.03	966	32,683	4.91	40.7	39	40	39.7	41.7	40.7
7	5.08	5.78	859	32,772	4.87	43.7	39.9	40	45.4	51.9	45.5
8	5.25	5.74	519	20,240	4.79	48.2	39.7	40	43.4	57.8	43.7

5.3 Literature Review

An HMA plant aims to produce a homogeneous asphalt mixture by blending aggregate and asphalt binder at an elevated temperature. Batch and drum mix HMA plants are currently used in the United States. Batch plants produce small, precise batches of HMA mixture until total tonnage is reached, while drum mix plants continuously manufacture HMA mixtures without interruption.

5.3.1 Batch Plants

A batch plant includes a cold-feed system, asphalt cement system, aggregate dryer, mixing tower, and emission-control system (NAPA & APWA, 2000). The major components of a batch plant are shown in Figure 5.2. The aggregates used in mixing are placed into individual cold-feed bins and output with a designed proportion. The gathering conveyor under the cold-feed bins transports aggregates to a charging conveyor and then to the dryer. After the drying operation, a bulk elevator transports the aggregates to the top of the mixing tower. It discharges them into various hot storage bins as they pass through vibration screens. A weigh hopper weighs the aggregates discharged from the hot bins to ensure the correct aggregate proportion. At the same time, a proper amount of asphalt cement (per Job Mix Formula, JMF) is pumped into a bucket above the pug mill. If RAP is used in the mixture, it is stored in a separate cold bin and added via either the bottom of the bulk elevator, the hot bins, or the weigh hopper, which is most common. The aggregates are then dropped into the pugmill and mixed briefly, discharging asphalt cement into the pugmill. The mixing process is finished in a short period. After mixing, the mixture is discharged from the bottom of the mixing tower into the mixing vehicle or conveyor that moves the mix to a silo (NAPA & APWA, 2000).

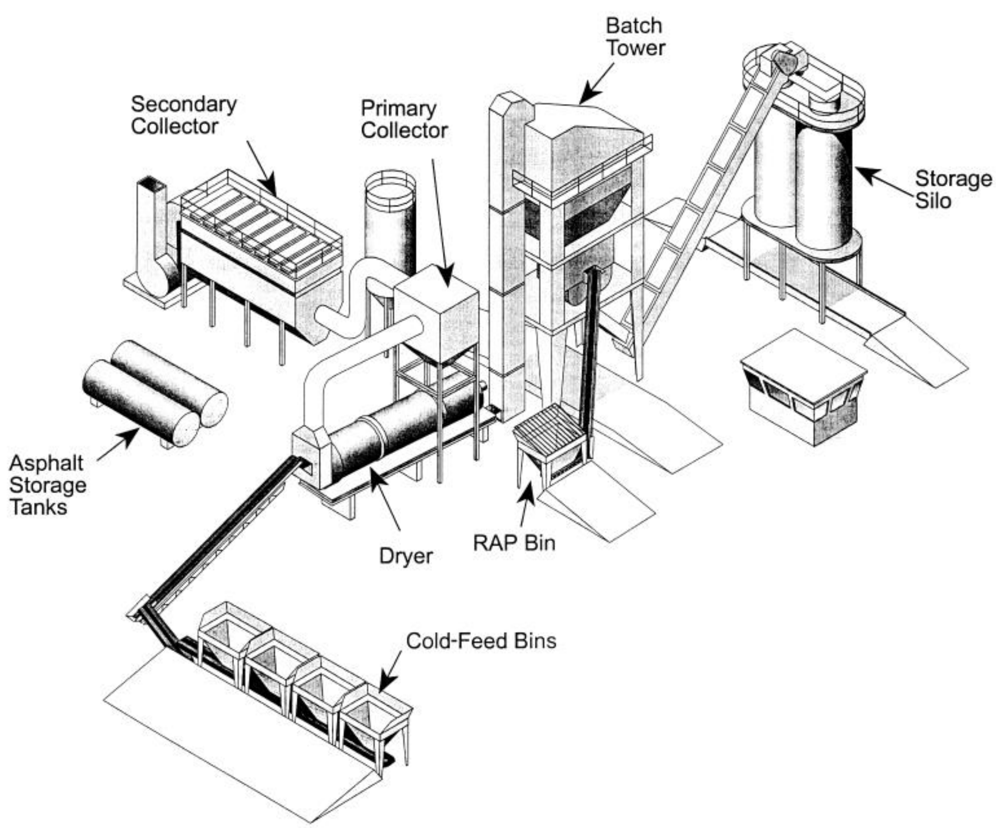

Figure 5.2. Major Components of a Batch Plant (Source: NAPA & APWA, 2000)

5.3.2 Drum Mix Plants

Drum mix plants are typically either parallel-flow or counter-flow; KDOT usually utilizes both types. Parallel-flow and counter-flow plants have similar mixing procedures and significant components, including a cold-feed system, an asphalt cement supply system, a drum mixer, and surge or storage silos. A diagram of a drum mix plant is shown in Figure 5.3.

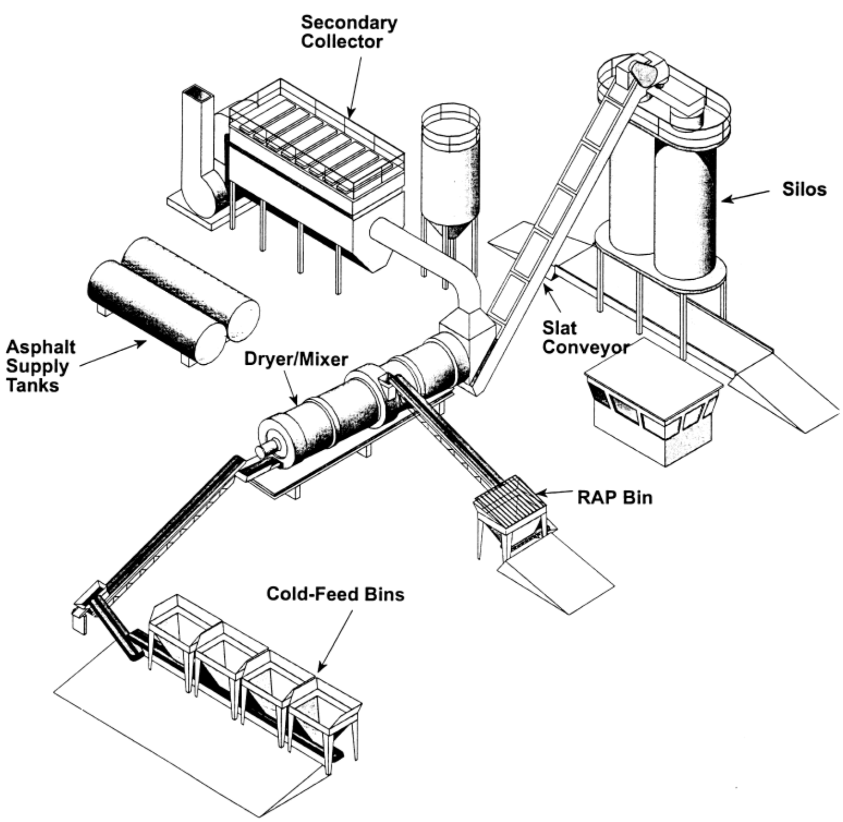

Figure 5.3. Major Components of a Drum Mix Plant (Source: NAPA & APWA, 2000)

5.3.2.1 Parallel-Flow Drum Mix Plants

In parallel-flow drum mix plants, cold-feed bins are typically used to introduce aggregates into the mixing process, and the gate size and the feeder belt's speed beneath the bin are used to control the proportion of the material. A gathering conveyor under the cold-feed bins gathers all the aggregates and delivers them to a charging conveyor via a scalping screen. The charging conveyor then transports the aggregate into the drum mixer. The charging conveyor typically contains a weighbridge and a sensor (Figure 5.4) to control the amount of aggregate needed in the mix. The weighbridge under the conveyor belt measures the weight of the aggregate passing over the weigh idler, which is attached to the load cell. The charging conveyor operates at a constant speed recorded with a belt sensor. The totalizer combines the information gathered from the two devices to determine the actual wet weight of the aggregates in tons per hour. The moisture information of the aggregates must be manually input into the control system to convert the wet weight to dry weight so that the proper amount of asphalt cement per JMF is calculated. The control system screen of a drum mix plant investigated in this research is presented in Figure 5.5.

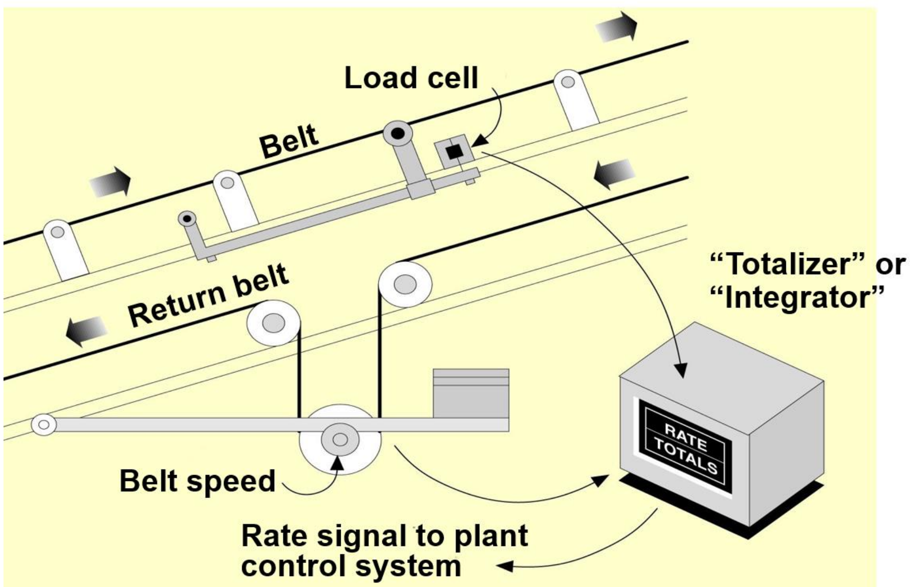

Figure 5.4. Weighbridge System **(**Source: NAPA & APWA, 2000)

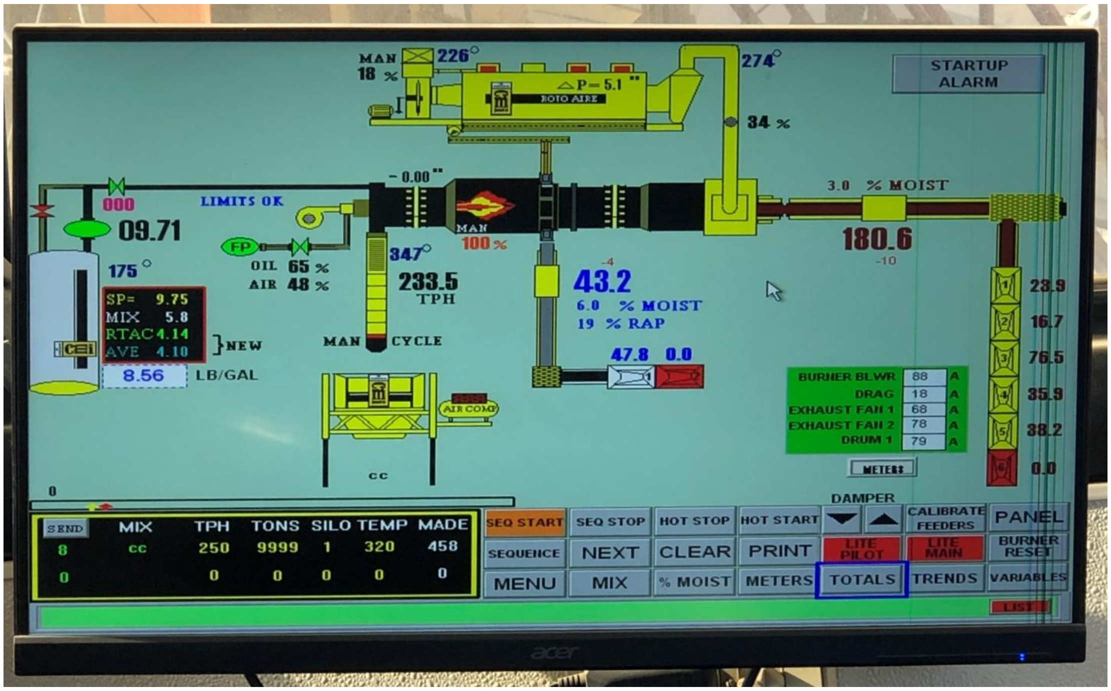

Figure 5.5. Sample Control System of Drum Mix Plant (Source: APAC, 2021)

In a drum mix plant, the burner is located at the upper end of the drum, and the aggregates are introduced into the drum through an inclined chute or a slinger conveyor. The inclined chute above the burner transports the aggregates by gravity. The slinger conveyor below the burner throws the aggregate into the drum with sufficient belt speed (Roberts et al., 1991; NAPA & APWA, 2000). As the aggregates travel into the drum, the moisture is removed and heated. If recycled materials are used, such as RAP and reclaimed asphalt shingles (RAS), they are delivered from a separate cold-feed bin with its conveyor system. Recycled materials are fed into the drum from a collar in the middle of the drum to prevent overheating. Once the virgin aggregates and reclaimed materials move to the discharge end of the drum, asphalt cement is pumped from the storage tank, fed through a meter, and injected into the aggregates, which are then coated with a binder while tumbling in the drum. The mixture then moves to the lower end of the drum and transits into a conveyor device. The conveyor, such as a drag slat conveyor or belt elevator, carries the HMA mixture into a storage silo, and the silo delivers the mixtures into haul vehicles in batches. The weight of each batch is weighed via silo scales, platform scales, or truck scales (NAPA & APWA, 2000).

5.3.2.2 Counter-Flow Drum Mix Plants

The operation process of counter-flow drum mix plants is like that of parallel-flow drum mix plants except for mixing. In the parallel-flow drum, the aggregates and hot airflow in the same direction through the drum, while in the counter-flow drum, the aggregates and hot gases flow in opposite directions. The drying and mixing processes in double-barrel counter-flow drums occur in separate barrels. The aggregates are introduced into the drum from the upper end and dried and heated via the burner at the lower back end. The dried and heated aggregates are then discharged downward into the outer barrel to mix with the asphalt cement. If applicable, RAP is added to the external drum. However, this mixing unit is not commonly used since the external drum does not rotate (NAPA & APWA, 2000). The most common counter-flow drum in Kansas is the conventional one, which contains a burner inside the drum near the lower end; the aggregates enter the drum from the upper end. The drum portion in front of the flame is the drying zone. The dried and heated aggregates are then moved to the mixing zone behind the burner and are mixed with asphalt cement. If applicable, RAP is introduced into the mixing zone behind the burner to avoid high temperature and further aging of RAP.

5.3.2.3 Calibration

Calibration is required to ensure accurate production of the HMA mixture for all drum mix plants. The plant should be calibrated before the start of production of new HMA mixtures, and whenever the portable plant is relocated, the plant has shut down for a relatively long time, the supply system for the ingredient proportions is broken, or the material changes (AASHTO, 2017a; Kennedy et al., 1986). Calibration procedures require running some aggregates on the charging conveyor and recording the weight that passes over the weigh idler. Instead of delivering the aggregates into the drum mixer, a truck collects all aggregates and weights. KDOT requires belt-scale accuracy within 2% of the material weight (KDOT, 2015). If the tolerance is exceeded, the weighbridge should be adjusted following the manufacturer's guide so that two consecutive tests are within tolerance. The cold-feed bins should be calibrated by determining the flow of aggregates with different gate openings and belt speeds. The gate openings should be calibrated above, at, and below the estimated plant production rate. To calibrate the belt speed, 20%, 50%, and 80% of the maximum feeder belt speed are selected (NAPA & APWA, 2000; Kennedy et al., 1986). The contractors typically set up the gate opening based on experience and then calibrate the speed of the feeder belt bracket to match the anticipated production rates. The drum mix plant's asphalt cement pump and meter system must be calibrated to ensure the correct amount of asphalt binder is injected into the mix. An empty, clean distributor truck must carry the binder and pump it back to the storage tank. After pumping the needed amount of asphalt cement, the weight of the distributor truck is taken over a certified scale, and the net weight is calculated. The plant console catches the reading of the metering system and calculates the weight. These two values should be within the required tolerance, typically 2% in Kansas (KDOT, 2015).

5.3.3 Reclaimed Materials in HMA Mixture Production

Using recycled materials such as RAP and RAS in asphalt pavement construction can decrease the demand for new materials such as virgin binders and aggregates, consequently lowering material costs and preserving natural resources.

5.3.3.1 Reclaimed Asphalt Pavement

Although 1,915 asphalt pavements were initially recycled, standard use of RAP did not become a practice until crude oil prices increased significantly due to the Arab oil embargo in 1973 (West, 2015; Copeland, 2011). RAP is collected from milling, full-depth pavement removal, and occasional plant waste during production. Asphalt milling is a pavement rehabilitation process that typically removes rutting from the surface to produce a smooth, even surface for repaving. In comparison, full-depth pavement demolition breaks down the entire pavement into chunks with heavy equipment and then crushes it into manageable sizes for reuse. Plant waste is stored in a separate stockpile or added to the unprocessed RAP stockpile for future processing (Copeland, 2011).

Although using an HMA mixture with RAP has many advantages, recycled materials often demonstrate decreased durability, precisely due to the aged asphalt binder from RAP. Most states allow 0% to 30% recycled materials in HMA mixtures. Studies have shown that in mixtures containing up to 20% RAP, aged binders do not significantly influence the blended binder properties (Kennedy et al., 1998). However, increased percentages of RAP could dramatically affect the performance of the blended binder (Al-Qadi et al., 2007). According to the AASHTO (2017b) Superpave mix design specification, the binder performance grade (PG) level of the binder performance grade (PG) must be reduced by one when using more than 15% RAP. When adding more than 25% RAP, the virgin binder PG should be determined according to the properties of the RAP binder.

Daniel and Lachance (2005) found that a mixture with 15% RAP had increased stiffness but lower creep compliance, indicating that the mix with RAP is more resistant to permanent deformation and less resistant to fatigue and thermal cracking. The 25% and 40% RAP mixtures had higher voids in mineral aggregate (VMA) and voids filled with asphalt (VFA), making the mixture soft, decreasing the dynamic modulus, and increasing creep compliance.

Shu et al. (2008) found that mixtures containing RAP demonstrated increased tensile strength and decreased post-failure tenacity. The dissipated creep strain energy and energy ratio decreased, resulting in a short fatigue life of HMA mixtures. Plateau values from the beam fatigue test showed that including RAP would need more input energy for damage, thereby shortening the fatigue life.

Izaks et al. (2015) concluded high RAP content decreases fatigue resistance. An HMA mixture could be designed with up to 50% RAP since RAP has no significant effect on volumetric and mechanical properties. They determined that increasing the effective asphalt content of the recycled asphalt mixtures increases mixture durability and fatigue resistance.

Hong et al. (2010) analyzed the field data of several pavement sections in Texas with 35% RAP from 1991 to 2007. Overall, the sections performed relatively satisfactorily during the monitoring period. However, the area with 35% RAP had more prevalent cracking, less rut depth, and similar roughness than the pavement without RAP. The researchers concluded that, with proper mix design, the performance of a pavement containing up to 35% RAP would be identical to that of pavements without RAP during an average pavement life span.

5.3.3.2Reclaimed Asphalt Shingles

RAS is typically derived from tear-offs of roofs and manufactured shingle waste. Three essential components comprise RAS: fibers, asphalt cement, and mineral granules. In the late 1980s, the first shingle recycling was established, and the investigation of HMA with RAS began (Epps & Paulsen, 1986; Aschenbrener, 2018). Most RAS is used for paving projects. After grounding the shingles into particles, the large particles can be used for base stabilization, while the small particles are used in the surface course. AASHTO MP 23-15 (2021) is the current standard specification for RAS usage in asphalt mixtures. Due to the angular and hard granules in RAS, the VMA of the HMA with RAS has increased, indicating that the mixture is less susceptible to cracking (Willis & Turner, 2016). However, the asphalt binder in RAS is more aged, oxidized, and much stiffer and brittle than virgin binders, likely decreasing the mixture's cracking resistance (Stroup-Gardiner, 2016). Typically, 3%–5% RAS by weight or approximately 15%–20% binder replacement is used in asphalt mix design (Aschenbrener, 2018; Hand et al., 2021). State DOTs also have specific requirements for RAS use in combination with RAP.

5.3.3.3 Summary

Although some DOTs allow increased amounts of recycled materials in HMA mixtures, the effect of high percentages of recycled materials on long-term pavement performance is a significant concern. Therefore, consistently controlling recycled materials during HMA processing and production in a drum mix plant is critical. An Asphalt Concrete (AC) mass-balanced method calculates the percentage of RAP and RAS with quality control (QC) and quality assurance (QA) data to verify the usage of recycled materials. Therefore, process control is crucial in the production of HMA.

5.4 Objective

This study investigated the QC/QA process in HMA production to ensure proper RAP feed in the drum-mix plant. The study studied time-series data from drum-mix HMA plant production and then compared the data to the calculated results to find improvement in process control.

5.5 Plant Investigation

Researchers for the current study visited four portable plants of projects on US-83, US-36, US-24, and K-23 in KDOT District 3 (northwest Kansas); two mobile plants for projects on K-15 and I-135 in District 2 (south-central Kansas); and one portable plant for a project in District 1 (eastern Kansas).

5.5.1 Project and Superpave Mixture Data

Process control and quality assurance data on RAP contents were collected from the seven projects, and the mixture information of these projects is shown in Table 5.3.

Table 5.3. Study Project and Superpave HMA Data

Project No.	U083-020 KA 5662-01	U036-20 KA 5663-01	24-90 KA-5343-01	32 KA 5550-01	15-106 KA 5865-01	K031-099 KA 6316-01	I135-85 KA 6064-01
Route	US-83	US-36	US-24	K-32	K-15	K-31	I-135
%RAP	25	25	25	25	20	25	25
Target % AC	5.30	5.20	5.20	5.20	5.60	5.90	5.20
% AC (Total Mix)	5.05	5.07	5.31	5.38	5.99	6.23	5.51
Absorbed % AC	0.66	0.51	0.44	0.12	0.74	1.29	0.80
Effective % AC	4.42	4.59	4.89	5.27	5.29	5.02	4.75
% VMA	13.6	14.0	14.0	14.6	14.7	14.0	14.8
% Air Voids	3.45	3.59	2.84	2.61	3.03	2.62	4.23
% VFA	74	74	80	82	79	82	72
Dust/Binder Ratio	1.1	1.0	0.9	0.8	0.7	1.1	1.0

5.5.2 Totalizer Data

The plant operation data was obtained periodically from seven projects for up to three days. Flow rates, such as the feed rate of the virgin aggregates and RAP from the totalizer, were collected every 10 to 15 minutes during mix production. Plant calibration was observed on the first day of the project. The weighbridge measured virgin aggregate and RAP weights, and after correcting for moisture, the system continuously calculated dry weight. This information was recorded for this project every 30 minutes. These weight values were used to calculate the RAP percentage in the HMA mixture, which is the percentage of the aggregate blend, including virgin aggregate and RAP, not a portion of the entire mix. RAP percentage calculation results are shown in Table 5.4, along with the JMF RAP percentage of each project.

Table 5.4. RAP Percentage Calculated from Totalizer Data

Project No.	JMF RAP Content (%)	Plant Operation Data							
		Feed Rate				Totalizer			
		Mean % RAP	Std. Dev.	COV (%)	No.	Mean % RAP	Std. Dev.	COV (%)	No.
U083-020 KA 5662-01	25	23.7	0.007	2.9	45	23.7	0.001	0.5	17
U036-20 KA 5663-01	25	23.5	0.008	3.3	52	23.9	0.005	2.3	24
24-90 KA-5343-01	25	22.7	0.010	4.3	78	23.4	0.006	2.6	23
32 KA 5550-01	25	23.5	0.009	4.0	78	23.2	0.010	4.3	25
15-106 KA 5865-01	20	19.8	0.008	3.8	86	19.9	0.008	3.8	25
K031-099 KA 6316-01	25	24.3	0.005	2.0	73	24.2	0.002	1.0	22
I135-85 KA 6064-01	25	25.0	0.006	2.5	85	24.5	0.009	3.5	19

As shown in the table, the totalized RAP percentage did not exceed the maximum RAP level in JMF, and the RAP percentages determined by the totalizer were consistent with the target feed rates. The low coefficients of variation of the rate data indicate precise process control.

5.5.3 AC Mass-Balance Method

The QC/QA data from the HMA mixture and RAP and the total quantity of HMA mixture and virgin AC were collected from the contractor and KDOT after construction. Table 5.5 shows the back-calculation results of the RAP percentages compared to the totalizer results.

Table 5.5. RAP Percentage Comparison

Project No.	JMF RAP Content	Mean RAP Quantity (%)		
		Back calculated (Equation (2))	Plant Operation Data	
			Feed Rate	Totalizer
U083-020 KA 5662-01	25	28.6	23.7	23.7
U036-20 KA 5663-01	25	27.6	23.5	24.0
24-90 KA-5343-01	25	26.6	22.7	23.4
32 KA 5550-01	25	26.7	23.5	23.0
15-106 KA 5865-01	20	18.4	19.8	19.9
K031-099 KA 6316-01	25	25.6	24.3	24.2
I135-85 KA 6064-01	25	29.7	25.0%	24.5%

Significant differences between the RAP quantities from the back-calculated (theoretical mass-balance) method and the totalizer data from the four projects were highly concerning to KDOT. RAP binder contents on K-32 from the contractor (QC) and KDOT (QA) differed significantly. The RAP samples were collected from different parts of a stockpile or milling site. In current QC practices for RAP in Kansas, the contractor collects RAP sample once during the first lot and once per 1,000 tons of RAP. For QA, KDOT conducts one test during the first lot and one per 4,000 tons of RAP (KDOT, 2015; KDOT, 2022b). The average values of the RAP binder content and calculated RAP percentages from Project 32 KA 5550-01 are shown in Table 5.6.

Table 5.6. RAP and AC Content from Project 32 KA 5550-01

Quantity (%)	JMF	Total	KDOT	Contractor
RAP Binder	5.2	6.3	7.8	5.8
RAP	25	23.3	18.7	25.4

The table shows that KDOT QA data showed a high RAP binder content (7.8%), decreasing the RAP percentage. The contractor's QC result for the binder content of RAP was 5.8%, which increased the RAP percentage, proving that the binder content of RAP significantly impacted the RAP percentage. Burn-off tests were done in the laboratory at Kansas State University to investigate the influence of binder contents in RAP and HMA mixtures further, and the RAP binder results from KDOT and the contractor were compared.

5.5.4 Burn-Off Tests

Two other projects (K-31 and I-135) were visited later as a follow-up to this study. Plant operation data were obtained, and RAP and HMA mixtures were collected for burn-off tests according to the Kansas standard test method KT-57. The HMA mixtures were randomly collected behind the paver, and the RAP samples were collected via the outlet on the RAP belt conveyor. The sampling of the HMA mixture and RAP was independent and not correlated. 1,500 grams of HMA mixtures and 2,000 grams of RAP samples were used for the burn-off tests. The test samples were preheated under 110 ±5 °C to dry to a constant mass and to ensure all particles were spread evenly on the basket. After cooling the samples to room temperature, the mass of the sample and basket was recorded. The initial sample weight was calculated from the mass of the sample and basket minus the mass of the empty basket. The sample was put into the ignition oven at a temperature of 500°C, burned until it was free of asphalt, and then removed from the furnace to cool to room temperature. The weight was re-recorded, and the total weight of the aggregate after ignition was calculated. Equation 5.3 was then used to calculate the binder content of the sample:

$$\boldsymbol{AC}\% = \left[\frac{(\boldsymbol{W_S}-\boldsymbol{W_A})}{\boldsymbol{W_A}} \times \mathbf{100}\right] - \boldsymbol{C_F} \qquad \text{Equation 5.3}$$

Where:

AC% is measured (corrected) asphalt content percent by mass of the sample;

W_A is the total mass of aggregate remaining after ignition;

W_S is the total mass of the sample before ignition; and

C_F is the calibration factor, the percent of the mass of the HMA sample.

Table 5.7 compares the burn-off test results to the QC and QA results obtained from KDOT and the contractor.

Table 5.7. AC Content from Burn-Off Tests

AC (%)	Project No.			
	K031-099 KA 6316-01		I135-85 KA 6064-0135	
	HMA	RAP	HMA	RAP
JMF	5.90%	-	5.40%	-
QC	6.00%	7.03%	5.38%	5.66%*
QA	6.07%	7.52%	5.38%	6.11%
KSU Lab	6.12%	6.57%	5.45%	5.57%

*in mix design submittal

Results in Table 5.7 show no significant differences between the asphalt binder contents for the HMA mixtures on both projects. However, the RAP asphalt content test results from multiple labs showed differences. That, in turn, affected the calculated RAP contents from Equations (1) and (2). The RAP percentage calculation results based on QC, QA, and laboratory results are shown in Table 5.8, along with the RAP content obtained from the plant operation data. KSU results indicate that much higher quantities of RAP than in the JMF were introduced.

Table 5.8. RAP Percentages Based on QC, QA, and Laboratory Burn-Off Test Results

Project No.	JMF	Mean RAP Quantity (%)				
		AC Mass-Balance Data			Plant Operation Data	
		QC	QA	KSU Lab	Feed Rate	Totalizer
K031-099 KA 6316-01	25	25.8	24.1	27.6	24.3	24.2
I135-85 KA 6064-0135	25	31.4	29.1	32.0	25.0	24.5

5.6 Data Analysis

5.6.1 Statistical Analysis

5.6.1.1 RAP Percentage

In this RAP percentage analysis, a one-way treatment design with a fixed factor: method at three levels - feeding rate, totalizer, and AC mass balance was applied. Project number was considered as a random factor at seven levels which accounted for the variability that was not attributable to the different methods. A linear mixed model was used to explore the differences in RAP percentages with various calculation methods:

$$y_{ij} = \mu + \alpha_i + \beta_j + \varepsilon_{ij} \qquad \text{Equation 5.4}$$

Where,

y is the response variable (RAP percentage);

μ is the intercept;

α_i is the effect of i^{th} level of method; i = 1, 2, 3;

β_j is the random effect of the j^{th} level of project number, j = 1, 2, 3, 4, 5, 6, 7;

ε_{ij} is the response error from the i^{th} method and j^{th} project.

The Type III test results are shown in Table 5.9. The p-value is smaller than 0.05, demonstrating that the method contributes significantly to the RAP percentage determination.

Table 5.9. Type III Tests of RAP Percentage

Effect	Num DF	Den DF	F value	Pr > F
Method	2	681	27.83	<.0001

Table 5.10. Differences of LS-Means for Multiple Comparisons of RAP Percentage

Method	Method	Estimate	Standard Error	DF	t Value	Pr > |t|
Feeding Rate	Totalizer	-0.03	0.08	681	-0.41	0.6829
Feeding Rate	AC Mass-Balance	-2.36	0.32	681	-7.46	<.0001
Totalizer	AC Mass-Balance	-2.33	0.32	681	-7.25	<.0001

Table 5.11. T Grouping for Method LS-Means of RAP Percentage (Alpha = 0.05)

Method	Estimate	
AC Mass-Balance	25.59	A
Totalizer	23.26	B
		B
Feeding Rate	23.22	B

*LS-means with the same letter are not significantly different.

LS-means results of RAP percentage are shown in Table 5.10 and Table 5.11. The p-value is larger than 0.05 for the comparison between the feeding rate method and totalizer method, which indicates that the feeding rate method and totalizer method will have no significant difference in determining RAP percentage. The difference between the AC mass-balance method and the totalizer or feeding rate method differed significantly since the p-values are less than 0.0001. Table 5.11 illustrates the same conclusion. The AC mass-balance method obtains a higher RAP percentage and shows a significant difference between the RAP percentages obtained from the totalizer method and the feeding rate method.

5.6.1.2 RAP Binder Content

In the RAP binder content analysis, two factors were considered. One was the operator at three levels: QC, QA, and KSU lab which defined the treatment structure as a two-way experimental design. The other one is a random factor: project number at seven levels which accounted for the variability that was not attributable to the operator level. The following linear mixed model was used to investigate the differences in RAP binder content with different operators:

$$\boldsymbol{y_{ij}} = \boldsymbol{\mu} + \boldsymbol{\alpha_i} + \boldsymbol{\beta_j} + \boldsymbol{\varepsilon_{ij}} \quad \text{Equation 5.5}$$

Where,

y is the response variable (RAP percentage);

μ is the intercept;

α_i is the effect of the i^{th} level of the operator; i = 1, 2, 3;

β_j is the random effect of the j^{th} level of project number, j = 1, 2, 3, 4, 5, 6, 7;

ε_{ij} is the response error from the i^{th} method and j^{th} project.

Table 5.12 illustrates the Type III test results of RAP binder content. The p-value is smaller than 0.05, indicating that the operator significantly influences the RAP binder content.

Table 5.12. Type III Tests of RAP Binder Content

Effect	Num DF	Den DF	F value	Pr > F
Operator	2	60	33.22	<.0001

Table 5.13. Differences of LS-Means for Multiple Comparisons of RAP Binder Content

Operator	Operator	Estimate	Standard Error	DF	t Value	Pr > │t│
QC	QA	-0.96	0.12	60	-8.06	<.0001
QC	KSU Lab	-0.18	0.09	60	-1.92	0.0593
QA	KSU Lab	0.78	0.12	60	6.54	<.0001

Table 5.14. T Grouping for Method LS-Means of RAP Binder Content (Alpha = 0.05)

Operator	Estimate	
QA	6.63	A
KSU Lab	5.85	B
		B
QC	5.67	B

*LS-means with the same letter are not significantly different.

LS-means results of RAP percentage are shown in Table 5.13 and Table 5.14. The p-value of comparison between QC and KSU lab RAP binder content results is larger than 0.05, indicating no significant difference in RAP binder content between QC and KSU lab. The difference between QA and QC or KSU lab differed significantly since the p-values are less than 0.0001. Table 5.14 illustrates the same conclusion.

5.6.2 Monte Carlo Simulation

The Monte Carlo simulation is a statistical method that predicts the probability of output using random variables and repeated random sampling. In other words, the technique can quantitatively account for risk in forecasting and decision-making (Kroese et al., 2014). This study used Scilab for the Monte Carlo simulations to randomly generate binder content in the RAP and HMA mixture, calculate the RAP quantity, and generate its probability distribution. Scilab is a user-friendly scientific computation software for numerical computations and algorithm testing (Baudin, 2010).

To start a Monte Carlo simulation, a functional equation was created in the software to determine the RAP quantity (Equation 5.2), and then the input parameters were defined in the software. The total amount of HMA mixture produced, and the total binder usage was considered constant values. Two variables, the binder contents measured in RAP and HMA, were randomly generated with a specified mean and standard deviation following a normal distribution. The average values were collected from each project's QC/QA burn-off test results, and standard deviation values were calculated and used as inputs in the software, as shown in Table 5.9. In addition, the multi-laboratory precision, which is 0.117%, from the Kansas test method KT-57 (2002b) was also used and compared to the simulation results of the collected RAP binder content standard deviation. An extensive random data set was needed to perform the simulation because more data provided an anticipated input variation, providing a reliable indication of the outputs. In this study, 5,000,000 was used for each variable to generate and obtain the RAP quantity. Histogram plots were also developed to show the RAP percentage distribution, as illustrated in Figures 5.6 and 5.7. Figure 5.6 shows the RAP quantity distribution gathered using the standard deviation of the QC/QA data, which simulated the "in-field" situation. Figure 5.7 shows an "ideal" distribution of the RAP quantity using the KT-57 standard precision. Also, the risks of the RAP quantity exceeding the JMF value were calculated, as shown in Table 5.9.

Table 5.15. Risk of RAP Percentages over JMF

Project No.	Design HMA P_b (%)	Average HMA P_b (%)	Std. Dev.	No.	Average RAP P_b (%)	Std. Dev.	No.	Risk* (%)	Risk** (%)
U083-020 KA 5662-01	5.30	5.26	0.001	45	5.41	0.003	11	91.0	94.2
U036-20 KA 5663-01	5.30	5.26	0.001	45	5.41	0.003	11	82.6	86.5
24-90 KA-5343-01	5.20	5.19	0.002	32	5.47	0.002	8	68.7	75.3
32 KA 5550-01	5.20	5.31	0.002	35	6.29	0.010	8	37.5	19.9
15-106 KA 5865-01	5.60	5.60	0.001	45	7.94	0.005	7	24.1	14.8
K031-099 KA 6316-01	5.90	6.02	0.002	68	7.07	0.002	14	59.1	63.6
I135-85 KA 6064-01	5.40	5.38	0.002	60	6.11	0.003	3	88.9	98.7

* Collected Data Std. Dev. Bias ** KT-57 Multi Lab Precision

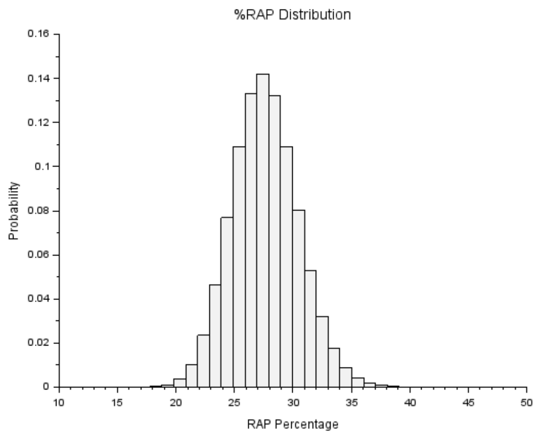

(a) U036-20 KA 5663-01

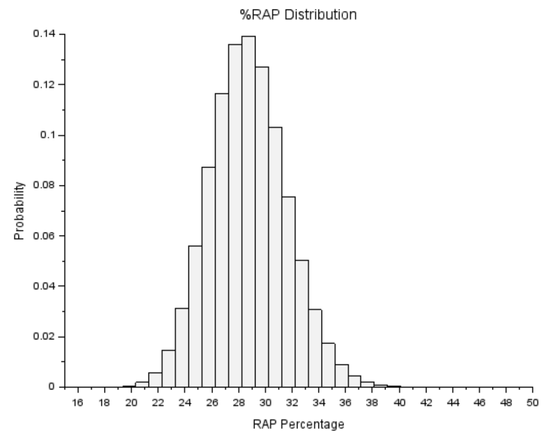

(b) U083-020 KA 5662-01

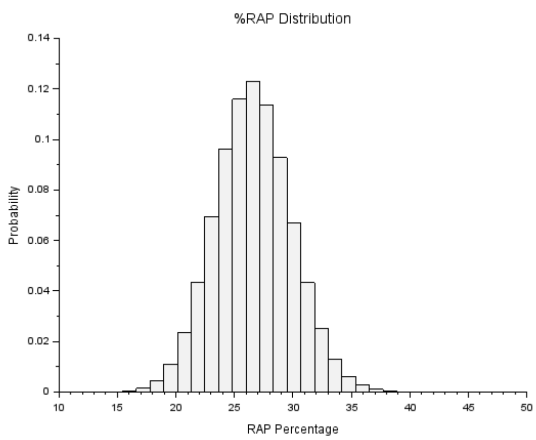

(c) 24-90 KA-5343-01

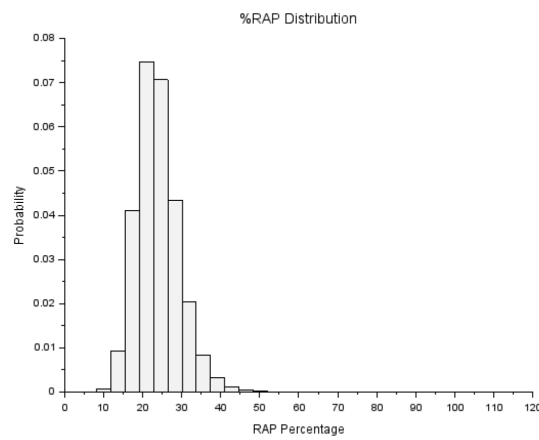

(d) 32 KA 5550-01

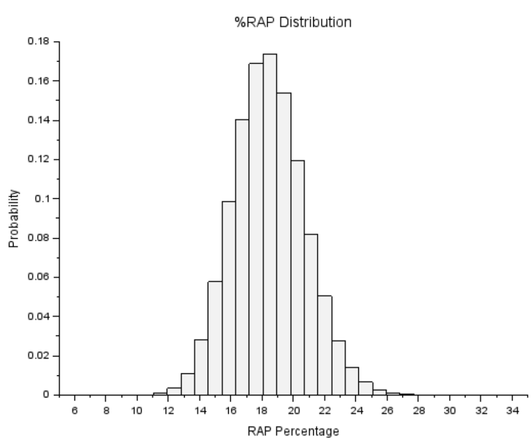

(e) 15-106 KA 5865-01

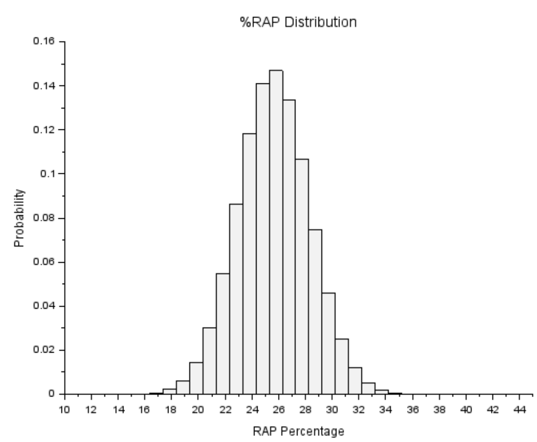

(f) K031-099 KA 6316-01

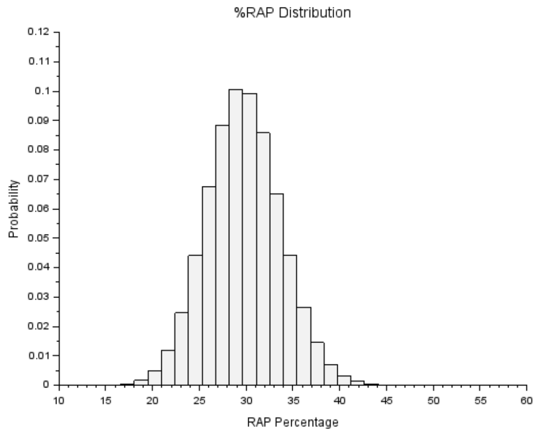

(g) I135-85 KA 6064-01

Figure 5.6. RAP Percentage Distribution based on Collected RAP Binder Content Standard Deviation

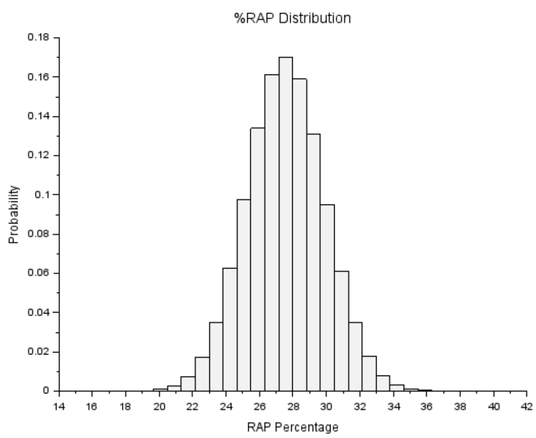

(a) U036-20 KA 5663-01

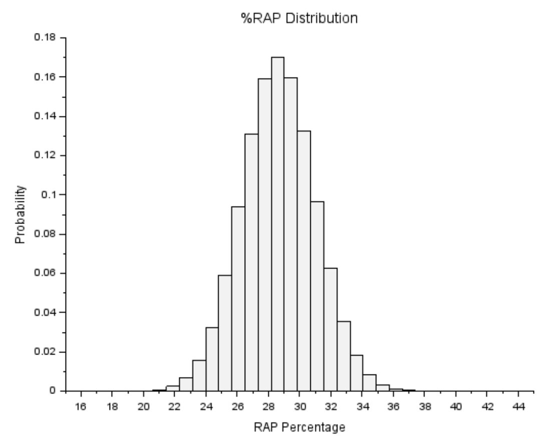

(b) U083-020 KA 5662-01

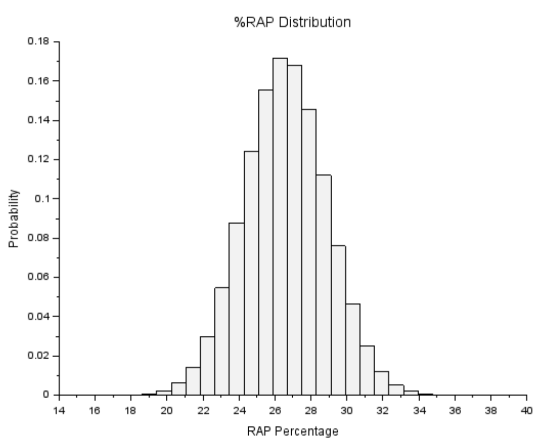

(c) 24-90 KA-5343-01

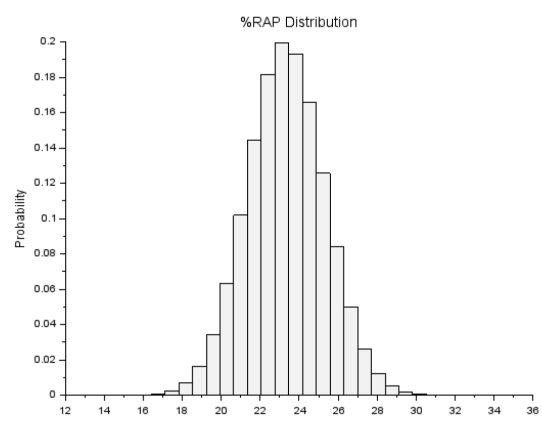

(d) 32 KA 5550-01

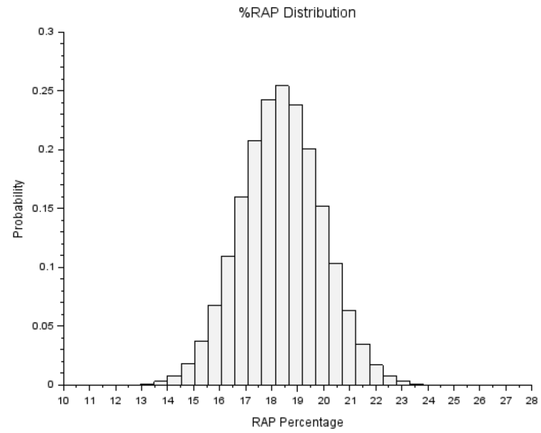

(e) 15-106 KA 5865-01

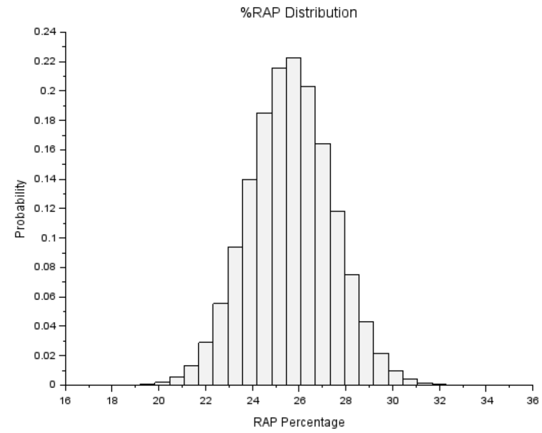

(f) K031-099 KA 6316-01

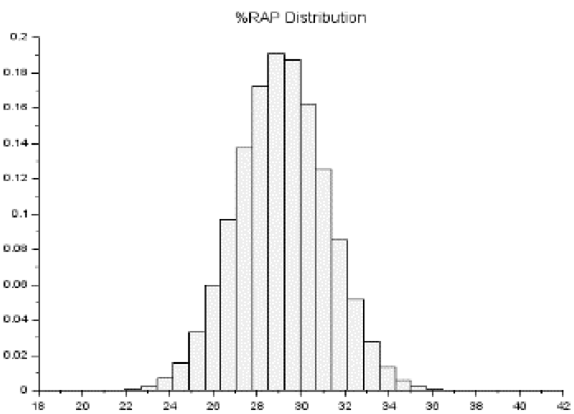

(g) I135-85 KA 6064-01

Figure 5.7. RAP Quantity Distribution based on KT-57 Multi Lab Precision

Figures 5.6 and 5.7 show that most simulated RAP quantities follow a normal distribution except the simulation with the collected data. The RAP quantity distribution chart is shifted to the left based on the collected data standard deviation. As shown in Table 5.9, the standard deviation of collected data of the 32 KA 5550-01 project went up to 0.01 because of the vast difference between QC and QA burn-off results and fewer data points, as shown in Table 5.8. This higher standard deviation would cause some “outstanding” simulation results. However, the probabilities were extremely low, which is hard to see in the distribution chart.

The burn-off results for the HMA mixture were very close to, or the same as, the design/JMF binder content of the HMA mixture, and the standard deviation values of QC/QA data were very close to 0.00117, the expected precision. The standard deviation of RAP binder content ranged from 0.002 to 0.010, resulting in fewer collected data points. Therefore, the RAP binder content was shown to be the variable that most significantly affected the RAP percentage, thereby increasing the risk of exceeding the target RAP percentage.

Comparing the distribution charts with different standard deviations, the graphs with KT-57 standard precision had narrow ranges of the RAP quantity but higher probabilities, thereby increasing the risk. However, for projects, 32 KA 5550-01 and 15-106 KA 5865-01, the risks with standard test precision decreased since the back-calculated results were within the target RAP percentage, and a lower standard deviation would further narrow down the possibility of exceeding the target value.

5.7 Conclusions & Recommendations

5.7.1 Conclusions

This study investigated computing RAP quantities using the totalizer method in the HMA drum mix plant and back-calculation after production. The RAP quantity determined by the totalizer method was steady and did not exceed the designed RAP percentage. However, a significant difference was sometimes observed between the theoretical RAP quantity and the totalizer. For example, when the burn-off test results of binder content in RAP from the contractor and KDOT differed, varying RAP quantities were observed; a high RAP binder content decreased the RAP feed rate in the drum mix plant. Follow-up investigations showed significant differences in burn-off test results from multiple labs, indicating that RAP AC binder influences the calculated (theoretical) RAP quantity. Statistical and Monte Carlo simulation analyses also supported this observation.

5.7.2 Recommendations

The percentage of RAP usage in the projects (20% –25%) and the volume of HMA production on each project limit the testing frequency for the RAP binder content. Small sample sizes may increase variability and decrease the precision of the RAP quantity analysis. Therefore, a higher frequency for testing the RAP AC content is recommended to enlarge the population and, in turn, reduce variability.

Chapter 6 - Conclusions & Recommendations

In this study, the performance properties of an HMA mixture with carbon char were first investigated via performance tests for moisture resistance and rutting. It was revealed that carbon char in small quantities can improve moisture resistance but reduce rutting resistance. No interaction with the asphalt binder was apparent. Next, the HMA mixture with coal combustion products was tested, and the results showed that adding 15% fly ash to the asphalt binder would have a similar performance in rutting, fracture cracking, and moisture susceptibility to the HMA mixture without fly ash. Statistical analyses confirmed these observations. Also, no interaction between the fly ash and the asphalt binder was apparent from the SEM study. Then, the rheological properties of asphalt binders with varying Recycled Engine Oil Bottom (REOB) content were studied. A hand-held XRF spectrometer can detect some of the "signature" elements of REOB. The addition of REOB reduced the stiffness at high temperatures and improved the low-temperature properties of the binder, as found in the statistical analysis. Finally, an investigation of QC/QA of recycled materials quantity in HMA was conducted. The theoretical RAP quantities in the produced mix varied due to differences in the RAP burn-off test results between the labs in the QC/QA process. Statistical and Monte Carlo simulation analyses confirmed this finding. A more frequent RAP binder determination was suggested as a remedy.

Using recycled materials in HMA mixtures looks enticing due to increasing environmental awareness and the need for sustainable construction practices. However, when selecting and managing recycled materials, one should be careful to achieve sustainable and cost-effective road construction practices while meeting performance requirements. The fundamental interaction between recycled material and asphalt binders should be studied first to ensure the role of recycled materials. Although suggested in the literature, no fundamental interaction was detected between carbon char and fly ash and asphalt. This resulted from these materials' role as mineral fillers, not asphalt additives. Also, the QC/QA process during HMA production using RAP should be enhanced since the input RAP properties determine the quantity of RAP being used. In most cases, there is a higher limit on this quantity.

References

AASHTO. (2009). *Determining Dynamic Modulus of Hot Mix Asphalt* (TP 62-07). American Association of State Highway and Transportation Officials.

AASHTO. (2017a). *Standard specification for requirements for mixing plants for hot-mixed, hot-laid bituminous paving mixtures* (M 156-13). American Association of State Highway and Transportation Officials.

AASHTO. (2017b). *Standard specification for Superpave volumetric mix design* (M 323). American Association of State Highway and Transportation Officials.

AASHTO. (2018). *Standard test method for Determining the Damage Characteristic Curve of Asphalt Mixtures from Direct Tension Cyclic Fatigue Tests* (TP 107). American Association of State Highway and Transportation Officials.

AASHTO. (2021). *Standard specification for reclaimed asphalt shingles for use in asphalt mixtures* (MP 23-15)—American Association of State Highway and Transportation Officials.

Ahmedzade, P., & Geckil, T. (2007). Influence of carbon black on the mechanical and electrical properties of asphalt mixtures.

Alfayez, S. A., Suleiman, A. R., & Nehdi, M. L. (2020). Recycling tire rubber in asphalt pavements: State of the art. *Sustainability, 12*(21), 9076.

Al-Qadi, I. L., Elseifi, M., & Carpenter, S. H. (2007). *Reclaimed asphalt pavement: A literature review* (FHWA-ICT-07-001). Illinois Center for Transportation.

Anderson, R. M., G. King, D. Hanson, and P. Blankenship. (2011). Evaluation of the Relationship Between Asphalt Binder Properties and Non-Load Related Cracking. Asphalt Paving Technology: Association of Asphalt Paving Technologists-Proceedings of the Technical, Sessions. 80.

Arnold, T. S., and A. Shastry. (2015). The Analysis of Asphalt Binders for Recycled Engine Oil Bottoms by X-ray fluorescence Spectroscopy. *TRB 94th Annual Meeting Compendium of Papers*, No. 15-2117.

Asi, I., and Assa'ad, A. (2005). "Effect of Jordanian oil shale fly ash on asphalt mixes." *Journal of Materials in Civil Engineering*, *17*(5): 553-559.

Aschenbrener, T. (2018). *FHWA division office survey on state highway agency usage of reclaimed asphalt shingles: Quantities, trends, requirements, and direction-Results from May 2017* (No. FHWA-HIF-18-009). Federal Highway Administration. https://rosap.ntl.bts.gov/view/dot/38319/dot_38319_DS1.pdf.

Asphalt Institute (AI). (2016). *State-Of-The-Knowledge: The Use Of REOB/VTAE In Asphalt*, IS-235, First Edition, AI, Lexington, KY.

Barborak, R. C., Coward Jr, C. E., & Lee, R. E. (2016). Detection and estimation of Re-refined engine oil bottoms in asphalt binders: Texas department of transportation's approach with wavelength dispersive X-ray fluorescence spectroscopy. *Transportation Research Record, 2574*(1), 48-56. Bautista, E. (2015). "Experimental evaluation of the effect of coal combustion products on constructability, damage and aging resistance of asphalt mastics." Theses and Dissertations. 858. Retrieved from http://dc.uwm.edu/etd/858

Baudin, M. (January 2010). Introduction to Scilab. Consortium Scilab. 34–56.

Bennert, T., Ericson, C., Pezeshki, D., Haas, E., Shamborovskyy, R., & Corun, R. (2016). Laboratory performance of re-refined engine oil bottoms (REOB) modified asphalt. In *Asphalt Paving Technology 2016, AAPT 2016* (pp. 163-207). Association of Asphalt Paving Technologist. Bolker, B. M. (2015). Linear and generalized linear mixed models. *Ecological statistics: contemporary theory and application*, 309-333.

Bruker. (2018). Handheld XRF: How it works, https://www.bruker.com/products/x-ray-diffraction-and-elemental-analysis/handheld-xrf/how-xrf-works.html. Accessed on Oct. 15, 2018.

Bukowski, J., & Harman, T. (2014). *The Use of Recycled Tire Rubber to Modify Asphalt Binder and Mixtures*. Research Report No. FHWA-HIF-14-015. Office of Asset Management, Pavements, and Construction, Federal Highway Administration, US Department of Transportation, Washington, DC.

Chesner, W. H., Collins, R. J., MacKay, M. H., & Emery, J. (2002). *User guidelines for waste and by-product materials in pavement construction* (No. FHWA-RD-97-148, Guideline Manual, Report No. 480017). Recycled Materials Resource Center. https://rosap.ntl.bts.gov/view/dot/38365/dot_38365_DS1.pdf

Chiu, C. T., Hsu, T. H., & Yang, W. F. (2008). Life cycle assessment on using recycled materials for rehabilitating asphalt pavements. *Resources, conservation and recycling, 52*(3), 545-556.

Copeland, A. (2011). *Reclaimed asphalt pavement in asphalt mixtures: State of the practice*. (No. FHWA-HRT-11-021). Federal Highway Administration. https://rosap.ntl.bts.gov/view/dot/40918/dot_40918_DS1.pdf

D'Angelo, J., K. Grzybowski, S. Lewis. (2013). Evaluation of the Performance of Asphalt Mixes Produced with Re-refined Heavy Vacuum Distillate Bottoms. Canadian Technical Asphalt Association, Vol. 58.

Daniel, J. S., & Lachance, A. (2005). Mechanistic and volumetric properties of asphalt mixtures with recycled asphalt pavement. *Transportation Research Record, 1929*(1), 28–36. https://doi.org/10.1177/0361198105192900104

Epps, J. A., & Paulsen, G. L. (1986). *Use of roofing wastes in asphalt paving mixtures: Economic considerations* (Report 709-2). Center for Construction Materials Research, University of Nevada.

Faheem, A.F., Cloutier, C., Bautista, E. and Sobolev, K. (2017). "Impact of coal combustion products incorporation in asphalt mixture performance." Paper presented at the TRB Annual Meeting, Transportation Research Board, Washington, D.C.

FHWA. (2015). FHWA Asphalt Binder ETG, REOB – Re-refine Engine Oil Bottoms Residue – Task Force, Report to the September 2015 FHWA Binder ETG, 2015.

FHWA. (2015, September). FHWA Recycled Materials Policy. Washington: Federal Highway Administration. https://www.fhwa.dot.gov/legsregs/directives/policy/recmatpolicy.htm. Accessed on October 4, 2022.

FHWA. (2021). Highway Statistics 2020. Washington: Federal Highway Administration.

Golestani, B. (2015). Sustainable material solution for flexible pavements; performance evaluation and impact assessment of utilizing multiple recycled materials in HMA.

Gong, F.; Guo, S.; Chen, S.; You, Z.; Liu, Y.; Dai, Q. (2019). Strength and durability of dry-processed stone matrix asphalt containing cement pre-coated scrap tire rubber particles. *Constr. Build. Mater. 214*, 475–483.

Hand, A., Aschenbrener, T., & Cooper, S. (2021). *Practices and lessons learned using reclaimed asphalt shingles in asphalt mixtures* (No. FHWA-HIF-22-001). Federal Highway Administration.

Henning, N.E. 1974. *Evaluation of lignite fly ash as a mineral filler in asphaltic concrete*. Report No. Item 2 (73). Twin City Testing and Engineering Laboratory, St. Paul, Minnesota.

Hesp, S. A. M., and H. F. Shurvell. (2013). Quality assurance testing of asphalt containing waste engine oil. 1st Int. Journal of Pavements Conf., International Journal of Pavements, São Paulo, Brazil.

Hong, F., Chen, D. H., & Mikhail, M. M. (2010). Long-term performance evaluation of recycled asphalt pavement results from Texas: Pavement studies category five sections from the long-term pavement performance program. *Transportation Research Record*, 2180(1), 58–66. https://doi.org/10.3141/2180-07

Horvath, A. (2003). Life-cycle environmental and economic assessment of using recycled materials for asphalt pavements. https://escholarship.org/uc/item/5jz3x91z

Izaks, R., Haritonovs, V., Klasa, I., & Zaumanis, M. J. P. E. (2015). Hot mix asphalt with high RAP content. *Procedia Engineering*, *114*, 676–684. https://doi.org/10.1016/j.proeng.2015.08.009

Kandhal, P. S. (1992). Waste materials in hot mix asphalt-an overview.

Kaskow, J., S. v. Poppelen, and S. A. M. Hesp. (2018). Methods for the Quantification of Recycled Engine Oil Bottoms in Performance-Graded Asphalt Cement. Journal of Materials in Civil Engineering, Volume 30, Issue 2, Content ID 04017269.

Karki, P., F. Zhou. (2018). Evaluation of Asphalt Binder Performance with Laboratory and Field Test Sections. Texas A&M Transportation Institute, Texas Department of Transportation, Federal Highway Administration, 102p.

KDOT. (2015). *Standard specifications for state road and bridge construction*. Kansas Department of Transportation.

KDOT. (2022a). *Resistance of Compacted Asphalt Mixture to Moisture-included Damage* (KT-56). Topeka, KS: Kansas Department of Transportation

KDOT. (2022b). *Determination of asphalt content and gradation of hot mix asphalt concrete by the ignition method* (KT-57). Topeka, KS: Kansas Department of Transportation

KDOT. (2022c). *Construction manual, Part V*: Materials. Kansas Department of Transportation

Kennedy, T. W., Scherocman, J. A., & Tahmoressi, M. (1986). *Drum mix plants: Equipment and operations.* The Center. https://library.ctr.utexas.edu/digitized/texasarchive/phase2/440-1f.pdf

Kennedy, T. W., Tam, W. O., & Solaimanian, M. (1998). Optimizing the use of reclaimed asphalt pavement with the Superpave system. *Journal of the Association of Asphalt Paving Technologists, 67.*

Kim, H.; Lee, S.; Amirkhanian, S. (2010). Rheology investigation of crumb rubber modified asphalt binders. *KSCE J. Civ. Eng. 14*, 839–843.

Kroese, D. P., Brereton, T., Taimre, T., & Botev, Z. I. (2014). Why the Monte Carlo method is so essential today. *Wiley Interdisciplinary Reviews: Computational Statistics, 6*(6), 386–392. https://doi.org/10.1002/wics.1314

Lee, J. C., Edil, T. B., Tinjum, J. M., & Benson, C. H. (2010). Quantitative assessment of environmental and economic benefits of recycled materials in highway construction. *Transportation research record, 2158*(1), 138-142.

Lenth, R. V. (2016). Least-squares means: the R package lsmeans. *Journal of statistical software, 69*, 1-33.

Lichte, F. E., Golightly, D. W., and Lamothe, P. J. (1987). “Inductively coupled plasma-atomic emission spectrometry.” Chapter B in: *Methods for Geochemical Analysis, US Geological Survey Bulletin 1770,* Baedecker, P.A. Eds., pp. B1–B10.

Martin, K. G. (1962). Preliminary microviscometer studies of carbon black/rubber/bitumen dispersions. In Australian Road Research Board (ARRB) Conference, 1st, 1962, Canberra (Vol. 1, No. 2)

Mirković, K., Tošić, N., & Mladenović, G. (2019). Effect of different types of fly ash on properties of asphalt mixtures. *Advances in civil engineering, 2019*, 1-11.

Mistry, R., Roy, T.K. (2016). "Effect of using fly ash as alternative filler in hot mix asphalt." *Perspectives in Science*, Volume 8, Pages 307-309.

Montaser, A. (1998), *Inductively Coupled Plasma Mass Spectrometry*, Wiley-VCH, Inc., NJ.

MPCA. (2014). Guidelines for managing industrial by-products from food, beverage and agro-industrial processing facilities. Minnesota Pollution Control Agency

NAPA (National Asphalt Pavement Association), & APWA (American Public Works Association). (2000). *Hot-mix asphalt paving handbook 2000* (No. AC 150/5370-14A, Appendix 1 (FAA)). United States Army Corps of Engineers. https://rosap.ntl.bts.gov/view/dot/42051

NAPA. (2024, April). *RAP Benefits for Pavement Owners*. https://www.asphaltpavement.org/uploads/documents/Sustainability/NAPA_RAP_Benefits_for_Pavement_Owners_1121.pdf

Notani, M. A., Arabzadeh, A., Satvati, S., Tarighati Tabesh, M., Ghafari Hashjin, N., Estakhri, S., & Alizadeh, M. (2020). Investigating the high-temperature performance and activation energy of carbon black-modified asphalt binder. *SN Applied Sciences, 2*, 1-12.

Oelofse, L. (2018). Using EDXRF to Quantify the Amount of Metals in Asphalt Binders. https://www.xenemetrix.com/images/Brochures/Articles/Article.pdf. Accessed on Oct. 1st, 2018.

Ozer, H., G. Renshaw, K. Hasiba, I. L. Al-Qadi. (2016). Evaluation of the Impacts of Re-Refined Engine Oil Bottoms (ReOB) on Performance Graded Asphalt Binders and Asphalt Mixtures. Civil Engineering Studies, Illinois Center for Transportation Series, University of Illinois, Urbana-Champaign, Illinois Department of Transportation, Federal Highway Administration, Issue 16-006, 55p

Park, T., Coree, B. J., & Lovell, C.W. (1996), Evaluation of Pyrolized Carbon Black from Scrap Tires as an Additive in Hot Mix Asphalt. Transportation Research Record: Journal of the Transportation Research Board, Vol. 1530, Issue 1, pp. 43–50.

Pihl, K. A., & Milvang-Jensen, O. (2001). The Motivation Factors in the Development and Sustainment of a Well-functioning Recycling Industry for Road and Non-road Byproducts in Denmark. *In Beneficial Use of Recycled Materials in Transportation Applications University of New Hampshire, Durham.*

RCB Nanotechnologies. (2023). Recovered Carbon Black. https://recovered-carbon-black.com/en/. Accessed on April 7, 2023.

Reinke, G., Hanz, A., Anderson, R. M., Ryan, M., Engber, S., & Herlitzka, D. (2016). Impact of re-refined engine oil bottoms on binder properties and mix performance on two pavements in Minnesota. In *Proceedings of the E&E Congress.*

Rosner, J.C., Chehovits, J.G., and Morris, G.R. (1982). Fly ash as a mineral filler and antistrip agent for asphalt concrete. Challenge of change-6th International Ash Utilization Symposium Proceedings. United States Department of Energy, Morgantown

Rostler, F. S., White, R.M., & Dannenberg, E.M. (1977), Carbon Black as a Reinforcing Agent for Asphalt. AAPT, Vol. 46, pp. 376 - 401.

Roberts, F. L., Kandhal, P. S., Brown, E. R., Lee, D. Y., & Kennedy, T. W. (1991). Hot mix asphalt materials, mixture design, and construction.

Rotational Viscometer. Pavement Interactive, Retrieved from https://www.pavementinteractive.org/reference-desk/testing/binder-tests/rotational-viscometer/. Accessed on Oct. 29, 2018.

Salehi, S., Arashpour, M., Kodikara, J., & Guppy, R. (2021). Sustainable pavement construction: A systematic literature review of environmental and economic analysis of recycled materials. *Journal of Cleaner Production, 313*, 127936.

SAS Institute Inc. (2018). The GLIMMIX procedure. In *SAS/STAT® 15.1 User's Guide*, pp. 1234-1278. SAS Institute Inc. Retrieved from https://documentation.sas.com/doc/en/statug/15.1/statug_glimmix_gettingstarted.htm

Shastry, A. (2018). Field Analysis of Asphalt Binders for Recycled Engine Oil Bottoms (REOB) Using Handheld XRF Spectrometers. TechBrief, 12p.

Shu, X., Huang, B., & Vukosavljevic, D. (2008). Laboratory evaluation of fatigue characteristics of recycled asphalt mixture. *Construction and Building Materials, 22*(7), 1323–1330. https://doi.org/10.1016/j.conbuildmat.2007.04.019

Stroup-Gardiner, M. (2016). *Use of reclaimed asphalt pavement and recycled shingles in asphalt mixtures* (No. Project 20-05, Topic 46-05). http://www.trb.org/Main/Blurbs/174969.aspx

Tapkın, S. (2008). "Mechanical evaluation of asphalt–aggregate mixtures prepared with fly ash as filler replacement." *Can. J. Civ. Eng*. 35: 27-40.

Tavakol, M. and Hossain, M. (2016). "Minimum Virgin Binder Limits in Recycled Superpave Mixes in Kansas." *Kansas State University Transportation Center*, Report No. K-TRAN: KSU-13-5

Texas Department of Transportation. (2014) Hamburg Wheel-Tracking Test (Twx-242-F). Taxes Department of Transportation. Retrieved from https://ftp.dot.state.tx.us/pub/txdot-info/cst/TMS/200-F_series/pdfs/bit242.pdf.

Tons, E. et al. (1983). Fly ash as an asphalt reducer in bituminous base courses. Report prepared by the University of Michigan, The Board of Water and Light. Consumer Power Co. and Detroit Edison Co. Detroit, Michigan.

U.S. Environmental Protection Agency. (2007, May). *Recycling and Reuse: Industrial By-Products: European Union Communication.* https://archive.epa.gov/oswer/international/web/html/byproducts-guidance-053007.html#:~:text=These%20examples%20include%20slags%20and,from%20a%20primary%20production%20process. Accessed on September 9, 2022

U.S. Environmental Protection Agency. (2016, February). *Scrap Tires – Basic Information.* https://archive.epa.gov/epawaste/conserve/materials/tires/web/html/basic.html. Accessed on May 17, 2021.

Vallerga, B. A., & Gridley, P.F. (1980), Carbon Black Reinforcement of Asphalt in Paving Mixtures. Asphalt Pavement Construction, New Materials and Techniques, ASTM STP 724, l.A. Scherocman, Ed., American Society for Testing and Materials, pp. 110 - 128.

West, R. C. (2015). *Best practices for RAP and RAS management* (No. QIP 129). http://www.asphaltpavement.org/PDFs/EngineeringPubs/QIP129_RAP_-_RAS_Best_Practices_lr.pdf

Wielinski, J. C., A. J. Kriech, G. A. Huber, A. Horton, and L. V. Osborn. (2014). The Impact of Asphalt Blended with Re-refined Vacuum Tower Bottoms (RVTB) and Its Effect on HMA Mixture Performance. Canadian Technical Asphalt Association, pp. 402–426.

Williams, B. A., Willis, J. R., & Shacat, J. (2022). *Asphalt pavement industry survey on recycled materials and warm-mix asphalt usage: 2021* (No. IS 138 (12e)).

Willis, J. R., & Turner, P. (2016). *Characterization of asphalt binder extracted from reclaimed asphalt shingles.* National Center for Asphalt Technology. https://www.eng.auburn.edu/research/centers/ncat/files/technical-reports/rep16-01.pdf

Wirth, K. (2018). X-Ray Fluorescence (XRF), Geochemical Instrumentation and Analysis, https://serc.carleton.edu/research_education/geochemsheets/techniques/XRF.html. Accessed on Oct. 15, 2018.

Witczak, M., and Bari, Javed. (2004). Development of a master curve (E*) database for lime modified asphaltic mixtures. National Lime Association.

Xie, Z., & Shen, J., Earnest, M., Li, B., and Jackson, M. (2015). “Fatigue Performance Evaluation of Rubberized Porous European Mixture by Simplified Viscoelastic Continuum Damage Model.” *Transportation Research Record: Journal of the Transportation Research Board*. 2506. 90-99. 10.3141/2506-10.

Yao, Z., & Monismith, L. C. (1986), Behavior of Asphalt Mixtures with Carbon Black Reinforcement, AAPT, Vo1.55, pp.564 - 585.

You, T., Y. Shi, L. N. Mohammad, S. B. (2018). Cooper. Laboratory Performance of Asphalt Mixtures Containing Re-Refined Engine Oil Bottoms Modified Asphalt Binders. *Transportation Research Record: Journal of the Transportation Research Board*, Volume 2672, Issue 28, pp 88-95.

Yildirim, Y., Jayawickrama, P. W., Hossain, M. S., Alhabshi, A., Yildirim, C., Smit, A. D. F., & Little, D. N. (2007). Hamburg wheel-tracking database analysis. No. FHWA/TX-05/0-1707-7.

Zimmer, F.V. (1970). Fly ash as a bituminous filler. United States Department of Interior, Bureau of Mines. Washington, D.C.